TESIS DE LA UNIVERSIDAD DE ZARAGOZA

2019 107

Jorge Escribano Jiménez

Modeling and simulation of cell-cel and cell-matrix interactions

Departamento
Ingeniería Mecánica

Director/es
Sánchez Rúa, María Teresa
García Aznar, José Manuel

ISSN 2254-7606

Prensas de la Universidad
Universidad Zaragoza

ISSN 2254-7606

Universidad Zaragoza
1542

Tesis Doctoral

MODELING AND SIMULATION OF CELL-CEL AND CELL-MATRIX INTERACTIONS

Autor

Jorge Escribano Jiménez

Director/es

Sánchez Rúa, María Teresa
García Aznar, José Manuel

UNIVERSIDAD DE ZARAGOZA

Ingeniería Mecánica

2018

Modeling and simulation of cell-cell and cell-matrix interactions

Universidad Zaragoza

Jorge Escribano Jiménez

Advisors:
José Manuel García Aznar
María Teresa Sánchez Rúa

Department of Mechanical Engineering
University of Zaragoza

This dissertation is submitted for the degree of
Doctor of Philosophy in Mechanical Engineering

April 2018

A mis padres . . .

Acknowledgements

I would like to express my gratitude to all the people that has accompanied me during this journey and that, one way or another, have made their mark on this thesis and, more important, on me.

First of all, I would like to thank my advisors Manu and Tere. Thank you for your trust, and for all your patience and comprehension. I know it has not always been easy, but, I know you will miss our endless discussions and, specially, our countless skype meetings.

To our collaborators from the IBEC: Roger, Raimon, Xavier and Pere. Thank you for trusting in me to be part of those fascinating projects and for all your advise. Gràcies.

To Taeyoon Kim and his team for letting me be a part of it during my stay at Purdue. They made me feel very comfortable during my time with them. Thanks to Jing for his friendship, without whom, my stay in Indiana would have not been the same.

To the people from MIT. Thank you Roger for welcoming me in your lab and giving me such a great opportunity. To all the Roger´s lab members for making me feel at home: Sossy, Ran, Vivek, Jean Carlos, Jordan... and every one else. Thanks to Fabian for the good advises and for appreciating all my efforts.

Quiero dar las gracias a toda la gente que me ha acompañado de la universidad de Zaragoza: María José, María Ángeles, Tirso. A mis compañeros y amigos de la sala de becarios, tanto a los que ya estaban cuando yo llegué, como a los que seguirán cuando me vaya: Sergio, Raquel, Marina, Sara, los Carlos, los Javis, Alberto, Diego, Bea... y tantos otros con los que he compartido incontables cafés, y algún que otro viernes de bombero. A L.E.S: Andrea, Mar e Ismael por acompañarme de principio a fin y vivir juntos "estos momentos tan

bonitos", por esas charlas interminables, paseos a la máquina y cervezas de contrabando a última hora.

A todos los amigos, que tan buenos momentos me han dado y que han hecho que los difíciles fuesen mucho mas llevaderos. A los de toda la vida (La Garita), que aún no tienen muy claro si todos estos años he estado estudiando, trabajando o viviendo del cuento, pero que siempre me reciben con una sonrisa y dispuestos a hacer un buen rancho y pasar juntos el día. A los Amiguis (María, Pedro, Oriol, Carlos, Isa, ...), ese grupo que todas las mañanas te daba los buenos días por whatsapp y que hizo que mi estancia en Boston fuera una experiencia inolvidable. A mis amigos de Zaragoza: Victor y Alecha por esas cenas y cervezas. A Valeron, Rivas, Raúl y Diego por perder una y otra vez en esas partidas de Risk y NBA y subirme la moral cada fin de semana. Aroa y Belén por tantos buenos momentos en nuestro piso de Chopitos. A mis actuales compañeros en el piso del calor (Mario, Tori y sí, Ana, tú también) por esos jueves de lardero, martes de champions y ruedas de prensa.

Especial mención merece Rebeca, mi mejor compañera, por sacar siempre lo mejor de mí, apoyarme y animarme en todo momento. Espero que no dejes nunca de dar tanta "guerrita". Y como no hay uno sin tres, gracias también a los "churritos", por pasarme el manual de instrucciones e introducirme en la "familia".

Por último gracias a mis padres, Javier y Pilar. Son tantas cosas, que sabría por donde empezar pero no por donde acabar, así que sólo diré: Gracias por los últimos treinta años. A mi hermano Javi y a mi abuela Nati por acompañarme y cuidar de mi desde que nací. Al pequeño de la familia, Javi III, por alegrar este último año y medio como sólo él sabe. A toda mi familia de Cervera del Río Alhama tíos y primos porque siempre me han recibido con los brazos abiertos. También me gustaría dar las gracias a mis abuelos Asunción, Sebastián y Teodoro, sé que estarían muy orgullosos de este trabajo y gran parte de él es también mérito suyo.

Abstract

Chemical and physical properties of the environment regulate diverse processes such as cell differentiation, proliferation, or apoptosis. To migrate, cells need to quickly adapt to the environmental characteristics. Cells are able to sense the properties of their surroundings by establishing adhesions and applying force through them. Adhesions are regulated by the engagement, clustering, and turnover of adhesion receptors. The interaction between the cell and the extracellular matrix (ECM) is mediated through focal adhesions (FAs) or focal complexes which present a high concentration of the integrin family adhesion receptors. Cells also interact with their neighboring cells through different adhesive structures like adherens junctions, which also contain high levels of another transmembrane receptors known as cadherins. These cell-ECM and cell-cell adhesions are crucial in mechanosensing processes. They are responsible for the transmission of cell generated forces to their surroundings and they participate in the transduction of mechanical cues into biochemical signals. The influence of these adhesive structures in cell movement is crucial. Cells use them to test their surrounding, reorganize their structure and exert forces needed for their movement. Moreover, cell movement and shape significantly vary depending on the stiffness of the substrates or depending if migration occurs on flat substrates or three-dimensional matrices. The presence of other cells has also an important impact on migration. When cells move collectively, they establish a collaboration between them, through cell-cell adhesions, to achieve a more efficient migration. Cell-cell junction stability in some cell monolayers, like the endothelium, is crucial during diverse processes, including inflammation and cancer metastasis. The rupture of adhesion results in the formation of gaps which are critical for enabling immune or cancer cells to effectively transmigrate through the endothelium into or out of the vasculature.

In this thesis, we study, from a mechanical point of view, the role of these different adhesion structures in diverse processes such as cell migration or endothelium cell junction integrity. We focus on how mechanical properties of the environment influence the formation of adhesion and force transmission. To achieve this goal, we design four different computational models to simulate the force transmission process through cell-ECM or cell-cell adhesion in different scenarios and we study the emergent behavior of the system for each case.

First, we propose a discrete approach to simulate cell-ECM adhesions during actin during filopodium retraction. We analyze how mechanical properties of a 2D substrate influence adhesion and force transmission. This numerical model provides an individual analysis of the proteins involved including spatial distribution, interaction between them, and study of different phenomena, such as clutches unbinding or protein unfolding.

Second, we create a model for simulating different local extracellular matrix properties in order to unravel the fundamental mechanisms that regulate the formation of cell-matrix adhesions in 3D. We aim to study the mechanical interaction of these biological structures through a three-dimensional discrete approach, reproducing the transmission pattern force between the cytoskeleton and a single extracellular matrix fiber.

Third, we simulate how cells migrate individually and collectively in 2D substrates with rigidity gradients. We use a hybrid approach that combines continuous formulation of truss elements and a particle-based approach to simulate the dynamics of cell-ECM adhesions and cell-cell interactions. This model allows us to understand how collective behavior emerges and shows the basic physics of cell movement under stiffness gradient conditions. We show that cells move towards the stiffer part of the substrates due to their ability to deform more the substrate in the part of lower stiffness than in the stiffer part. This effect explains why cell collective movement is more efficient than single cell movement in stiffness gradient conditions. In addition, we numerically evaluate how gradient stiffness properties, cell monolayer size and force transmission between cells and extracellular matrix are crucial in regulating durotaxis.

Finally, we simulate an endothelial cell monolayer and show how the dynamic nature of the endothelium leads to spontaneous gap formations, without interference from the transmigrating tumor cells. The proposed model is based on contractile mechanical elements (stress fibers and actin cortex) within single cells, which are connected to neighboring cells through VE-cadherin based cell-cell adhesions. These adhesions can randomly bind and unbind in a force-dependent manner. We use the model to show that these gaps preferentially

appear at the vertices of three endothelial cells, as opposed to the edges between two cells. In addition, this model is capable of predicting gap lifetime and size. We perform parameter studies and identify how the competition of tightly balanced mechanical properties, including cell stiffness, radial or tangential contractility or adhesion strength critically affect gap formation or duration.

Table of contents

List of figures

Chapter 1

Introduction

1.1 Motivation and research objectives

The development of technologies to simulate the micro-environment, in which cells interact with tissues, is fundamental in many areas of biomedical research, such as regenerative medicine, cancer treatment or drug development. In the past recent years, the tendency to develop computational simulation models capable of reproducing and even predicting biological phenomena under different conditions has increased. The fundamental objective of these models is to provide a physical-chemical base able to explain the different phenomena and to reduce both in-silico and in-vivo experimentation, with the consequent economic and ethical impact that this fact entails.

This thesis focus on both cell-extracellular matrix interactions and cell-cell interactions. These interactions are crucial in different processes such as differentiation, migration, wound healing and cancer metastasis. Due to this importance, in the recent years, authors have focused on trying to understand the chemical and physical mechanisms underlying these interactions. Aberrant cell motility contributes to diseases such cancer metastasis whereas failure in the cell-cell junctions of a cell monolayer could lead to tumor cell extravasation [58]. These interactions involve multi-protein complexes combined to form the adhesion between cells and their environment. Adhesions are mainly governed by mechanical processes which determine the cell fate. For example, they are able to regulate the type of migration of the cell [53, 204] or the stability of the cell-cell junctions in a cellular monolayer [91]. It is

also known that cells adhere and migrate differently when they are located in 2D or 3D matrices [86] and they also present different behavior when they move isolated or in groups (collective migration) [189]. Cells are able to differentiate the environment characteristics through these multi-protein complexes that conform the different adhesions. It is therefore essential to understand how these adhesions work and how the force is transmitted through them to understand cell behavior in these different scenarios.

The fundamental objective of this thesis is to advance in the understanding of the mechanical mechanisms that regulate the adhesive properties of cells. In particular, the interaction between the cytoskeleton and proteins that regulate adhesion to the extracellular matrix (integrins) and other cells (cadherin) will be studied (See Fig 1.1). More specifically, we will focus on the role of these interactions in phenomena such as cell migration or cell monolayer cell-cell junction integrity. To this end, algorithms will be developed to simulate the biomechanics of the different molecules involved in the adhesions and observe the emergent behavior of the system in different scenarios. The different implemented models are discrete or hybrid (continuous and discrete) and they combine elemental mechanical equations with Brownian dynamics and biochemical laws for adhesion binding and unbinding. The scenarios analyzed with the different models are the following:

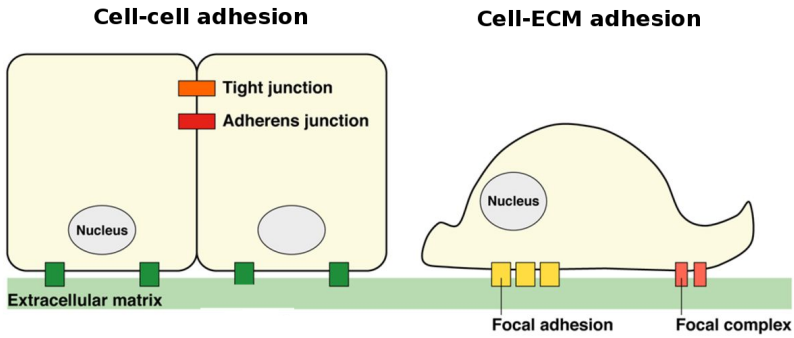

Fig. 1.1 Adhering cells. Cells can adhere to other cells through different structures such as tight or adherens junctions (left). They can also bind to the extracellular matrix through focal adhesions or focal complexes (right). Adapted from [130].

- The interaction between a cell and a 2D substrate. We try to unravel the mechanism of force transmission during actin retraction. We focus on understanding the role of the different elements involved: matrix stiffness, ligand distribution, myosin activity or adhesion availability.

- Cell-ECM interactions in a 3D environment. The objective is to observe the same phenomena studied before but with 3D fibers instead of a flat substrate. We focus on analyzing how different aspects such as crosslinking stiffness, adhesion binding laws and geometrical positions between fiber and cell might influence the force transmission and adhesion characteristics.
- The role of cell-ECM and cell-cell contacts in cell migration. We aim to understand how force transmission at both levels (cell-cell and cell-ECM) influence migration in 2D. We analyze how extracellular matrix properties might guide migration directions and which aspects (cell contractility, cell-ECM adhesion size, collective vs single movement,...) promote migration.
- Mechanisms that leading to the failure of the cell-cell junctions in the cell monolayer. The objective is to study how mechanical properties of the cell, cell-cell adhesion properties, and force distribution may lead to the generation of gaps in the cellular monolayer barrier.

1.2 Cell adhesion and migration

Cells are the smallest units of life that can replicate independently. Cells can be divided into eukaryotic cells, which contain a nucleus, and prokaryotic cells, which do not, and they all vary in structure, shape, and function [19]. In this manuscript, we will study some features of only eukaryotic animal cells. There are about 10^{14} cells in a human body and their size is in the range of tens of micrometers [4]. Between them we can find about 200 major cell types and all of them have the same genome; however, due to differentiation process, they all have different gene expression [177].

Cells are delimited by a plasma membrane which consists of a fluid lipid bilayer that carries a wide variety of membrane bound proteins. The actin cortex is located underneath the cell membrane, it consists of a polymer structure formed by crosslinked actin filaments that govern the mechanical response of cell deformations. The cytoplasm is contained within the limits of the membrane and corresponds to the cell volume (excluding the nucleus); it contains the cytosol, different cell organelles and highly crosslinked polymer networks of actin filaments, microtubules, and intermediate filaments that are collectively known as cytoskeleton (CSK)[19, 177, 89]. Inside the CSK, molecular motor proteins myosin II pulls from the actin filaments provoking cell contraction and being responsible for the force

generated process inside the cell. Migrating cells present typical structures like lamellipodia and filopodia. The lamellipodium is located at the edge of the cell, it is a very dynamic structure that is constantly moving as consequence of myosin activity. It grows due to processes of actin filament polymerization, capping, cross-linking and branching [154, 155, 161]. In the lamellipodium, protruding finger-like structures known as filopodia are originated (see Fig. 1.2).

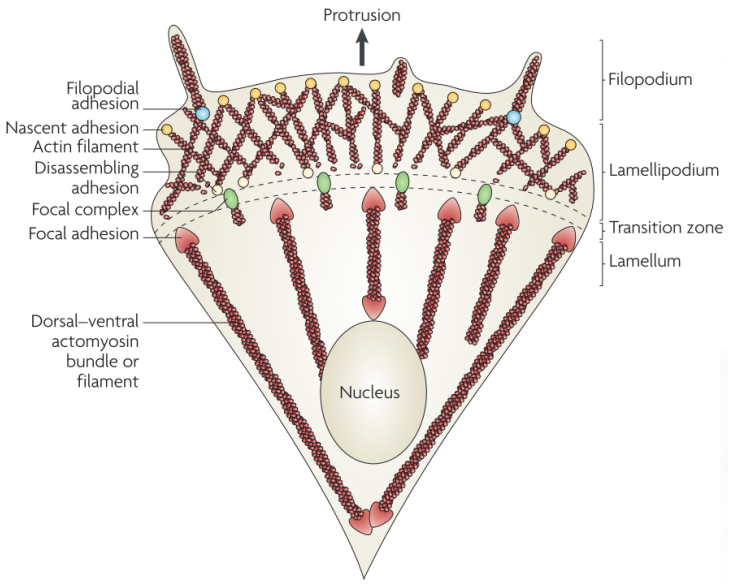

Fig. 1.2 Structure of an adhering cell. At the leading edge of the cell, filopodia and lamellipodia create protrusions and establish dynamic adhesion with low stability known as nascent adhesions. Adhesion maturation to focal complexes and focal adhesions occurs in the inner part of the lamellipodium and in the lamelum. Adapted from [148].

The extracellular matrix (ECM), a fibrous network made of different components like fibronectin or collagen, is located outside the cell boundaries. Cells are able to adhere to the extracellular matrix through trans-membrane proteins called integrins. Integrins are located in the cell membrane and bind the actin filaments inside the CSK with the ligands in the ECM through different adapter proteins (talin, vinculin, paxillin,...) [96]. These adhesions have different names depending on the cell location where they occur and on their stability. Adhesion sites are typically located in between the polymerization dominated lamellipodium and the myosin-dominated contractile structures (stress fibers) located closer to the lamella. The stress fibers and lamellipodium are actin assemblies that constitute the two main force-

generating structures for adhering cell, creating pulling and pushing forces. Adhesion located in the lamellipodium and filopodium are usually called nascent adhesion. They are transient adhesions with low stability that tend to appear and disappear at high frequencies. The exact organization of the lamellipodium varies as a function of cell type, motility state, and external signals [196, 206]. One of the most important aspects of lamellipodium growth is the force-velocity relation, objective of various modeling approaches [31, 218, 175, 114]. As we move to the inner part of the lamellipodium, adhesions start to mature and become more stable; they are usually called focal complexes. The lamellum is the part behind the lamellipodium closest to the cell body. Actin filaments gather together and form more stable structures known as stress fibers. The adhesions in this part are generally referred as focal adhesions (FAs) and they have greater stability. They constitute the main sources of cellular forces that are exerted on the substrate since they are often found at large adhesion sites correlating with large forces [11].

Through the cell-ECM adhesions, the cell is able to transmit the force generated by the cytoskeleton to the ECM. Cells can only respond to the physical properties of the environment when they are able to actively generate and transmit forces to their surroundings. Therefore, this force transmission is crucial for cell fate since it allows the cell to sense and consequently react to the environment that surrounds it. This opens a new line of applications for tissue engineering and regenerative medicine since these physical signals are more permanent and easy to control than biochemical or genetic manipulations [177]. For example, mechanical properties of the substrate and adhesive characteristics are crucial in regulating cell differentiation [64, 98]

Adhesions not only occur at the cell-ECM level, cells also interact with each other through a different adhesion complexes known as tight junctions (TJs) and adherens junctions (AJs). Cadherins, located in the AJs, are one of the main proteins involved in cell-cell force transmission [125]. Cell-cell interactions are also crucial for different cellular processes. For example, cells behave in a different way when they are isolated or when they are surrounded by other cells. They develop a mechanism based on the force transmission to cell-cell contacts in order to migrate in a more efficient way than when they move isolated. Cell monolayer integrity is also regulated by these kinds of interactions; rupture of cell-cell adhesion provokes gap generation between cells allowing other cells to trespass the monolayer barrier. Due to its relevance in different biological phenomena, it seems crucial to understand how this force transmission at both cell-ECM and cell-cell levels influence them and, at the same time, understand how these forces modify the level of adhesion in both scenarios.

Adhesion assembly (at both levels, cell-ECM and cell-cell) depends on different factors. First of all, the proteins that bind should be close to each other in order to perform the adhesion. The concentration of binding proteins or binding sites in the ECM as well as force level are also relevant. Adhesions grow as the force does, this is due to a reinforcement phenomenon. Force provokes protein unfolding, this unfolding leads to an increase in the available binding sites for vinculin recruitment . When vinculin attaches, it provokes a strengthening of the adhesion [148].

Adhesion breaking is a force dependent process. There are two main laws that describe adhesion lifetime depending on the force: Slip bond law and catch bond law. These laws will be explained further in this chapter.

Cell migration is a complex process that all nucleated cells do. It is involved in tissue maintenance, formation, and regeneration as well as pathological conditions like cancer invasion [72]. Motile cells adapt to the different environmental conditions such as ECM dimensions, density, stiffness, presence of other cells and which define their way migration. In general, cell movement involves different stages (see Fig. 1.3).

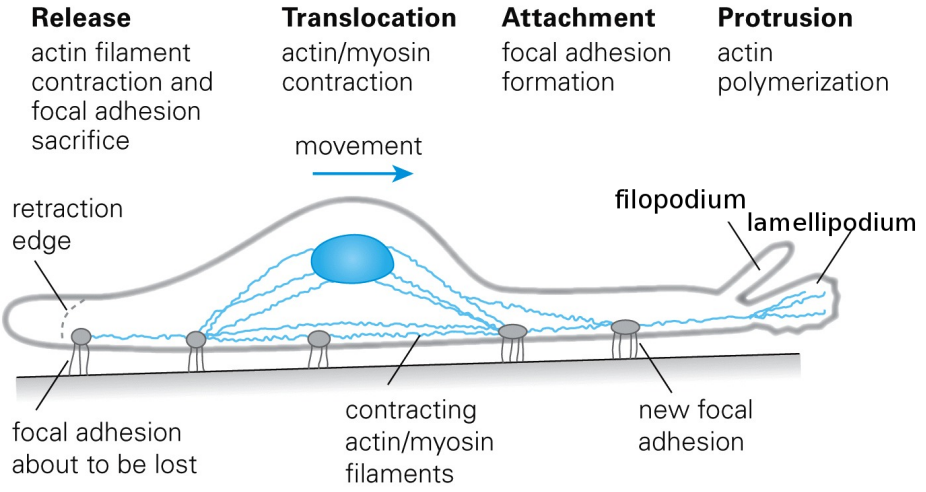

Fig. 1.3 Cell migration stages. Cell movement involves the formation of protrusion at the front of the cell, adhesion of such protrusions, detachment of adhesions at the rear of cell and translocation of the cell body. For this chain of events myosin generated forces are essential. Adapted from [41].

1.2.1 Cell-ECM adhesion

Focal adhesions (FAs) are multifunctional organelles that mediate cytoskeletal regulation and signaling, force transmission and cell–ECM adhesion [76]. FAs consist of a complex network [215] of cytoplasmic proteins and membrane integrins that form a 200-nm plaque [69, 38] which links the cytoskeleton with the ECM. FAs have been deeply studied in the recent years due to their well-known importance in phenomena such as morphogenesis, immunity and wound healing [96]. Through them, cell generated forces are transmitted to the extracellular matrix allowing the cell to sense the mechanical properties of the tissue that surrounds it and respond consequently. These forces deform the substrate in the short term but, at longer time scales, they can provoke reorganization of substrate fibers and cytoskeleton polymers [177]; in fact, substrate characteristics modify the size of adhesive regions and provokes reorganization of the cellular cytoskeleton. This means that cellular function and structure are very sensitive to the substrate stiffness[54]. For example, cells tend to spread more and have larger adhesive regions on stiffer substrates. They also prefer to move from softer to more rigid substrates (a process known as durotaxis) [194, 189].

The complexity of focal adhesion composition and dynamics implicate an intricate molecular machine [96]. Studies with super-resolution microscopy have provided insight of the nano-organization of FAs [93] and the molecular layers present in them (see Fig. 1.4). Paxillin and highly signaling proteins focal adhesion kinase (FAK) are located in the signaling layer, the closest to integrins in the membrane. The next layer binds the actin filament with the integrins and it is known as the force transduction layer. It contains talin and vinculin proteins: talin proteins unfold under stress forces and bind the actin monomers in the cytoskeleton with the integrins in the membrane. Mechanical stretching of talin promotes its binding to vinculin and, at the same time, vinculin binding inhibits talin refolding after the force is released [212]. This force-dependent interaction between vinculin and talin is crucial for the initiation and growth of focal adhesions. Actin stress fibers and actin regulatory are the next layers, containing VASP, zyxin and α-actinin [93].

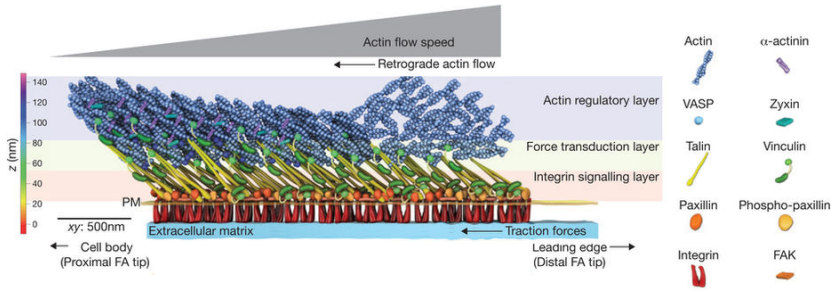

Fig. 1.4 Focal adhesion architecture. Actin filaments in the cytoskeleton are bound to the integrins placed in the membrane through different force sensitive proteins. Integrin binds with the extracellular matrix outside the cell and transmit the force generated inside the cell to the substrate. Adapted from [33].

1.2.2 Cell-cell adhesion

For both epithelium and endothelium layers, cell-cell junctions are crucial for the remodeling and integrity of the entire cell layer. Multiple physiological and patho-physiological processes such as wound healing, barrier function, angiogenesis, and inflammation require a mechanically stable connection of cells [3]. Cell-cell interaction also plays an important role in cell migration. The way cells migrate changes when they are isolated or when they are located in a monolayer with other cells. Endothelial cells have at least two different adhesive regions that which are comparable to tight junctions (TJs) and adherens junctions (AJs) found in epithelial cells. Adherens junctions are involved in starting cell-cell contacts and maintain their stability. On the contrary, TJs control the passage of soluble factors [50]. Adherens junction proteins might vary depending on the cell type, however, the cadherin/catenin complex and actin filaments are always present, mediating adhesion of adjacent cells and constituting a precondition for overall junction differentiation and regulation [25, 3].

Endothelial monolayer integrity Vascular endothelial cadherin (VE-Cadherin) is one of the main proteins that regulates endothelial cell-cell junctions, responsible for maintaining the vascular integrity. Intracellular signals caused by inflammatory cytokines or permeability-increasing agents provoke the formation of gaps in the cell-cell contacts which allow solutes or cells to cross the endothelial barrier [16, 104]. In general, these gaps are reversible and can close quickly, unless chronic inflammation occurs [49]. Disturbed endothelial junctions are often found in patho-physiological conditions such as inflammation, vascular leakage, atherosclerosis, and tumor-associated angiogenesis [12, 91] (see Fig 1.5).

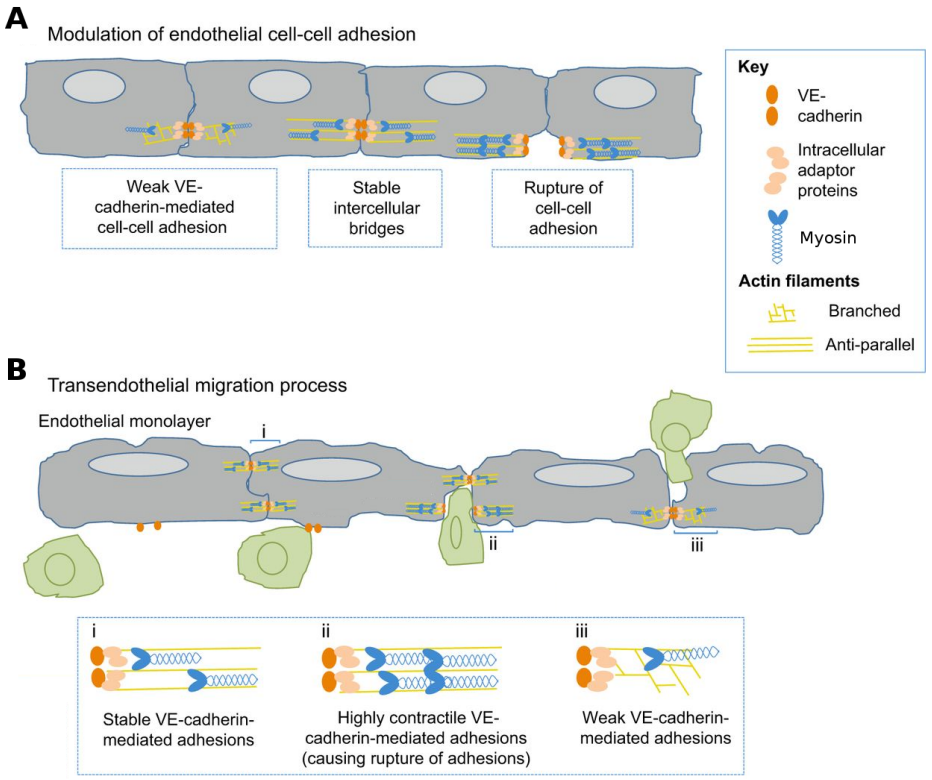

Fig. 1.5 Endothelial gap formation and transmigration. A) VE-cadherin rupture and gap formation. B) Cell migrating through a gap and trespassing the endothelial barrier. Adapted from [138].

VE-Cadherins are linked with the actin in the cytoskeleton by proteins such as α -Catenin, Eplin, and Vinculin [61, 2]. Cadherin and vinculin complexes transmit forces and also act as active mechanosensors [110]. In the same way as in FAs, in cell-cell adhesions although vinculin recruitment is not necessary for junction formation, maintenance, or remodeling, it promotes adhesion stability and protects endothelial junctions from opening during force-dependent remodeling [91]. The strength of VE-cadherin adhesive bonds also works in a stress-dependent manner [107].

1.2.3 Physical laws for bond adhesion and rupture

The stability of adhesions was first addressed by Bell [18]. Unbinding was assumed a force dependent process and the author proposed an unbinding rate (k_{off}) of:

$$k_{off} = k_0 e^{F_b/F^0}, \tag{1.1}$$

where k_0 is the unbinding rate for zero force (in s^{-1}) and F^0 the molecular-scale force (typically of the order of pN) and F_b is the modulus of the current force of the bound. This equation is known as the Bell's equation and it can be used to simulate the exponential force dependent behavior seen in the slip bond law. This law has been used for different authors to simulate focal adhesion formation [34, 62, 63].

A pure catch bond law is the opposite to a slip bond law: higher forces mean higher stability. Different works have shown that cell-ECM and cell-cell contacts can also behave as catch bonds until a point where force increment also provokes less stability [146, 106]. This kind of behavior is known as catch-slip bond, since it shows a response of catch bond law for low forces and a response of slip bond law for high forces. It can be simulated as the sum of two exponential curves (of catch and slip bond) [141]:

$$k_{off} = k_0 exp(\Phi_c - \Phi) + exp(\Phi - \Phi_s), \tag{1.2}$$

where $\Phi = F_b/F^*$ and Φ_c, Φ_s are the parameters of the catch and slip bond regimes respectively. F^* is used to normalize the force and F_b is the modulus of the current force of the bound.

Fig 1.6 shows the comparison between two types of law. Slip bond law lifetime decreases exponentially as the force increases, having its most stable point when forces are null. On the contrary, cath-slip bond law has medium stability when force is null. As the forces increases so does the lifetime of the bond until it reaches a maximum point of stability. After that point lifetime decreases exponentially with force. During this thesis, we will use these two laws, but sometimes, for simplicity reasons we will refer to the catch-slip bond law as simply catch bond. Pure catch bond law will not be considered during this thesis.

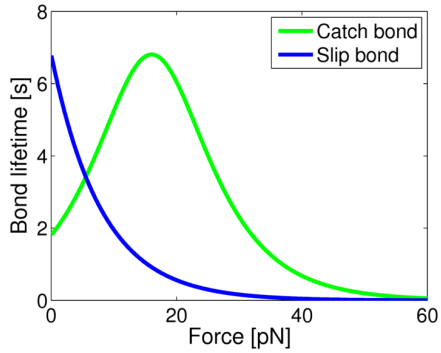

Fig. 1.6 Typical adhesion unbinding law. Catch and slip bond. Bond lifetime depending on the force for the two typical laws for adhesion unbinding (Slip and catch-slip bond).

1.2.4 Cell migration

Cell migration is a complex and heterogeneous process which affects all nucleated cell types during some time of their development. Cells present different modes of migration depending on different factors, being particularly important the extracellular matrix characteristics [72].

Modes of migration can be classified into different categories: ameboid or mesenchymal migration for single cells and collective migration for a group of cells. Ameboid migration refers to a movement where the cell barely establishes adhesions with the extracellular matrix and lacks of stress fibers and mature focal adhesions. They normally generate weak adhesions localized at the filopodia leading edge with low force transmission [213, 183]. If the cell does not have focal contacts at all, it is also known as blebby migration and, in this particular case, there is no pulling or pushing the substrate [68, 170]. In mesenchymal migration, cells can present high levels of attachment with the ECM and develop a consistent cytoskeletal contractility [121, 81]. Cell movement is produced as a response to the environmental characteristics. These different environmental characteristics (ECM ligands with different macromolecular and structural organization, which includes orientation, dimension, stiffness, and density) impact critically migration type and efficiency. In response to these different characteristics, the CSK adapts in a dynamic way modifying its geometry in time and space [81, 97]. When cells have no adhesion (blebby migration), cells are rounded and they use a propulsive-pushing way of migration (see Fig. 1.7) [68, 170]. When cells present strong adhesions they transmit the myosin generated forces to the surrounding tissue. In this scenario, cells create protrusions through actin polymerization which bind to the available adhesion sites at the ECM [210].

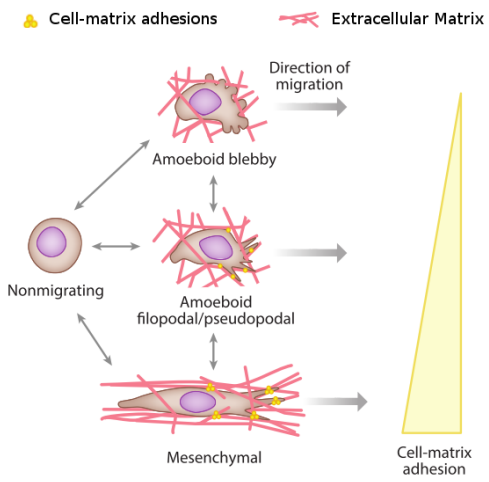

Fig. 1.7 Cell migration modes depending on the adhesion to the substrate. Movement can be mesenchymal, ameboid or blebby depending on the level of adhesion. Adapted from [191].

In response to environmental determinants, the actomyosin cytoskeleton adapts in a dynamic manner and generates different geometries in space and time, ranging from flat and spread out to roundish, elongated, or multipolar shapes [81, 97]. To transmit actomyosin-driven forces to surrounding tissue structures, the cell either develops actin-polymerization–driven protrusions that bind to adhesion sites of the tissue through adhesion receptors [210], or it uses poorly adhesive intercalation and propulsion [145]. In both cases, subsequent to leading edge protrusion, actomyosin contraction leads to retraction of the cell rear and translocation of the cell body [145]. The cyclic repetition of protrusion, cell-ECM interaction and cell rear retraction is what provokes the cell movement [72].

Cells can also move in groups, this is known as collective migration. Collective migration is vital during cell development and in processes such as building, shaping, and remodeling complex tissues. It also contributes to cancer progression by local invasion [71]. Different factors can affect collective migration such as the strength of adhesion, cell density or ECM constraints [72]. As in single cell migration, communication between matrix and cell is crucial for the process; for collective migration, it is also important to consider the role of cell-cell contacts. Collective behavior is not the result of an independent group of cells that moves in the same direction. Chemical and mechanical coupling through cell-cell contacts allow cells to influence the behavior of one another and modify the supracellular front-rear polarity [48]. A hierarchy is established between the group of cells, where some

cells act as the leaders guiding the others. These leaders sense the mechanical and chemical cues that guide migration. Cells communicate and cooperate each other by transmitting the force through cell-cell contacts. This results in a more efficient migration [189, 190, 48] (see Fig 1.8).

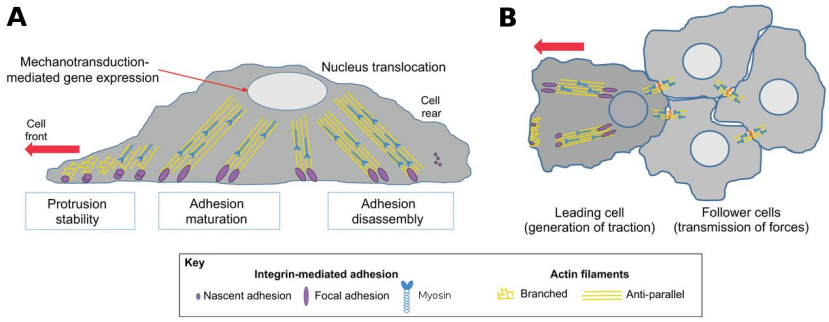

Fig. 1.8 Cell migration. Single vs collective. A) Single cell migrating by establishing adhesions at the front and disengaging adhesion at the rear. B) Collective migration. Cell is bound through cell-cell contacts and one of the cells creates strong adhesion with the substrate leading the others by force transmission through the cell-cell adhesion. Adapted from [138].

Cell movement direction can be guided by different external stimuli that cells are able to sense. Some examples of guided movement are: haptotaxis (cells migrate as a consequence of gradient in the adhesion binding sites of the ECM), chemotaxis (movement is guided by chemical cues), electrotaxis (electrical stimuli) or durotaxis (movement depends on the substrate rigidity, cells tend to migrate to stiffer substrates).

3D vs 2D Different physical properties of the ECM provoke significant difference between cell migration in 2D and 3D. In 2D migration, cells are flat and rounded and move on top of the substrate. The ECM characteristics that cells are able to sense are mainly mechanical rigidity and ligand availability for establishing adhesions. However, cell migration in 3D tissues is more complex and there are more aspects needed to be considered. Cells move inside a fiber network, they need to deform the matrix and degrade it to generate some space to go through. Cells also have to deform their body to pass through these gaps between the fibers. Moreover, they have to establish adhesions along the matrix fibers during the process. It is clear that to understand cell 3D migration, more variables than in 2D migration have to be considered: cell deformability, matrix degradation, matrix density and matrix mechanical

stiffness. During the past recent years, many authors have focused their work on trying to unravel the mechanisms behind 3D cell migration.

1.3 Computational modeling background

Computational models are a useful tool that can help us to understand the fundamental physics and biology regulating the dynamical behavior of different systems. They are able to predict biological behavior in different scenarios and with relative accuracy. This could help in determining the direction of future experimental work, reducing considerably costs and time. Throughout this thesis, different computational models will be presented to simulate cell-ECM adhesion and cell-cell interactions. In this section, we show a brief review of the most relevant models for the work developed during this thesis. For cell-ECM interaction, we show a brief review of the different clutch models. The clutch model has served us as a base for designing the model of the second chapter. We have expanded this model in the two following next chapters to analyze different phenomena. For cell-cell interactions, we present a brief review of the agent-based models which are typically used to mimic cell monolayer behavior. Further modeling review is done in the introduction of each chapter.

Different attempts have been made in order to simulate cell-ECM interactions during these last years, between all them it is particularly interesting the clutch model (see Fig . 1.9). Chan and Odde [34] first presented a clutch model to simulate cell-ECM force transmission during actin retrograde flow in filopodia formation. They analyzed how the dynamical behavior of adhesions influence force transmission and actin velocity for different substrates rigidities. They observed a biphasic response of the traction forces transmitted to an increase of substrate stiffness. In a first stage, traction forces increased as stiffness was increasing. In a second stage, when substrate rigidity was high enough, adhesion failure occurred and traction forces critically dropped. However, experimental observation suggested that force always increased as a consequence of substrate stiffening. More recently, Elosegui *et al.* [62] improved the clutch model proposed by Chan and Odde by including an adhesion reinforcement phenomenon. They showed that there is a rigidity threshold above which adhesion probability is increased, leading to the reinforcement of the bond. Later, Elosegui *et al.* [63] found that talin is needed for force transmission when this rigidity threshold is exceeded. The threshold also correlated with integrin recruitment, the growth of vinculin-rich FAs, and the nuclear translocation of the mechanosensitive transcription factor YAP. They stated that the observed rigidity threshold occurred due to talin unfolding, and found that,

depletion of talin resulted in the biphasic behavior between traction forces and ECM stiffness showed by Chan and Odde [34]. Recently, Oria *et al.* [144] improved the clutch model to simulate heterogeneous distance distribution between the ligand in the substrate which affects force distribution between the bounds. They observed how this force distribution affects adhesion reinforcement threshold and adhesion size.

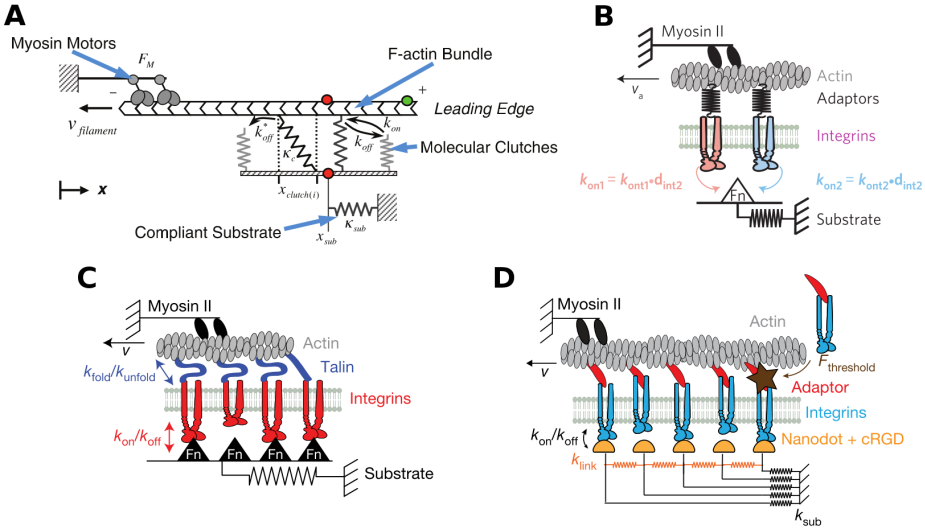

Fig. 1.9 Clutch model evolution. A) First clutch model, proposed by Chan and Odde. Figure from [34]. B) Clutch model adaptation to simulate different integrin proteins and clucth reinforcement. Figure from [62]. C) Clutch model that incorporates Talin effect. Figure from [63]. D) Clutch models modified to simulate distance between integrins through a network of springs in series and in parallel. Figure from [144].

Agent-based models are one of the most used models to mimic the mechanical and physiological behavior of cell populations. These models are discrete approaches that consider cells as individual units, and they allow us to simulate the interactions between different cells, and at the same time integrate intracellular processes [199]. Agent-based models can be divided in three different categories (see [199]): center-based models (CBM)[73], vertex models [117] and deformable models (DFM) [92]. Most of the recent models simulating monolayers correspond to vertex, center-based or continuum approaches. Different DFM [92, 149] offer the possibility to simulate cell-cell interaction and to observe the response of the cell cluster in different conditions. We will propose a DFM appraoach to simulate cell-cell adhesions dynamics in an endothelial monolayer.

1.4 Thesis outline

This thesis dissertation is divided into six chapters and two appendices. Each chapter is based on a journal publication and all of them are self-contained. The thesis is organized as follows:

- Chapter 1: (Current chapter) introduces the motivation and objectives of the thesis and provides biological background to the questions addressed. Moreover, it provides a brief overview of computational models.
- Chapter 2: We develop a computational framework to simulate focal adhesions during filopodium retraction and study the importance of mechanical properties of the substrate as well as cell and adhesion properties.
- Chapter 3: Filopodium retraction is studied in 3D matrices. We employ the previous model with some modifications and observe how adhesion level is fundamental for matrix realignment.
- Chapter 4: We extend the model from Chapter 2 into a whole cell model. This allows us to study durotaxis in single and collective cell migration. We show the importance of different mechanisms in the process such as level of adhesion, force generation or cell monolayer size.
- Chapter 5: We introduce an agent-based model of an endothelial cell monolayer that allows us to investigate the mechanisms behind cell-cell junction instability and paracellular gap formation.
- Chapter 6: We summarize the most important findings and conclusions of this thesis. We also indicate some possible future lines of research to continue with the work started in this thesis.

In the appendices, a list of the contributions made during the writing of this thesis is given. We also provide a thesis summary in Spanish.

Chapter 2

A discrete approach for modeling cell-matrix adhesions

In this chapter, we develop a discrete computational model for cell-ECM adhesion during actin filopodium retrograde flow. This chapter is published as [65]:

Escribano J, Sánchez MT, García-Aznar JM (2014) A discrete approach for modeling cell–matrix adhesions. Comput Part Mech 1:117–130.

2.1 Introduction

Cell migration is crucial in a wide range of biological processes like chemotaxis, cancer metastasis, tissue regeneration and development. Nevertheless, despite the importance of this phenomenon, it still exists a deep unawareness of the main mechanisms that mediate this process. This lack of knowledge is due to the high variability of morphology that cells show during migration and its strong dependency on environmental factors, such as dimensionality, stiffness of the matrix and chemical gradients [148]. During migration, cells can present two different extreme main migration modes: amaeboid (weak adhesions) and mesenchymal (strong adhesions). Therefore, the understanding of cell-matrix adhesions is essential for advancing in the comprehension of cell migration. Cell adhesion is the mechanism that ensures structural integrity of tissue [178], and it is mainly regulated by mechanical processes

[53, 204]. Moreover, forces generated by cells are crucial in morphological tissue changes during cell migration, along with other processes such as spreading, migration and division [112, 209, 176]. The force generating processes in the cytoskeleton are closely related to the building of adhesion sites, called focal contacts or focal adhesions (FAs) [77, 176]. These connections make the mechanical forces generated in the cytoskeleton (usually by myosin proteins) to reach the extracellular matrix (ECM), allowing the cell to sense the mechanical properties of their surroundings, which will regulate the cell behavior. Focal contacts are mainly localized in the edge of cells in like-protrusion structures such as lamellipodium and filopodia [76]. When they are found in high concentration (i.e. in these kind of structures), they are called focal adhesions. These adhesions are strongly related with the retrograde flow of the actin filaments, which is driven by actin polymerization and myosin contractility [168].

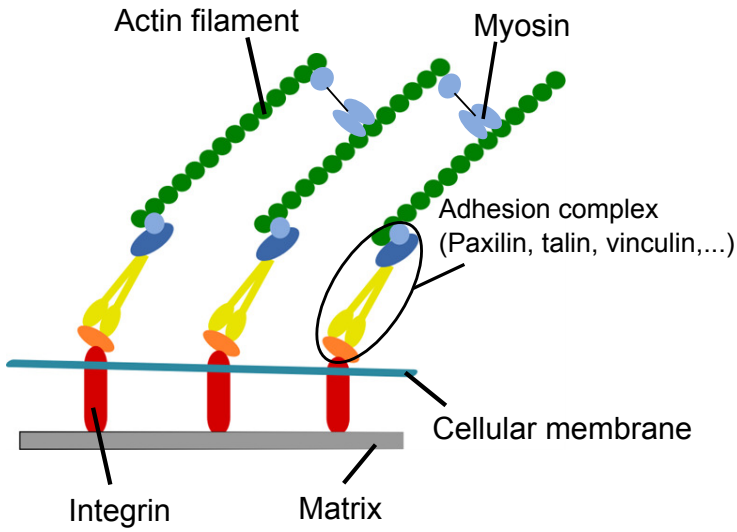

Fig. 2.1 Cell-Extracellular matrix adhesion schematic. Representation of the main components that define the cell-matrix attachment through actin cytoskeleton.

In fact, migrating cells are governed by a cycle of membrane protrusion, cell adhesion to the matrix, cytoskeleton contraction and de-adhesion at the cell rear [193]. This cyclic process in protruding lamellipodia is mainly regulated by the cell cytoskeleton through the filamentous actin (F-actin) assembly and retrograde flow (see Fig. 2.1). These adhesions connect the cytoskeleton of a cell to the extracellular matrix by means of a dynamic and complex set of proteins. Actually, these adhesions are implemented by transmembrane receptors from the integrin family [47] (which are placed in the cell membrane and reach both sides), binding protein ligands of the ECM, like fibronectin family [167], with the

actin cytoskeleton through a clutch of proteins that include talin, α-actinin, vinculin and paxilin [216, 178]. The polymerization of actin filaments provides the force for membrane deformation causing membrane protrusion. Contractile forces are generated by the myosin II, which moves antiparallel actin filaments past each other and thereby provides the force that rearranges the actin cytoskeleton [148]. Finally, these protrusions must adhere to the matrix to define cell locomotion. If they do not attach, protrusions are unproductive and tend to move rearward in waves in response to the tension generated in the cell, in a process known as membrane ruffling [23]. Therefore, actin retrograde flow is strongly dependent on cell contraction and focal adhesion size, concentration and strength [99].

In this chapter, we propose a discrete computational model for the simulation of the actin retrograde flow in filopodia growth-cone structures. Filopodia are found interposed along the lamellipodium leading edge and they consist of bundles of actin filaments that are packed together and protrude forward [131]. Filopodia not only play a role as adhesion sites, but also as sensors of the environment that surrounds the cell and signaling [217], and they also contain the receptors for the guidance molecules [17, 137, 159, 186].

Mathematical modeling of cell adhesion is crucial for advancing in the understanding of how cells regulate their cytoskeleton to lead their locomotion [78]. Therefore, a high number of conceptual [163, 40] and mathematical works [74, 15] have been developed to unravel how mechanical stimulus and cell-matrix properties regulate the dynamics of FAs. Most of these works are based on stochastic dynamics of multiple receptor-ligand bonds [74]. So, for example, Nicolas *et al.* [139] proposed that the FA mechanosensitivity can be enhanced by deformation-induced increase in the affinity of plaque proteins that form the adhesion. Shemesh *et al.* [181] considered FA growth as a consequence of enhanced aggregation of FA proteins in the direction of force application. Deshpande *et al.* [52] proposed a model of cellular contractility that accounts for dynamic reorganization of cytoskeleton. Chan and Odde [34] investigated ECM rigidity sensing of filopodia via a stochastic model of the motor-clutch force transmission system, where integrin molecules work as mechanical clutches linking F-actin to the substrate and mechanically resisting myosin-driven F-actin retrograde flow. More recently, Novikova *et al.* [141] proposed an original mathematical model for stiffness-sensing at focal adhesions, based on the interplay of catch-bond dynamics in the integrin layer and intracellular force generation through contractile fibers. One of the main limitations of these approaches is the assumption that total force is equally transmitted to all the bonds, not considering the spatial distribution of the focal adhesions. Another different strategy is based on a continuous approach considering energetic basis. Olberding *et al.* [142] proposed a theoretical treatment of focal adhesion dynamics as a nonlinear

rate process governed by a classical kinetic model. Kong *et al.* [105] treated the focal adhesion as an adhesion cluster and studied the stability of this cluster under dynamic load by applying cyclic external strain on the substrate. There are also other works that were not specifically conceived for cell adhesions, but their methodology can be applied to model them. For example, Sauer and Wriggers [172] presented a three dimensional finite element method for contact problems developing a computational contact formulation that captures intermolecular forces such as van der Waals adhesions.

In focal adhesions sites it is important to assess the impact that protein folding phenomena has on them. In this chapter, a force dependent model is implemented, but this phenomenon has been the focus of numerous numerical and mathematical studies during the last years. Thanks to technological advances in computer hardware and software, the possibilities of performing numerical analysis on this subject has increased and improved. Different numerical approaches have been developed in order to simulate protein folding, from making predictions of a folded peptide from its primary sequence to Monte Carlo simulations [120, 184] or different molecular dynamics simulations [197]. For example, Monte Carlo simulations are used to obtain an approximation of a dynamically folding pathway. However, in order to understand how the mechanism of the whole folding process is, atomistic molecular dynamics simulations are used, since they provide information about the transitions between structures [70]. The accuracy of these simulations relies on the capacity of the different physical models (force fields) to reproduce the true potential energy surfaces of proteins [27, 152]. Freddolino *et al.* [70] analyzed the challenges that molecular dynamic simulations face, mainly due to the amount of sampling needed in order to model protein folding and the accuracy required from empirical force fields that represent the true free energy surface on which a protein folds. It is also interesting to remark the work of Waisman and Fish [205], in which they originally proposed a variant of the full approximation storage (FAS) technique [24]. This method allowed the consideration of different force fields at various scales, enhancing in that way the flexibility and the computational performance. More recently, Piana et al [152] evaluated the accuracy of the force fields typically used in folding simulations.

The binding phenomenon treated in this chapter has also been simulated in other numerical works. They are based on the estimation of the binding energy and different computational approaches are widely discussed in Vietś work [203]. These approaches can be divided in docking methods, where scoring functions are used to identify the most stable receptor ligand conformation, and methods based in Brownian dynamics simulations. They used conformational sampling to generate thermodynamical averages. There are a wide

variety of methods used to compute the binding free energy such as linear interaction energy (LIE), linear-response approximate (LRA), molecular mechanics Poisson-Boltzmann surface area (MM-PBSA) [103] and thermodynamics integration (TI). Generally, these methods are more accurate than docking methods but, they are more time consuming.

Here, we present a mathematical model to simulate filopodia protrusion phenomenon during the actin retrograde flow process. This model takes into account the different set of proteins involved: from myosin and actin filaments to the ligands on the ECM, including the linking proteins that perform the adhesion. Therefore, in this work we aim to understand through numerical discrete simulations how the spatiotemporal assembly, disassembly and reorganization of focal adhesions influence on the force transmission from the acto-myosin contractile system to the extracellular matrix. This model is also designed to be the starting point from which we build different models which are detailed in the next chapters.

2.2 Material and methods

In this section we present the simulation model together with the equations that govern its behavior and the hypotheses in which it is based. The main goal of this model is to reproduce the retrograde flow of actin filaments in filopodia protrusions due to the dynamics of cell-matrix adhesions. The number of components involved in this phenomenon is considerable, therefore some simplifications are required due to its complexity. More than 150 hundred types of proteins are involved in the linkage between the cytoskeleton and the extracellular matrix, but in this chapter we only consider the effect of myosin proteins, actin filaments, extracellular ligands and protein complexes. These protein complexes, called adhesion complexes (ACs), are formed by a myriad of intracellular proteins (paxilin, vinculin, talin,...), and also by the integrins in the cell membrane [178]. These bind the actin filaments with the extracellular ligands in the matrix, addressed from now on as simply ligands.

2.2.1 Brief description of the simulation model

The development of a full discrete model that includes all the protein complexes and their interactions involved in the formation of a filopodium would imply a huge computational cost. Due to this, a simplification of the actual case is proposed, presenting a model that consists on a single actin filament bound to the ECM. The system movement starts when myosin proteins exert a force on the actin filament provoking its retrograde flow as it is

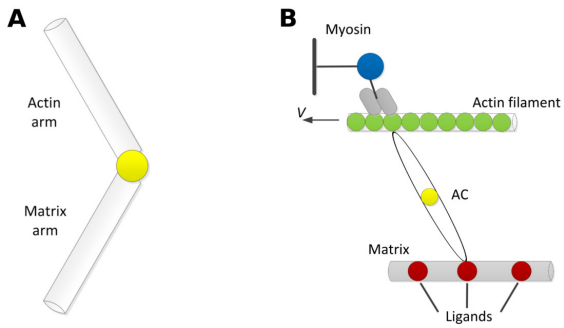

Fig. 2.2 Model schematics. (A) AC with its two arms in a non-equilibrium status. (B) Representation of the whole simplified system proposed. The actin filament is parallel to the ECM. ACs bind the actin monomers of the filament with the ligands that are fixed to the matrix.

shown in Fig. 2.2B. As the actin filament is driven backwards, it starts to bundle with the matrix through the ligands, which are located in the substrate of the ECM. Therefore, the ligands perform a role of anchoring points. ACs oppose to the actin filament movement by transmitting the force to the matrix causing its deformation. ACs are considered as a complex with two diferent arms (see Fig. 2.2A): one of them binds to the actin filament (actin-arm), and the other binds to the ECM (matrix-arm). In this model, as a first approach, the effect of the cellular membrane is not taken into account. Therefore, the actin filament is connected directly with the ligands through the ACs. The model scheme is shown in Fig. 2.2B.

The simulation model can be divided in three different components, where force balance is considered. In the following sections, the mathematical equations that govern the model are described.

2.2.2 Actin-Myosin complex

We assume that the actin filament presents a solid rigid behavior and it only moves in the horizontal direction; therefore, only forces in that direction are considered. In addition, we consider that the myosins can only exert a force to pull from the actin filaments. The magnitude of this force depends on the number of myosin heads attached to the actin filament. The force exerted by the myosin heads is considered constant and equal between them. Thus, the total force is given by:

$$F_m = F_c \cdot n_m, \tag{2.1}$$

where F_c is the force exerted by each myosin head and n_m is the number of myosin heads attached to the filament. The ACs bound to the actin filament oppose to that force and, as a result of the balance of these two forces, the actin filament velocity can be obtained [34]:

$$v_{filament} = v_u(1 + \frac{F_r}{F_m}), \tag{2.2}$$

where F_r is the force applied by the bound ACs and v_u is the actin velocity for the unloaded filament, that is, when $F_r = 0$.

2.2.3 Adhesion Complexes (ACs)

The AC is the clutch of proteins that binds the actin filament with the extracellular matrix through the ligands. It is considered as two different bars (arms) with the same model behavior and linked between each other for one side, leaving the free one to bind with the actin filament and ligands, respectively. One arm is only capable to clutch with the actin and the other only with the ligand.

The behavior of the ACs is expressed in terms of Brownian dynamics. The equations that govern this behavior are now detailed together with the different phenomena that have been proposed for them: binding-unbinding and folding-refolding.

Brownian Dynamics

We assume that the Langevin equation governs the dynamical behavior of the ACs [101]. Therefore, if we consider the i-th AC,

$$m_i \frac{d^2\mathbf{r}_i}{dt^2} = \mathbf{F}_i - \zeta_i \frac{d\mathbf{r}_i}{dt} + \mathbf{F}_i^B, \tag{2.3}$$

where m_i is the mass of the AC, $\mathbf{r}_i$ corresponds to its current position, $\mathbf{F}_i$ are the interaction forces among proteins, ζ_i is the drag coefficient and $\mathbf{F}_i^B$ is a stochastic force. This equation allows the computation of the new position of each particle for each time increment. In addition, considering that the inertial effects of the ACs barely have an influence on the system in the considered time scale, the acceleration term in equation 2.3 can be neglected, and therefore:

$$\frac{d\mathbf{r}_i}{dt} = \frac{1}{\zeta_i}(\mathbf{F}_i^B + \mathbf{F}_i). \tag{2.4}$$

In order to satisfy the fluctuation-dissipation theorem, the stochastic force, $\mathbf{F}_i^B$, is chosen from a random distribution verifying the following expectation values:

$$\left\langle \mathbf{F}_i^B(t) \right\rangle = 0, \qquad \left\langle \mathbf{F}_i^B(t)\mathbf{F}_j^B(t) \right\rangle = \frac{2k_B T \zeta_i \delta_{ij}}{\Delta t}\boldsymbol{\delta}, \tag{2.5}$$

where k_B is the Boltzmann constant, T the absolute temperature, δ_{ij} is the Kronecker delta, $\boldsymbol{\delta}$ the second order unit tensor and Δt the time increment considered in the simulation. As a first approach, it is considered for simplicity that the geometry of the AC corresponds to a sphere, therefore the drag coefficient is:

$$\zeta_i = 3\pi\eta\sigma_i, \tag{2.6}$$

with σ_i being the diameter of the sphere and η the viscosity of the medium.

For the interaction forces, we consider that $F_i = F_s + F_b$, where F_s is the internal force of the AC and F_b is the force induced by the moment created for the orientation of the ACs arms respect to their balance position. Then, $F_s(r_{12})$ is given by [102]:

$$F_s(r_{12}) = \begin{cases} \frac{k_B T}{p}\left[\frac{(2l_{0,i}-r_{12}-r_0)(r_{12}-r_0)}{4l_{0,i}^2(1-r_{12}/l_{0,i})^2(1-r_0/l_{0,i})^2} + \frac{r_{12}-r_0}{l_{0,i}}\right] & \text{if } r_{12} \geq r_0, \\ \\ k_{s,ACP}(r_{12}-r_0) & \text{if } r_{12} \leq r_0, \end{cases} \tag{2.7}$$

where r_{12} is the current length of the AC, r_0 is its length at rest state, p is the persistence length, $l_{0,i} = 40 + 10i$ is the maximum extension for the i^{th} unfolding, phenomenon that will be presented in the next section.

The force induced by the orientation is given by

$$M_b = \frac{1}{2}K_b(\theta - \theta_0), \quad F_b = M_b/l_{AC}, \tag{2.8}$$

where K_b is the bending stiffness, θ_0 is the balance orientation for the AC arms and l_{AC} is the lenght of one arm of the AC. Fig. 2.3 shows the schemes of an AC subjected to the interacion forces F_s and F_b, respectively.

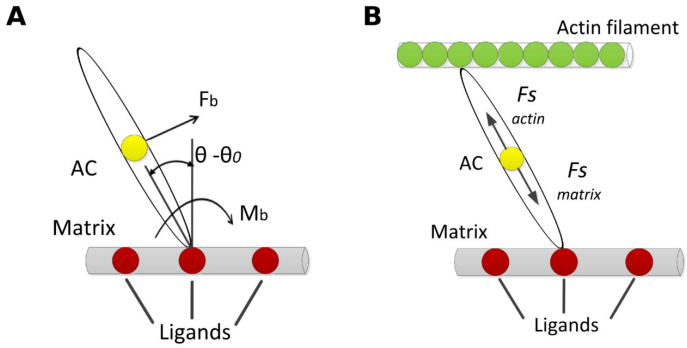

Fig. 2.3 Scheme of ACs subjected to different interaction forces. (A) Internal forces on ACs. Each arm is subjected to a different force depending on their own length. In the central point, the balance between these two forces is carried out and, as a consequence, the central point moves until the forces are in equilibrium. (B) Scheme of an AC subjected to the moment created by the AC orientation respect to the balance position, M_b. This moment is applied on the central point of the AC causing its movement towards the balance position, θ_0. In this figure it is only shown an AC bound to the ligands, but the same methodology is applied when it is bound to the actin filament.

Unfolding/refolding

Experimental tests show that some proteins such as fribonectin or actin crosslinkers can sustain unfolding under determined extensional forces [13, 102]. We assume that the ACs present a similar behavior. Therefore, the internal force-extension curve of the AC exhibits a saw-tooth behavior; this curve presents peak values around 30 pN, at 10nm intervals (see Fig. 2.4). Then, unfolding phenomena is regulated by the unfolding rate, k_{uf} [102]:

$$k_{uf} = \begin{cases} k_{uf}^0 exp(\frac{\lambda_{uf} F_s}{k_B T}) & \text{if } r_{12} \geq r_0, \\ \\ 0 & \text{if } r_{12} \leq r_0, \end{cases} \tag{2.9}$$

where λ_{ub} is the mechanical compliance, k_{ub}^0 is the zero-force unfolding rate coefficient and F_s is the internal force of the AC seen in previous section, equation 2.7.

When unfolding happens, it exists the possibility that the inverse phenomenon occurs, phenomenon known as refolding. This happens when the AC shrinks below the length at which the last unfolding occured, then i^{th} unfolding decreases by 1.

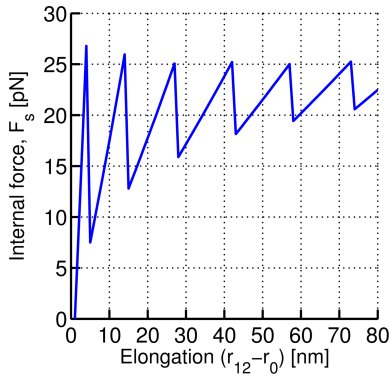

Fig. 2.4 Unfolding curve: Internal force of an AC arm against its elongation. The saw-tooth behavior is clearly observed: when the force reach values around 30 pN, unfolding occurs. This provokes a reduction in the internal force for the same arm elongation.

Finally, k_{uf} corresponds to the rate parameter of an exponential distribution function, therefore the probability of the event is:

$$P = 1 - e^{k_{uf}\Delta t}. \tag{2.10}$$

Binding/Unbinding

ACs present the possibility of separating from the actin filament or the ligands when they are bound to them. This phenomenon is similar to the unfolding one, and it is governed by the unbinding rate, k_{ub} [102]:

$$k_{ub} = \begin{cases} k_{ub}^0 exp(\frac{\lambda_{ub} F_s}{k_B T}) & \text{if } r_{12} \geq r_0, \\ \\ 0 & \text{if } r_{12} \leq r_0, \end{cases} \tag{2.11}$$

where λ_{ub} is the mechanical compliance of the bond in the unbinding case and k_{ub}^0 is the zero-force unbinding coefficient. In this model, when unbinding occurs, both arms of the AC refold completely and return to their rest state ($r_{12} = r_0$). The probability of this event is given by an exponential distribution function, similar to equation 2.10.

Free ACs can also bind to the actin filament or the ligands. This process is determined by the distance between them, occurring when

$$d_{12} \leq 2^{1/6}\sigma_{12}, \tag{2.12}$$

d_{12} being the distance between the two particles and σ_{12} the average diameter of both particles.

2.2.4 The extracelullar matrix (ECM)

The extracellular matrix is considered as a set of truss elements, which only bears axial forces. Therefore, its behavior can be explained in terms of the global stiffness matrix

$$\mathbf{F}_{str} = \mathbf{K}_{str}\mathbf{U}_{str}, \tag{2.13}$$

where $\mathbf{F}_{str}$ is the force vector, $\mathbf{K}_{str}$ is the stiffness matrix of the ECM and $\mathbf{U}_{str}$ is the displacement vector corresponding to all their ligands.

The values of the stiffness matrix depends on the product of the elastic modulus of the ECM, E, and its surface area, A. We consider that A presents a fixed value and we only change the value of E for all the simulations. We also assume that in each node the discretization of the elements is occupied by one ligand. Hence, the force vector is obtained from the forces exerted by the ACs on each ligand, and the displacement vector is applied on them. Initially, as a first approach, we are working under the assumption of small strains and displacements. Therefore, we assume a linear elastic behavior for the ECM and K_{str} remains constant.

2.3 Numerical implementation

In this section, an explicit algorithm is proposed to implement all the equations seen in the previous section, based on the following steps: First, given the initial conditions, an analysis of the current position of the ACs, actin monomers and ligands is performed in order to check the different phenomena considered (binding-unbinding and unfolding-refolding). Next, the actin filament moves, and as a consequence, the force balance in the system breaks the mechanical equilibrium. This provokes ACs and ECM deformation, requiring an iterative process to reach the force balance again. Finally, the new force on the actin filament is calculated and therefore its velocity is obtained.

As a first approach, we consider that the actin filament polymerizes by setting one actin monomer after another creating in that way a straight filament. The ECM is considered parallel to the actin filament with the ligands distributed on it with a random distribution. The ACs are placed randomly in the spatial domain set for the simulation. Both actin and ligands are considered as particles and they are defined only by their central point. Nevertheless, although the ACs are also considered as particles when random movement, they are defined by three points and behave like two attached arms for the rest of scenarios. From now on, these three points are known as: AC-actin point, that binds the AC with the actin monomers in the filament and corresponds to the edge of the actin-arm; AC-matrix point, which corresponds to the edge of the matrix-arm and binds to ligands; and AC-central point that corresponds to the point where both arms intersect.

2.3.1 Development of the algorithm

We present an algorithm for the spatiotemporal resolution of this problem, which is solved in a discrete form, for each time increment, n. The algorithm is schematically shown in Fig. 2.5, and it is mainly based on three balances of forces.

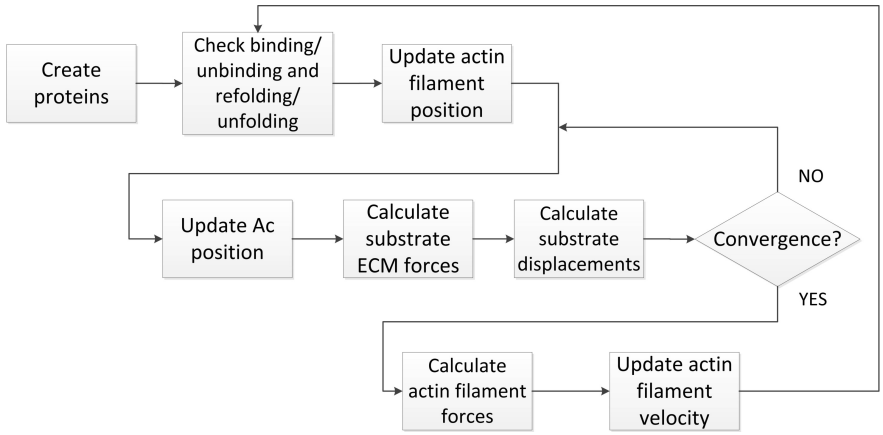

Fig. 2.5 Flow chart of the implemented algorithm.

The whole system mechanism starts by creating the different components involved as it was explained before. Next, the iteration process begins. Firstly, an analysis of the current situation of the different proteins involved in the system is carried out. This let the algorithm know if some protein binding phenomenon is occurring. If an AC-actin point is sufficiently

close to a free actin monomer, they automatically clutch. The same process occurs with the ligands and the AC-matrix points. Then, the algorithm separates the ACs in four different scenarios depending on their linkage:

- Case 0: Fully free. The ACs moves randomly in the medium.
- Case 1: Bound to actin filament. The entire AC moves with the actin filament in its balanced position.
- Case 2: Bound to matrix. The entire AC moves with the matrix in its balanced position.
- Case 3: Fully bound to actin filament and to matrix. The AC is deformed under the effect of the actin movement and the resistance that the matrix exerts to it.

For the ACs in Case 3, the unbinding and unfolding-refolding phenomena are studied. Firstly, refolding is checked, that is, when the AC arm has shrink below the length at which the last unfolding occurs. If there is no refolding, then the unfolding phenomenon is studied as it was explained in the mathematical model. After, the unbinding is checked. All these analysis are carried out in both arms of the AC.

Next, the actin filament is moved, modifying its position. The AC-actin points attached to the filament move with it (Case 1 and Case 2), elongating the ACs actin-arm and breaking the force balance of the system. It is important to remark that the actin filament only moves in horizontal direction.

Due to this, a force balance in the matrix is evaluated. An iterative process starts and it is repeated until the equilibrium is fulfilled. The matrix balance begins by performing a local force balance in each AC of Case 3. This local force balance consists of an internal iterative process. Internal forces (equation 2.7) are calculated for both arms of the ACs and their AC-central point are moved as a result, following equation 2.4. When the difference between the two forces is below a threshold, the AC is in balance again and therefore the internal iterative process ends. After all the ACs are in equilibrium, the forces over the ECM are calculated. These forces correspond to the ones exerted by the AC matrix-arm over the ligands. Once these forces are known, the ECM displacements are calculated by using the stiffness matrix (equation 2.13). When the matrix is deformed, the AC-matrix point moves with it, causing the elongation of the matrix-arm if the AC is in Case 0, or just a displacement, if it is in Case 2. This process breaks again the internal force balance of the AC, so it is necessary to recalculate the AC force balance, the force vector and the new displacements. This process is repeated until the displacements are lower than a threshold. It also exists the

possibility that the increment of the ligand displacements diverges. In that case the loop is restarted recovering the initial values, and the time increment is divided by two.

Once the matrix balance is achieved the forces exerted by the AC over the actin filament are calculated. Finally, the new actin filament velocity is computed through equation 2.2 and a new time iteration starts.

2.4 Numerical simulations: Reference cases

In order to evaluate the potential of the model, several simulations are conducted. The aim of these simulations is to asses the influence of the ECM stiffness on the actin retrograde flow velocity and its effect on the adhesion size on the traction forces. The values of the parameters used in the model are shown in Table 2.1. The exact values of the mechanical properties of the ACs and some parameters related to unbinding and unfolding phenomena are yet unknown, therefore, we have estimated their values in order to simulate this experiment.

As mentioned in previous sections, we have designed a discrete algorithm to model the retrograde flow of the actin filament and to study the effect of the CAs in the process. The results shown in this section corresponds to nine seconds of simulation and the actin velocity is computed as the average value of the 6 last seconds of simulation (for the cases where a velocity analysis is considered), in order to show the velocity when the system is already stabilized and not when the clutches are being created and the randomness of the system is considerable. The results obtained for the initial values of the variables shown in Table 2.2 can be seen in Fig. 2.6. For a soft matrix, the actin speed is almost maximum, but as the stiffness increases, the actin speed starts to decrease. The velocity keeps decreasing until it reaches a point and, after it, the speed abruptly increases again to almost maximum values. A similar tendency has been observed in some experimental results [34].

This kind of behavior can be justified from our simulations. When the matrix is very soft, it can be deformed by minimum forces (considerably lower than the ones exerted by the myosin), so it moves along with the actin. The fully bound ACs move with them, almost without deforming. When the matrix stiffness increases, the matrix deforms slower exerting gradually more force to oppose to the actin filament movement. Due to this, the ACs are subjected to an increasing elongation and, therefore, to an increasing stress to bear. The abrupt increment in the speed occurs when the matrix is not able to deform enough due to its high stiffness and the elongation of the ACs leads to the adhesion failure. As the ACs start to disengage, the force required to remain the others bound increases, accelerating in this way

the unbinding process. Therefore, in a short period of time, all the ACs are found unbound. In order to see clearly these three kind of behaviors, we have reproduced the state of each component at the following time steps: 0s (initial), 3s, 6s and 9s (end). The results are shown in Figs. 2.7, 2.8 and 2.9 for soft, intermediate and stiff matrix, respectively.

Table 2.1 Numerical values for the mechanical data and phenomena parameters.

Parameter	Symbol	Value	Source
Myosin head force	F_c	-2(pN)	[34]
Unloaded actin filament velocity	v_u	$-120(\mu$m/s)	[34]
AC balance length	r_0	30 (nm)	estimated
AC arm length	L_{AC}	30 (nm)	estimated
Boltzman energy	k_BT	$4,142 \cdot 10^{-21}$ (J)	[101]
AC stiffness against compression below the equilibrium length	$k_{s,AC}$	$4,23 \cdot 10^{-5}$(N/m)	estimated
Zero-force unfolding rate coefficient	k^0_{uf}	$3 \cdot 10^{-5}(s^{-1})$	[102]
Mechanical compliance for the actin arm	$\lambda_{uf,actin}$	1,442 (nm)	estimated
Mechanical compliance for the matrix arm	$\lambda_{uf,matrix}$	2,884 (nm)	estimated
Zero-force unbinding rate coefficient	k^0_{ub}	$0,115(s^{-1})$	[102]
Mechanical compliance of the actin bond for unbinding	$\lambda_{ub,actin}$	0,25 (nm)	estimated
Mechanical compliance of the matrix bond for unbinding	$\lambda_{ub,matrix}$	0,5 (nm)	estimated
Persistence length for the actin arm	p_{actin}	0,04 (nm)	estimated
Persistence length for the matrix arm	p_{matrix}	0,04 (nm)	estimated
Maximum number of unfolding for the marix-arm	n_{uf}	2	estimated
Simulation step time	Δt	0,003 (s)	estimated
Total time of the simulation	t	9 (s)	estimated
Actin monomer diameter	σ_A	7 (nm)	[101]
Ligand diameter	σ_L	7 (nm)	estimated
Medium viscosity	η	$8,599 \cdot 10^{-4}$ (kg/m s)	[101]
Bending stiffness	K_b	15,74 (nN nm)	estimated
Balance orientation for the AC arms	θ_0	$\pi/2$(rad)	
Matrix surface	A	$2 \cdot 10^{-4}(nm^2)$	estimated

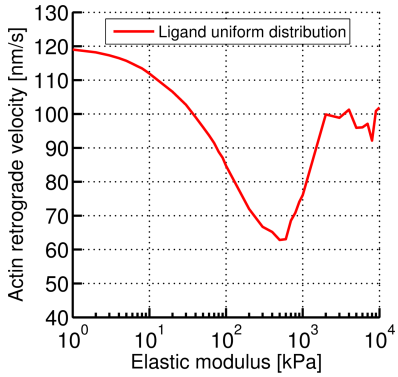

Fig. 2.6 Actin retrograde velocity under different ECM stiffness for a uniform distribution of ligands. For a soft matrix, the ACs deform without almost opposing to the actin filament movement. The matrix moves along with the actin filament. As the matrix stiffness increases, its deformation becomes slower, and the ACs that conform the linkage starts to elongate and to transmit the reaction force from the matrix to the actin filament. Hence, a reduction in the actin retrograde flow speed is produced. This behavior continues until the velocity reaches a minimum, $7 \cdot 10^2$ KPa. After that point, the ACs cannot bear the stress and start to quickly disengage, provoking a considerable increment on the actin speed.

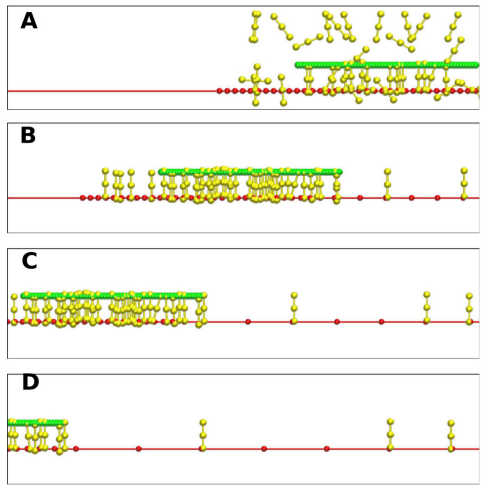

Fig. 2.7 Simulation for soft matrix. (Actin: green; ACs: yellow; Matrix: red; Ligands: red points). The actin filament starts to move as a consequence of the myosin action. The ACs are moving around the medium until they get close to an actin monomer or a ligand and bind to them. When they are bound to both of them they start to transmit forces to the matrix. Since the matrix is very soft it deforms very easily, moving almost at the same velocity that the actin filament and avoiding the ACs to bear big forces.

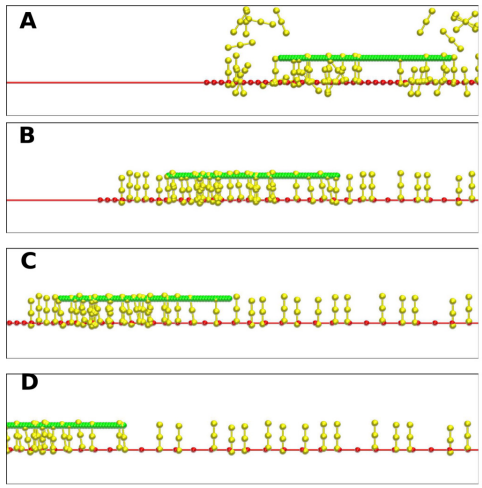

Fig. 2.8 Simulation for intermediate compliance matrix. (Actin: green; ACs: yellow; Matrix: red; Ligands: red points). The matrix deforms as a consequence of the force transmitted from the actin filament through the ACs. Since the stiffness is considerable, the matrix deformation is slower than the actin filament movement causing the ACs deformation. This provokes the unbinding phenomenon on some of the ACs and the reduction on the actin filament velocity.

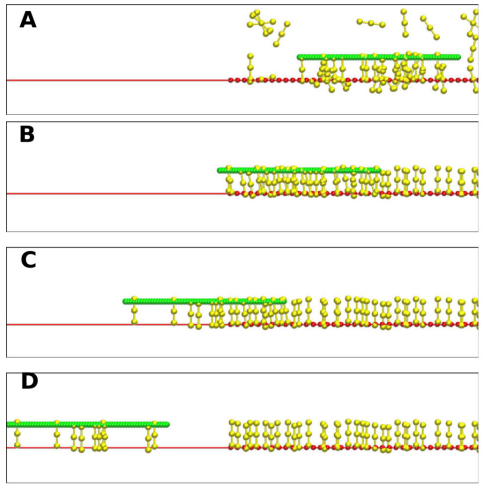

Fig. 2.9 Simulation for stiff matrix. (Actin: green ; ACs: yellow; Matrix: red; Ligands: red points). The matrix stiffness is very high, therefore it barely deforms under the force transmited by the ACs. Hence, the ACs have to bear all that force, deforming at high velocity. This provokes the rupture of the bounds and the dead of the adhesion, causing the free movement of the actin filament.

It has also been experimentally observed that the traction forces that the matrix exerts increase with the size of the adhesion [176]. In Fig. 2.10, this behavior is reproduced for different matrix stiffness. As the adhesion grows, more ACs are conforming the union between actin filament and matrix; therefore, the force on the ECM also increases. In stiffer matrix, the relation is more linear since the ACs quickly disengage as the traction forces increase in the ECM. For intermediate matrix compliance, the clutches starts to build as the traction force increases slowly, but it reaches a point where the adhesion cannot grow more because of the actin filament length and it remains constant as the traction force keeps increasing.

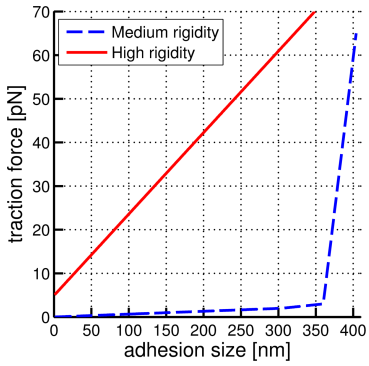

Fig. 2.10 Dependence of the adhesion size respect to actin retrograde speed. The more ACs are conforming the adhesion or the bigger the adhesion is, the bigger the traction force is. In intermediate compliance matrix the clutches starts to grow as the traction force increases slowly, but there is point at which the adhesion cannot grow further. The actin filament, limited by its own length, cannot host more clutches. At this point the size of the adhesion remains constant as the traction force keeps increasing. In stiffer matrix, the relation is almost linear since the ACs quickly disengage when the traction forces grows in the matrix.

2.5 Sensitivity analysis

To a better understanding of the mechanical behavior of our approach, it is important to analyze the influence that some of the components might have on it. For this purpose, a sensitivity analysis has been carried out, varying some parameters that are crucial for understanding the role of cell-matrix adhesions. For this analysis, we consider a random spatial distribution of the ligands. The variables subjected to analysis are shown in Table 2.2.

Table 2.2 Reference value and values for the sensitivity analysis of the initial conditions.

Parameter	Ref. value	Sensitivity analysis
Ligands concentration	40	20-60-80
Number of myosin heads	75	45-60-90
Number of actin monomers	60	20-40-80 (nm)

2.5.1 Effect of the ligand concentration

Initially, we analyze the role of the concentration of ligands. The results for a concentration of 20, 40, 60 and 80 ligands are shown in Fig. 2.11. The ligands have been located randomly in a surface that occupies a 40 percent longer than the actin filament length. Ligands are anchoring points with the matrix, therefore a lack of these elements would drive to a weaker adhesion. When the number of ACs linking actin filament and ECM decreases, the force that holds the actin filament decreases as well. For the same reason, the stiffness at which the ACs start to disengage (provoking the filament speed to rise) decreases with the number of ligands too.

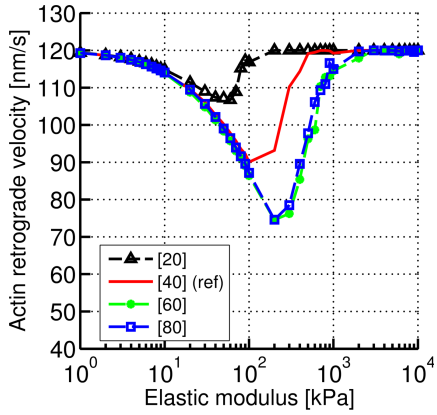

Fig. 2.11 Actin retrograde velocity under different matrix stiffness for different ligands concentration. When the concentration of ligands decreases to 20, the actin retrograde velocity is higher. On the contrary, when it increases to 60, the velocity decrease as a consequence of the formation of more clutches. When the concentration is equal to 80, there is no further decrease of the velocity. This is due to a saturation of ligands on the matrix and therefore, the ACs are not able to clutch with them.

2.5.2 Impact of the actin filament length

The actin filament length is related with polymerization and depolymerization processes, hence it is a variable subjected to considerable changes and it is worth to study. As the filament length increases more ACs are capable of creating bounds, provoking the linkage to grow stronger and increasing its life time. Moreover, not only new ACs have more possibilities to bind, but also the ones that were bound and at some point broke that union have more chances to re-bind. Consequently, this behavior causes a reduction in the actin filament retrograde speed. In Fig. 2.12 the effect on this variable is observed for actin filaments composed of 20, 40, 60 and 80 actin monomers. When more monomers are added to the actin filament, its velocity decreases considerably and a stiffer matrix is required to reach the point of minimum velocity.

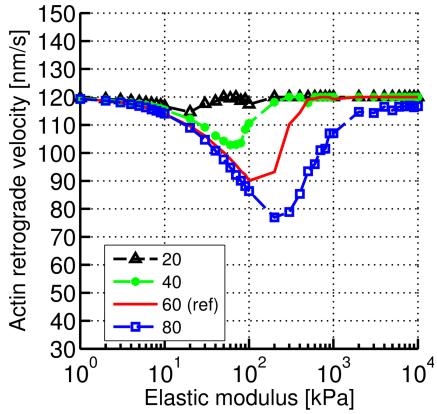

Fig. 2.12 Actin retrograde velocity under different matrix stiffness for different actin filament length. For a short actin filament of 20 actin monomers, few adhesion can grow, and therefore, it barely exists an opposition to the actin filament movement. When the actin filament increases to 40 actin monomers, the adhesion starts to grow stronger, provoking a velocity drop. This phenomenon continues when the actin filament grows to 60 and 80 actin monomers, being its effect clearly noticed on the corresponding curves.

2.5.3 Influence of the myosin traction force

Finally, the influence of the force exerted by the myosins to pull from the actin filament is analyzed. To do this, the number of myosin heads is changed in order to reproduce this effect. Each myosin head exerts a constant force to pull from the actin filament, therefore as the number of myosin heads rises the pulling force increases in a linear relation too. Results are

shown in Fig. 2.13 for 45, 60, 75 and 90 myosin heads. As expected, when the force exerted by the myosins to pull from the actin filament increases, the actin filament velocity increases as well.

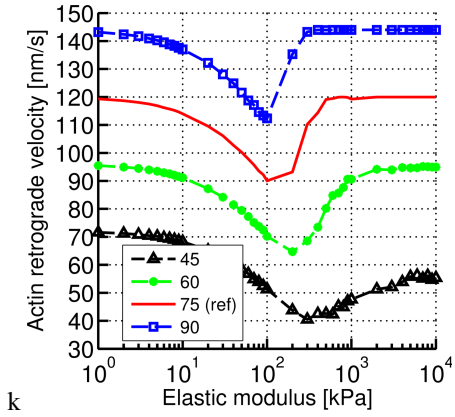

k

Fig. 2.13 Actin retrograde velocity under different matrix stiffness for different myosin traction force values. The myosin heads determines the force exerted to pull from the actin filament. When the number of myosin heads is low, 45, the actin retrograde flow speed decreases. When the number of myosin heads increases, the actin filament is driven backwards with a stronger force. This effect is observed for 60, 75 and 90 mysosin heads. It can also be noticed that, the minimum velocity point for each case occurs at lower stiffness for higher number of myosin heads.

2.6 Conclusions and discussion

A significant amount of conceptual works regarding focal adhesions have been carried out during the last few years. Generally, they can be divided into two different groups: theoretical and numerical studies. The first ones set the basics used in the numerical ones, which, at the same time, provide a deeper insight of the phenomena, allowing to improve theoretical models. Consequently, it emerges an enriching feedback process from which both sides get benefits. In addition, numerical models can be classified in continuous or discrete. In this chapter, we have developed a discrete model, since they offer the possibility of incorporating individual behavior at each complex of proteins involved in the biological phenomenon. We have provided for an insight view of these types of adhesions, that let improve our understanding of how each component individually behaves and how it interacts with the other ones that surrounds them.

Here, we have presented a discrete algorithm to model the cell-matrix adhesions. We have shown that this discrete model is consistent with experimental data from the literature [34, 176], and it presents a new approach to simulate this phenomenon. Hence, we have considered that ACs are flexible elements with a non-linear behavior and with some important properties, such as binding-unbinding or unfolding-refolding. We have also considered the spatial distribution of the ligands on the ECM, that determines the pattern of how the traction forces are transmitted to the matrix. This model offers the possibility of analyzing, individually, the influence of the different proteins involved in the mechano-biological process: myosins in their role of traction motors or the length of the actin filament, which is constantly changing because of the polymerization and depolymerization processes. It also considers the ligand concentration in the ECM, which determines the location of the adhesions and their size.

It is fair to say that, in spite of the considerable quantity of parameters and different phenomena analyzed, there are still a great amount of factors that has not been taken into account in this model. This is due to the implicit need of establishing some simplifications in the quantity of elements considered, or the need of formulating some hypothesis due to the lack of information produced by the deep unawareness that still exists about these biological processes. For example, the ACs are formed by a myriad of different proteins, but for this work, they are simplified to two main protein complexes.

During the last years, it has been shown that at high forces there is a recruitment of adhesion proteins provoking the growth and strengthening of the adhesion. Since the model presented in this chapter does not include this aspect, the predictions made in the stiffer gels are not as accurate as for the softer gels (where these two phenomena have a lower impact). Some recent experimental works have shown that for stiff substrates the adhesion and the forces grow as a consequence of the adhesion reinforcement [62]. This is key aspect to be included in our model and it is further discussed in the SI. Although the present model does not offer accurate results for the stiffer gels, it is a relevant tool to improve the understanding of cell matrix-adhesions and to go deeper into the biological knowledge of these processes. It serves us as a base to build different new models that will be presented in the next chapters. In addition, in the supplementary information of this chapter we show that by including a reinforcement phenomenon we are able to reproduce the experimental results observed for the stiffer gels. This proves that the model is robust and can be used for further extensions.

Supplementary Information: Reinforcement

In this second chapter, we have proposed a model for simulating cell-matrix adhesion during filopodia retraction. This work studies how forces are transmitted from the cell to the ECM through the focal adhesion complexes and how the system responds to different ECM rigidity conditions during filopodia retraction. When the model was designed, we focused on two main purposes: to obtain a better understanding of the phenomenon and to create a computational framework that could be used as a base to build different models from it. After finishing this study we continued by adapting it to different situations shown in the following chapters, however during this time new works were conducted giving new insight into the phenomenon studied. Some of these recent works show that for stiffer gels there is not a general failure in the adhesion as it was believed before. On the contrary, an adhesion protein recruitment occurs that results in the strengthening of the union and in the increment of the force transmission from the cell to the substrate[62, 63, 144]. Although the work shows important results previously observed in experimental works (especially the response of the system for low substrate stiffness), it is true that when analyzing the stiffer gels, predictive results from our model are no longer in line with these recent experimental observations.

It has been reported that adhesions subjected to high level of stress provoke the unfolding of some proteins present in the adhesive clutch such as talin [212]. This unfolding enables more binding sites for different proteins to bind which provokes the strengthening of the union. This event prevents from the total failure of the adhesions, in fact, it is in stiffer substrates where cells develop higher levels of adhesion and stability.

In this section, we expand the model to simulate with more accuracy these recent experimental observations. We add a catch-slip bond law for adhesion unbinding and incorporate reinforcement phenomena, to observe how the system responds to these new adjustments.

Model modifications

We add three important modifications to the previous model:

1) First of all, the actin filament is modeled as continuous bar which polymerizes and depolymerizes in order to maintain always actin monomers on top of the ligands of the substrate. The actin filament moves as a consequence of myosin activity, so if we want to simulate longer time scales we would have to simulate an infinite actin filament in order to

ensure that there is always actin pulling on the substrate domain. In order to ensure this, instead of making an infinite actin filament, polymerization and depolymerization of actin monomers is included in the model. If an actin monomer at the end of the actin filament which previously was on the substrate domain goes beyond this domain as a consequence of the actin movement, it is removed from that end and added to the other end of the actin filament so it could be again available for binding.

2) Second, we substitute the slip bond law for a catch bond law.

$$k_{ub}^{cb} = exp(\Phi_c - \Phi) + exp(\Phi - \Phi_s), \tag{2.14}$$

with $\Phi = F_b/F^*$, where Φ_c, Φ_s are the parameters of the catch and slip bond regimes respectively, F^* is used to normalize the force and F_b is the modulus of the current force for the specific adhesion complex.

3) Finally, we add a reinforcement phenomenon. We simulate the reinforcement by incrementing the probability of ACs to bound to the ECM. If an AC goes beyond a force threshold then this reinforcement is triggered and it affects to the ligands that are within a distance range of this specific AC. For these ligands the binding law is modified: maximum distance for binding (which before was σ_{12}) is incremented up to a maximum (d_{bind}^{max}), which provokes an overall increment of the binding probability on these ligands. If this force goes again below the threshold (due to unbinding) reinforcement is deactivated.

Results

After modifying the numerical model, some simulations for the different substrate stiffness and for different distances between ligands are carried out. Fig. S2.1 shows that in softer gels, actin velocity gradually decreases as a consequence of AC loading; however, as the substrate gets stiffer, the actin velocity keeps decreasing instead of increasing again, as seen in the previous results (Fig. 2.6). This effect is caused by the adhesion reinforcement; for stiffer substrates, ACs start to load and disengage but some of them trespass the force threshold that triggers reinforcement before unbinding. When reinforcement occurs, it provokes an increment of the binding probability in the neighboring regions of the AC that is over the force threshold. This results in the formation of more adhesions around that area, which provokes a higher transmission of force and therefore less actin retrograde velocity. This trend is similar to experimental observations made by Oria *et. al.* [144]. If we change the ligand density, the results present the same trend, however, a smaller distance between

ligands means a higher probability of binding and therefore bigger adhesions and greater force transmission. Note that even with reinforcement, adhesion failure can still occur for extreme rigidity cases, causing a drop in the actin velocity (Fig. S2.1D with 100nm of ligand distance). In our model, we have not tested the response at those extreme levels. However, from a theoretical point of view, it is reasonable to think that if we keep increasing substrate stiffness, we will reach a point whether the system stalls (Fig. S2.1D with 50 nm of ligand distance) or the unbinding occurs faster than binding (Fig. S2.1D with 100 nm of ligand distance).

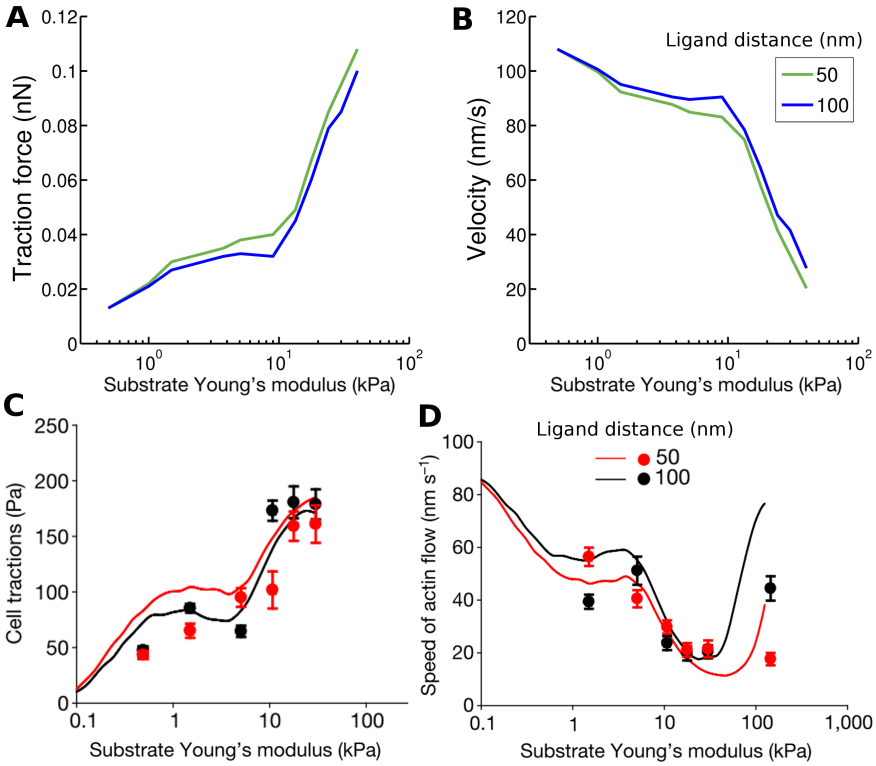

Fig. S2.1: Model vs experimental results for cell-ECM adhesion with reinforcement. A and B show model results for forces transmited to the substrate and actin retrograde velocity respectively when reinforcement is added. C and D results from Oria *et al.* [144] for traction force and actin velocity respectively. Lines represent clutch model results and dots are experimental results.

Discussion

Once reinforcement is included, we have observed how the model is able to simulate with experimental observations more accuracy, and to show sensitivity to different ligand distributions. In addition, previous results without reinforcement, correlate with experimental works where talin unfolding was blocked [63]. Catch bond law is important to stabilize the reinforcement phenomenon since it gives a force range of maximum stability for the bond after which reinforcement is activated.

Nevertheless, we have to keep in mind that the model still has some limitations observing results of recent works. Oria *et al.* [144] showed how reinforcement phenomena could be controlled by the ligands distribution. By changing the distance between the ECM ligands or even setting a non-homogeneous distance distribution between them, it is possible to change the rigidity at which reinforcement is triggered. These different conditions affect how force is distributed between the bounds, which ultimately affects when reinforcement is activated. They also propose a phenomenological model able to simulate all the scenarios by combining springs in parallel and in series to reproduce substrate rigidity and ligand distance distribution (see Fig. 1.9D). The model presented here since it considers ligand spacing, it also offers the possibility of simulating these different conditions. However, results do not show the same sensitivity to those experimental observations. In our model, the substrate is simulated as a bar, and by definition, when an AC exerts a force on it, it deforms the whole area of the bar homogeneously. This critically influences force transmission since some of ACs carry all the load and other are barely stressed. Previous models [34, 62, 63] assumed that force loading process was homogeneously distributed by the bound ACs. From this recent work by Oria *et al.* [144] it seems clear that how load variation is distributed between the ACs is critical in determining how reinforcement is triggered. Due to this, the previous clutch models (including the model proposed here) do not offer a high accuracy in terms of how the load is distributed between the ACs, although these models could reproduce the overall response of the system by including reinforcement phenomenon.

Although the model presents some limitations, it is still a powerful tool that allows us to simulate cell-ECM force transmission and that can be used in many different scenarios where a high level of precision is not needed. During this document, we extend the model and use it in other different scenarios probing to be very useful in giving insight on how different cellular systems work.

Chapter 3

Modeling the formation of cell-matrix adhesions on a single 3D matrix fiber

In this chapter we extend the model from previous chapter to simulate cell-ECM adhesions over a 3D matrix fiber. This chapter is published as [66]:

Escribano J, Sánchez MT, García-Aznar JM (2015) Modeling the formation of cell-matrix adhesions in 3D matrices. J Theor Biol 384:84–94

3.1 Introduction

Cell-matrix adhesions are crucial in a wide range of biological phenomena, playing a key role in tissue formation, immune responses, cell migration or extracellular matrix (ECM) remodeling [32]. These interactions are performed by a large multi-protein assembly that binds both parts forming the adhesion. These adhesions are commonly known as complex adhesions when they have matured, and nascent adhesions when they begin to form, which occurs in the cell edge in like-protrusion structures such as filopodia and lamellipodia [76]. This process of cell adhesion is the mechanism that ensures structural integrity of tissue [178], and it is mainly regulated by mechanical processes [53, 204].

Myosin contractility and actin polymerization produce the forces responsible for the cyclic process of membrane protrusion and retrograde flow of F-actin at the leading edge [156, 154, 168]. These forces are transmitted to the ECM through trans-membrane receptors of the integrin family placed on the cell membrane [167]. These receptors serve as traction points over which the cell moves as well as sources of migration-related regulatory signals [148, 162, 37, 119]. The integrins are bound to the actin filaments in the cytoskeleton through a clutch of proteins that include talin, α-actinin, vinculin and paxilin [216, 178, 1]. On the other hand, integrins bind to protein ligands of the ECM, like fibronectin family [167]. Finally, the formed membrane protusions must adhere to the matrix to define cell locomotion. If they do not attach, protrusions are unproductive and tend to move rearward in waves in response to the tension generated in the cell, in a process known as membrane ruffling [23]. Therefore, actin retrograde flow strongly depends on cell contraction and focal adhesion size, concentration and strength [99].

Numerous studies over the past three decades have revealed a wealth of information detailing cell adhesion in two-dimensional surfaces. However, in *in-vivo* experiments many cells are completely surrounded by ECM, which may have an influence on the size, composition and dynamics of adhesive structures. The study of cell adhesion in three-dimensional environments still remains in its infancy. This lack of knowledge together with the inherent computational cost of the corresponding simulations make these kind of 3D computational models a quite unexplored and challenging field. It is known that the way cells migrate changes between 2D and 3D environment [86]. Furthermore, in a 3D environment, cells of the same type migrate in different ways depending on the physical properties of the extracellular matrix, the degree of extracellular proteolysis and the soluble signaling factors [151, 169, 207]. Since cells use focal adhesions to sense and interact with their surroundings, it seems essential to understand adhesion behavior in order to clarify the mechanism of these migration changes.

Specific experiments in 3D environments were difficult to perform, but in the last two years this kind of studies has increased. Friedl and Wolf [72] analyzed how the ECM architecture along with some cellular determinants (such as concentration of some specific proteins) influence the different modes of cell migration in 3D environments. Haeger *et al.* [83] studied what triggers the change on the invasion mode (single or collective) of mesenchymal tumor cells, observing that the ECM mechanical properties are the determining factor. Alessandri *et al.* [5] studied how mechanical cues from the surrounding microenvironment may trigger cell invasion from a growing tumor. They used a revolutionary microfluidic technique that consists of the encapsulation and growth of cells inside permeable, elastic, hollow micro-spheres.

Another interesting study is the work by Kubow *et al.* [108], where the authors identified the different mechanisms that determine adhesion in 3D matrices, observing cells growing along the ECM fibers.

Computational modeling is a useful tool for integrating the multiple subprocesses that govern cell motility and migration. In this field, Chan and Odde [34] investigated ECM rigidity sensing of filopodia via a stochastic model of the motor-clutch force transmission system in 2D. In their model, integrin molecules work as mechanical clutches linking F-actin to the substrate and mechanically resisting myosin-driven F-actin retrograde flow. More recently, Elosegui-Artola *et al.* [62] have improved this model adjusting it for two different types of integrins and adding a reinforcement mechanosensing event. This phenomenon provokes an increment on the number of adhesions when the traction forces exceed a threshold. Another interesting work is developed by Cirit *et al.* [43], in which they created a model that analyzes the dynamical interplay between cell protrusion and adhesion at the cell's leading edge. Milan *et al.* [129] developed a 3D model able to analyze the signals involved in cell adhesions in stem cells using the Cytoskeleton Divided Medium model (CDM). This model describes the cell like a set of particles interacting with each other, and generating a discrete force network able to mimic the discrete filament network of the cytoskeleton in the cell. The model was also implemented to simulate how a cell adheres on plain substrates by filopodia formation. With this cell model they were able to predict cytoskeleton reorganization and reinforcement during cell spreading.

In vivo, ECM consists of a myriad of fibers that are crosslinked between them, forming a complex network which serves as a scaffold for the cells to migrate. When the cell adheres to the matrix and migrates, it moves over these fibers, deforming and reorienting them. Three aspects of the ECM are crucial for cell adhesion: mechanical properties, density and grade of fiber crosslinking. In this chapter, we assume that the local behavior of the ECM when a filopodium adheres to it does not depend on the global properties of the matrix. We also assume that the fiber is pre-stressed; therefore, we focus our study on the level of fiber crosslinking. The grade and strength of fiber crosslinkings determine the difficulty of the matrix to reorganize under cell forces. Alignment of the filopodia protrusion structures with the matrix fibers is necessary for the migration. If a protrusion adheres to a fiber and they are not aligned, the protrusion tries to reorient it in order to have more surface to adhere; if this is not possible, the protrusion cannot grow further and eventually disappears.

In this chapter, we present a simulation model to reproduce the adhesion degree between a cell filopodium (guided by non-muscle myosins) and a collagen fiber of the ECM, depending

on their relative orientations. Model is similar to the one showed in the previous chapter with changes in the ECM modeling.

3.2 Materials and Methods

Myosin force-generating process in the cytoskeleton provokes actin filaments dynamics. The forces are transmitted through an adhesion complex (AC) to the extracellular matrix. These adhesion complexes consist of a clutch of proteins that include cytoskeleton proteins (paxilin, talin, vinculin and so on) and transmembrane proteins called integrins. Extracellular matrix is deformed under these forces reorienting its fibers.

Due to the high variability of the studied phenomenon, it is indispensable to assume some simplifications and hypotheses for the development of a simulation model. The computational cost and the complexity of a model that will include all the proteins involved in this phenomenon would make the problem inaccessible.

In this model, we have consider the effect of myosin proteins, only an actin filament, extracellular ligands, only a matrix fiber and adhesion complexes. Myosin exerts a force over a single actin filament causing its movement. This actin filament is oversized in order to simulate a pack of filaments of a filopodium and it moves on a plane. Force is transmitted through the ACs to the matrix fiber which posseses a 3D movement and rotation in order to try to align with the actin filopodium. The ACs bind the actin monomers with the extracellular ligands that are distributed on the matrix fiber surface. They can be found in different scenarios: bound to actin and ligands, bound only to one of them and completely free. When they are bound to actin and ligand, the adhesion grows and transmits the force to the ECM and cell. Although the ECM is a complex network of fibers, Kubow *et al.* [108] experimentally quantified that the adhesion size mainly depends on the alignment of one single fiber.

Therefore, the simulation can be divided into three different components: Actin-Myosin contractile complex, Adhesion complexes and ECM.

The present model is a 3D extension of a previous one, developed by the authors in the 2D case [65], with the addition of novel properties. Actin-Myosin complex and ACs approximations are similar to the ones presented in the previous chapter, however simulation of the ECM is completely different in order to reproduce. We detail again the properties of the different parts simulated, although some of the are repeated, to make the chapter self-contained.

3.2.1 Actin-Myosin complex

The actin filament consists of a straight line of actin monomers, that only moves on the direction of its direction vector; therefore, only forces in this direction are considered. It is considered as a rigid solid under the assumption that the crosslinking stiffness of the matrix fibers is much lower than the union between monomers.

Myosins only exert pulling forces over the actin filament. The number of myosin heads bound to the actin filament determines the magnitude of the force. Each head is considered to produce a constant force of a fixed value. Thus, the total force is given by:

$$F_m = F_c \cdot n_m,$$

where F_c is the force exerted by each myosin head and n_m is the number of myosin heads attached to the filament. The ACs bound to the actin filament oppose to that force and, as a result of the balance of these two forces, the actin filament velocity can be obtained [34]:

$$v_{filament} = v_u(1 + \frac{F_r}{F_m}), \tag{3.1}$$

where F_r is the force applied by the bound ACs and v_u is the actin velocity for the unloaded filament, that is, when $F_r = 0$.

3.2.2 Adhesion Complexes (ACs)

The AC consists of a clutch of proteins with the function of binding the actin filament with the extracellular matrix. An AC is considered as two different arms bound together, with the two free sides bound to the actin monomers or the ligands in the ECM. One arm is only able to bind to the actin and the other only with the ligand. Both arms present the same constitutive law but different mechanical properties. This is because one arm simulates the cytoskeleton proteins and the other one simulates the integrin proteins. Brownian dynamics regulate ACs behavior. In the next subsections, the equations that govern their behavior along with the different phenomena proposed for them are detailed: binding-unbinding and folding-refolding.

Brownian Dynamics

We assume that the Langevin equation governs the dynamical behavior of the ACs [101]. Therefore, if we consider the i-th AC,

$$m_i \frac{d^2\mathbf{r}_i}{dt^2} = \mathbf{F}_i - \zeta_i \frac{d\mathbf{r}_i}{dt} + \mathbf{F}_i^B, \tag{3.2}$$

where m_i is the mass of the AC, r_i corresponds to its current position, $\mathbf{F}_i$ are the interaction forces among proteins, ζ_i is the drag coefficient and $\mathbf{F}_i^B$ is a stochastic force. This equation allows the computation of the new position of each particle for each time increment. In addition, considering that the inertial effects of the ACs barely have an influence on the system in the considered time scale, the acceleration term in equation 3.2 can be neglected, and therefore:

$$\frac{d\mathbf{r}_i}{dt} = \frac{1}{\zeta_i}(\mathbf{F}_i^B + \mathbf{F}_i). \tag{3.3}$$

In order to satisfy the fluctuation-dissipation theorem, the stochastic force, $\mathbf{F}_i^B$, is chosen from a random distribution verifying the following expectation values:

$$\left\langle \mathbf{F}_i^B(t) \right\rangle = 0, \qquad \left\langle \mathbf{F}_i^B(t)\mathbf{F}_j^B(t) \right\rangle = \frac{2k_B T \zeta_i \delta_{ij}}{\Delta t}\boldsymbol{\delta}, \tag{3.4}$$

where k_B is the Boltzmann constant, T the absolute temperature, δ_{ij} is the Kronecker delta, $\boldsymbol{\delta}$ the second order unit tensor and Δt the time increment considered in the simulation. As a first approach, it is considered for simplicity that the geometry of the AC corresponds to a sphere, therefore the drag coefficient is:

$$\zeta_i = 3\pi\eta\sigma_i, \tag{3.5}$$

with σ_i being the diameter of the sphere and η the viscosity of the medium.

For the interaction forces, we consider that $F_i = F_s$, where F_s is the internal force of the AC, which is given by [102]:

$$F_s(r_{12}) = \begin{cases} \frac{k_B T}{p}\left[\frac{(2l_{0,i}-r_{12}-r_0)(r_{12}-r_0)}{4l_{0,i}^2(1-r_{12}/l_{0,i})^2(1-r_0/l_{0,i})^2} + \frac{r_{12}-r_0}{l_{0,i}}\right] & \text{if } r_{12} \geq r_0, \\ \\ k_{s,AC}(r_{12}-r_0) & \text{if } r_{12} < r_0, \end{cases} \tag{3.6}$$

where r_{12} is the current length of the AC, r_0 is its length at the rest state, p is the persistence length, $l_{0,i} = 40 + 10i$ is the maximum extension for the i^{th} unfolding, phenomenon that will be presented in the next section. In Fig. 3.1, an AC subjected to internal forces is shown.

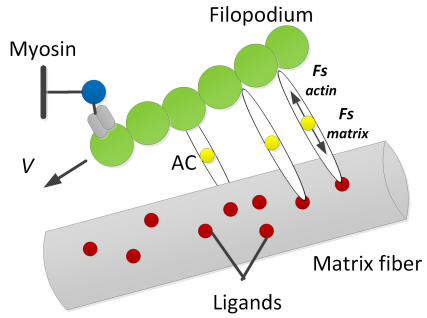

Fig. 3.1 System representation: Internal forces on ACs. Each arm is subjected to a different force depending on their own length. In the central point, the balance between these two forces is carried out and, as a consequence, the central point moves until the forces are in equilibrium.

Unfolding/refolding

Experimental tests show that some proteins such as fibronectin or actin crosslinkers can sustain unfolding under determined extensional forces [13, 102]. We assume that the ACs present a similar behavior. Therefore, the internal force-extension curve of the AC exhibits a saw-tooth behavior; this curve presents peak values around 30 pN, at 10nm intervals. Then, unfolding phenomena is regulated by the unfolding rate, k_{uf} [102]:

$$k_{uf} = \begin{cases} k_{uf}^0 exp(\frac{\lambda_{uf} F_s}{k_B T}) & \text{if } r_{12} \geq r_0, \\ \\ 0 & \text{if } r_{12} < r_0, \end{cases} \tag{3.7}$$

where λ_{uf} is the mechanical compliance, k_{uf}^0 is the zero-force unfolding rate coefficient and F_s is the internal force of the AC seen in previous section, equation 3.6.

When unfolding happens, it exists the possibility that the inverse phenomenon occurs, process known as refolding. This happens when the AC shrinks below the length at which the last unfolding occurred, then i^{th} unfolding decreases by 1.

Finally, k_{uf} corresponds to the rate parameter of an exponential distribution function; therefore, the probability of the event is:

$$P = 1 - e^{k_{uf}\Delta t}. \tag{3.8}$$

Binding/Unbinding

ACs present the possibility of separating from the actin filament or the ligands when they are bound to them. This phenomenon is similar to the unfolding one, and it is governed by the unbinding rate, k_{ub} [102]:

$$k_{ub} = \begin{cases} k_{ub}^0 exp(\frac{\lambda_{ub} F_s}{k_B T}) & \text{if } r_{12} \geq r_0, \\ \\ 0 & \text{if } r_{12} < r_0, \end{cases} \tag{3.9}$$

where λ_{ub} is the mechanical compliance of the bond in the unbinding case and k_{ub}^0 is the zero-force unbinding coefficient. In this model, when unbinding occurs, both arms of the AC refold completely and return to their resting state ($r_{12} = r_0$).

The unbinding phenomenon proposed above follows a slip bond law, that is, the bond lifetime is shortened as the force is increased. However, different authors have shown that some integrin bonds can behave following a catch bond law [171, 106]. In order to assess the impact of this assumption, we also propose a catch bond law to compare it with our first assumption. In general, under a catch bond behavior, there is a force range at which the bond is more stable. When the force value is out of this range the unbinding probability increases (Fig. 3.2). A catch bond law can be modeled as the addition of two exponential curves, one catch curve that is opposed by the applied force, and one slip curve that is promoted by it [141]. The expression for this law is the following:

$$k_{ub}^{cb}(\Phi) = e^{-(\Phi - \Phi_c)} + e^{(\Phi - \Phi_s)}, \tag{3.10}$$

with $\Phi = \frac{|F_s|}{F^*}$, where Φ_c, Φ_s and F^* are parameters of the simulation and $|F_s|$ is the modulus current force for the specific bond.

The probability of this event is given by an exponential distribution function, similar to equation 3.8.

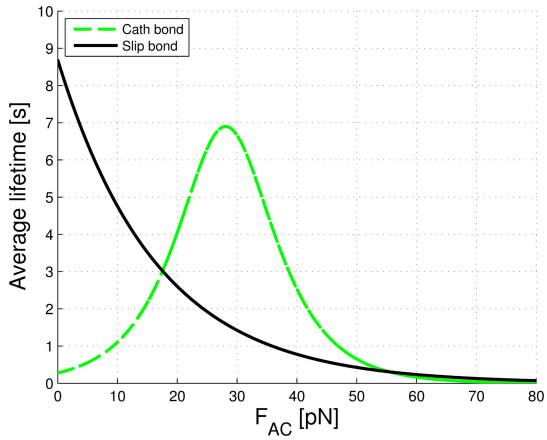

Fig. 3.2 Lifetime average depending on the force for slip and catch bond situation. The parameters values for the slip bond are: $\lambda_{ub} = 0.25\ nm$ and $k^0_{ub} = 0,115(s^{-1})$. For the catch bond, the values are: $f^* = 7,21\ pN$, $\Phi_c = 1,2864$ and $\Phi_s = 6,5352$.

Free ACs can also bind to the actin filament or the ligands. This process is determined by the distance between them, occurring when

$$d_{12} \leq 2^{1/6}\sigma_{12}, \tag{3.11}$$

d_{12} being the distance between the two particles and σ_{12} the average diameter of both particles.

It is important to remark that when an AC is bound only for one side (matrix fiber or actin filament), it is found in its equilibrium position. This equilibrium position corresponds to the radial direction of the matrix fiber or actin filament, respectively.

3.2.3 The Extracelullar Matrix (ECM)

As it was described before, the ECM is a complex network of fibers which are crosslinked. The ECM is deformed and reorganized by cell-generated forces. As a first approach, we only simulate a single matrix fiber. This fiber is considered as a 3D rigid solid element with six degrees of freedom in each extreme. Actually, we assume that there are three longitudinal and rotational springs in each direction to simulate the restriction exerted by the joints at each extreme of the fiber. In particular, these longitudinal and rotational springs model the stiffness associated to the the crosslinkers. This is given by the following expression:

$$\mathbf{F}_{fib,i} = k_{fib,i}\mathbf{U}_{fib,i}, \qquad \mathbf{M}_{fib,i} = \tilde{k}_{fib,i}\boldsymbol{\theta}_{fib,i}, \tag{3.12}$$

where $\mathbf{F}_{fib,i}$ and $\mathbf{M}_{fib,i}$ are the force and torque vectors, respectively; $k_{fib,i}$ and $\tilde{k}_{fib,i}$ are spring constants for displacement and torque, and $U_{fib,i}$ and $\boldsymbol{\theta}_{\mathbf{fib,i}}$ are the displacement and the rotation vectors for the matrix fiber, where the subindex i denotes the corresponding vector component.

We assume that the springs at the ends of the fiber have a similar behavior; so, we consider the same value for the corresponding constants $k_{fib,i}$ and $\tilde{k}_{fib,i}$. The force vector is obtained from the forces exerted by the ACs attached to the ligands, and the torque vector is calculated by multiplying each discrete force by its distance to the fiber gravity center. Initially, as a first approach, we assume a linear elastic behavior for the springs and $k_{fib,i}$ and $\tilde{k}_{fib,i}$ remain constant. This kind of approach allows to model the 3D movement of the fiber due to the deformation that suffer each spring.

3.2.4 Numerical implementation

We have implemented a 3D computational model to reproduce the adhesion building phenomenon between a cell filopodium and an ECM fiber. Firstly, we set the initial conditions: The actin filament is a cilinder-like shape formed by a straight line of actin monomers with a fixed orientation. The matrix fiber is located forming an initial angle θ_0 with the actin filament and the perpendicular plane between both actin filament and ECM fiber. The ligands are placed randomly or with a uniform distribution on the matrix fiber surface. Finally, the ACs are set randomly in the spatial domain of the simulation. Actin monomers and ligands are considered as spheres defined by their central point. ACs are defined by three points corresponding to two arms attached: the AC-actin point, that binds the AC with the actin monomers in the filament and corresponds to the edge of the actin-arm; the AC-matrix point, which corresponds to the edge of the matrix-arm and binds to ligands; and the AC-central point that corresponds to the point where both arms intersect.

The algorithm proposed for the spatio-temporal resolution of this problem is schematically shown in Fig. 3.3. It is solved in a discrete form, for each time increment, n. The algorithm is based on the following steps. First, given the initial conditions, an analysis of the current position of the ACs, actin monomers and ligands is performed and the binding phenomenon is checked. Next, the actin filament moves, and as a consequence, the force balance in the system breaks the mechanical equilibrium. This provokes the deformation of

the ACs bound for their both arms and consequently the increment of their stress. This stress provokes the matrix fiber displacement and rotation, requiring an iterative process to reach the force balance. When the ACs bound for their both arms are in balance, the unbinding and unfolding phenomena are analyzed. Finally, the new force on the actin filament is computed and therefore its velocity is obtained.

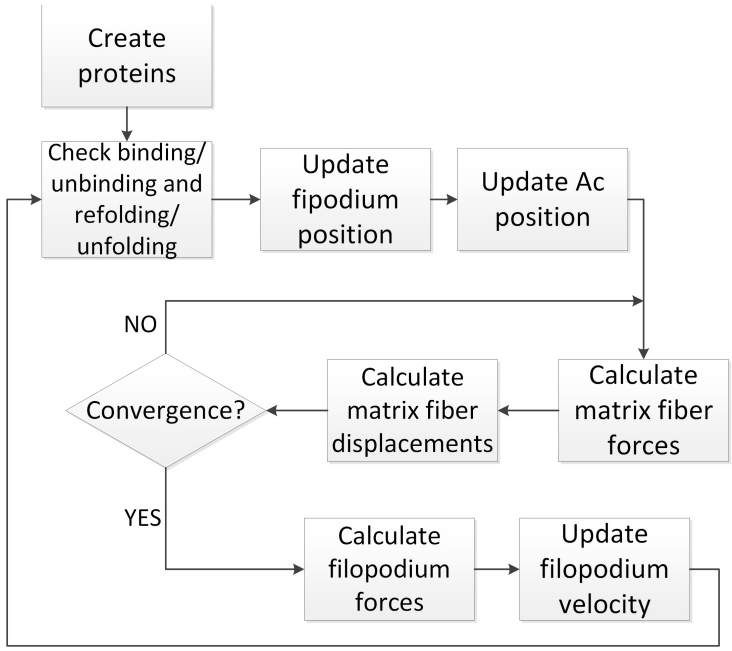

Fig. 3.3 Flow chart of the implemented algorithm.

Fig. 3.4 shows the initial state of the simulation and the position of all the elements after 4 seconds of simulation.

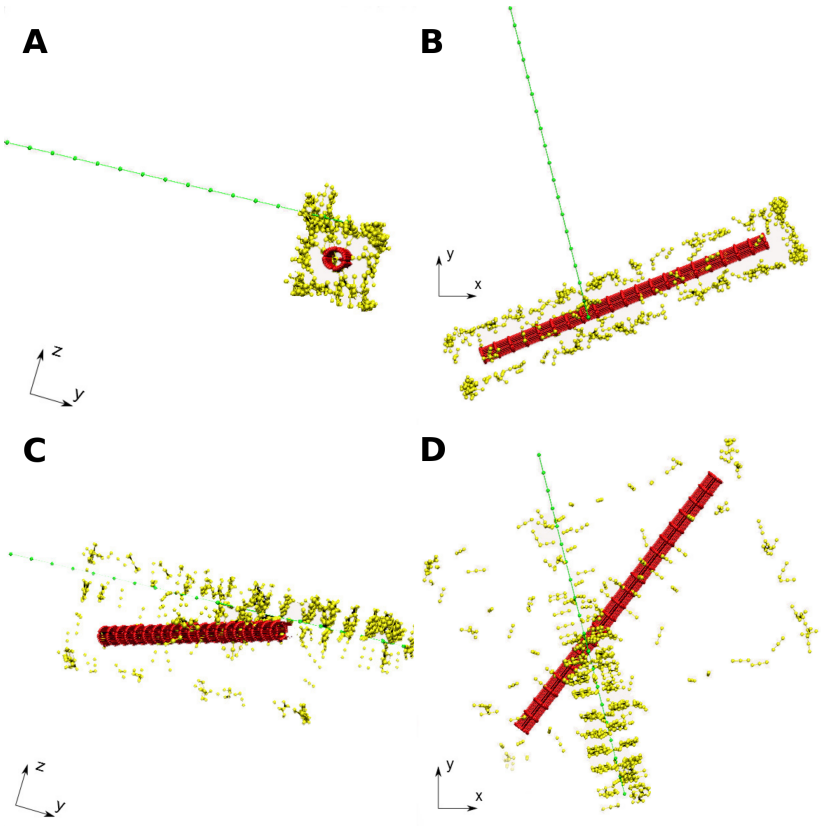

Fig. 3.4 Representation of the different elements of the simulation. (Actin: green ; ACs: yellow; Matrix fiber: red; Ligands: red points) at two different time steps: initial situation (A,B) and after 4 seconds (C,D). At the beginning, there are no interactions and the matrix fiber remains at its resting state. After 4 seconds, the actin filament has moved over the matrix fiber, provoking the focal adhesion building and reorienting the fiber. (A) Initial state, view from plane z. (B) Initial state, view from plane x. (C) After 4 seconds of simulation, view from plane z. (D) After 4 seconds of simulation, view from plane x.

3.3 Results

We perform an analysis of the studied phenomena, observing the influence of the relative orientation between the cell protrusion and the matrix fiber on the size of the adhesion. The local adhesion forming occurs during retrograde flow of actin filaments which is driven by myosin contraction. After that, we study how some matrix and protein properties may also

influence on the size of the adhesion. Since the proposed model present random properties, all the gathered results correspond to the average of 20 simulations. The values of the parameters used in the simulations are shown in Table 3.1. For the reference cases, a slip bond law is applied and two unfolding events are allowed to occur in the AC arms.

Table 3.1 Numerical values for the model parameters.

Parameter	Symbol	Value	Source
Myosin head force	F_c	-2(pN)	[34]
Unloaded actin filament velocity	v_u	$-120(\mu$m/s)	[34]
AC balance length	r_0	30 (nm)	estimated
AC arm length	L_{AC}	30 (nm)	estimated
Boltzman energy	k_BT	$4,142 \cdot 10^{-21}$ (J)	[101]
AC stiffness against compression below the equilibrium length	$k_{s,AC}$	0,004(N/m)	estimated
Zero-force unfolding rate coefficient	k^0_{uf}	$3 \cdot 10^{-5}(s^{-1})$	[102]
Mechanical compliance for the actin arm	$\lambda_{uf,actin}$	2.118 (nm)	estimated
Mechanical compliance for the matrix arm	$\lambda_{uf,matrix}$	2.118 (nm)	estimated
Zero-force unbinding rate coefficient	k^0_{ub}	$0,115(s^{-1})$	[102]
Mechanical compliance of the actin bond for unbinding	$\lambda_{ub,actin}$	0,25 (nm)	estimated
Mechanical compliance of the matrix bond for unbinding	$\lambda_{ub,matrix}$	0,25 (nm)	estimated
Force to normalize parameters in catch bond law	F^*	7,21 (pN)	estimated
Nondimensionalized force of catch curve in catch bond law	Φc	1,2864	estimated
Nondimensionalized force of slip curve in catch bond law	Φs	6,5352	estimated
Persistence length for the actin arm	p_{actin}	0,04 (nm)	estimated
Persistence length for the matrix arm	p_{matrix}	0,04 (nm)	estimated
Maximum number of unfolding for both arms	n_{uf}	2	estimated
Simulation step time	Δt	0,005 (s)	estimated
Simulation total time	t	10 (s)	estimated
Actin monomer diameter	σ_A	70 (nm)	estimated
Ligand diameter	σ_L	7 (nm)	estimated
Medium viscosity for the AC arms	η	$8,599 \cdot 10^{-4}$ (kg/m s)	[101]
Fiber crosslinking stiffness to translation [x,y,z]	$k_{fib,i}$	$[5,5,5]N/m$	estimated
Fiber crosslinking stiffness to rotation [x,y,z]	$\tilde{k}_{fib,i}$	$[5,5,5](nN \cdot nm/rad)$	estimated
Fiber length	L_{fib}	5000 nm	estimated

3.3.1 Local fiber alignment regulates the adhesion size

The results of simulating an initial situation of 80 degrees between the actin filament and the matrix fiber are shown in Fig. 3.5. The adhesion size increases as the matrix fiber and the actin filament are more aligned. Qualitative interpretation of these results from the

perspective of the model is straightforward: as the filament moves over the fiber, it starts to build adhesions; these adhesions begin to exert force on the matrix fiber provoking its movement (matrix reorganization) and a change on their relative position, increasing their alignment. This results in a closest position between the actin filament and the matrix fiber and the consequent increment on the number of adhesions.

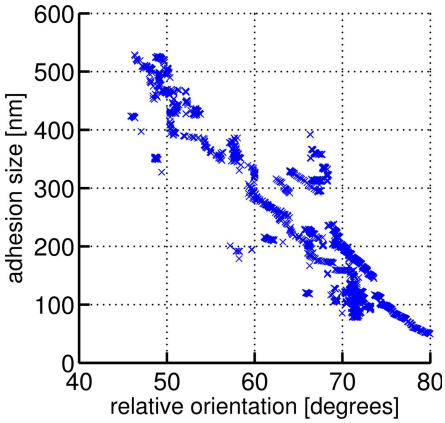

Fig. 3.5 Adhesion size depending on the level of alignment between the actin filament and the matrix fiber. The initial angle between them is 80 degrees. As the actin filament starts to build adhesions, the fiber is reoriented by the cell forces, increasing in this way their alignment (therefore, the relative angle between them decreases), which also increases the size of the adhesion.

3.3.2 Effect of the fiber crosslinking stiffness and the initial orientation

We analyze the effect of four different matrix crosslinking rigidities (1000, 200, 50 and 5 N/m) on the adhesion size, varying the initial orientation between the filopodium and the matrix fiber (80, 45 and 10 degrees). Fig. 3.6A shows the average of the adhesion size during each simulation for the reference values. We observe that, in general, as the initial alignment increases, the size of the adhesion grows bigger. When decreasing the stiffness, the size of the adhesion increases for 80 and 45 degrees of initial relative orientation since the more flexible the crosslinking is, the more fiber reorientation is permitted. However, when the initial relative orientation is 10 degrees, this behavior is not observed. In this case, the fiber and actin filament are almost fully aligned; therefore, the reorganization of the matrix fiber is not needed and the adhesion size mainly depends on the stochastic behavior of binding and unbinding phenomena. This behavior can be seen clearly in Fig. 3.7, in which the relation

between adhesion size and fiber alignment is shown. We can observe that, for this case, proportionality between alignment and adhesion size shown in Fig. 3.5 is lost.

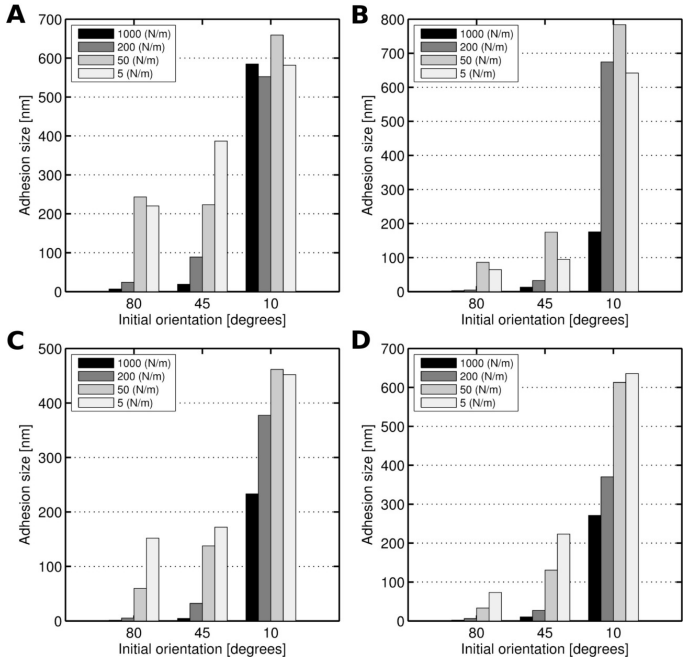

Fig. 3.6 Sensitivity analysis for different simulation conditions. Graphs represent the average of the adhesion size, for 10 seconds of simulation, depending on the initial orientation between actin filament and matrix fiber, considering different fiber crosslinking stiffness. For initial angles of 80 and 45 degrees, increasing the stiffness has a negative impact on the adhesion size. When the initial orientation is 10 degrees, the adhesion size is barely affected by fiber crosslinking stiffness since they are almost fully aligned from the beginning. (A) Reference case. Reference values are used in this case: diameter= 300nm, unfolding allowed and slip-bond law for the ACs unbinding. (B) Sensitivity analysis of the fiber diameter (diameter= 150nm). The adhesion size is influenced by the ECM fiber diameter for different fiber crosslinking stiffness and different grade of initial alignment. In general, as the fiber diameter increases, more surface the cell protrusion has to bind to; therefore, the adhesion size increases. This fact loose importance when the fiber is initially aligned, or when the fiber crosslinkers are very soft, since the cell filopodium quickly alines to the fiber. For these cases, the adhesion occurs along the length of the fiber, resting importance to its diameter size. (C) Sensitivity analysis for the unfolding. In this case the unfolding event has been blocked. As a consequence the ACs charge faster resulting in less stable adhesions provoking a general drop on their size. (D) Simulation using a catch bond law for the ACs. The adhesion size is lower than for a slip bond case. This due to the higher possibility of unbinding for low force cases that does not allow the adhesions to mature.

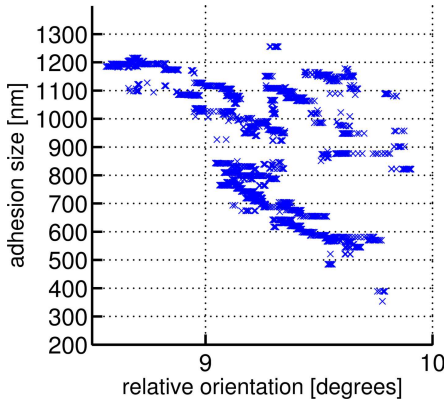

Fig. 3.7 Adhesion size against level of relative orientation between matrix fiber and actin filament. The initial value for the orientation is 10 degrees. Fiber orientation barely changes and it is not determinant on the adhesion size.

Now, we perform a sensitivity analysis varying different conditions in order to observe their effect on the adhesion size. The parameters used in the sensitivity analysis are gathered in Table 3.2.

Table 3.2 Reference values and range of variation for the sensitivity analysis of the initial conditions.

Parameter	**Ref. value**	**Sensitivity analysis**
Matrix fiber diameter (r_{fib})	300nm	150nm
Ligands concentration	$1.5 \cdot 10^{-3} (ligands/nm^2)$	$(1.2-0.9-0.6) \cdot 10^{-3}$ $ligands/(nm^2)$
Initial orientation	$80(degrees)$	$10-45(degrees)$
Fiber crosslinking stiffness, translation and rotation [x,y,z]	$[5,5,5](N/m)-(nN \cdot nm/rad)$	$[5,5,5] \cdot 10-[2,2,2] \cdot 10^2$ $-[1,1,1] \cdot 10^3 (N/m)-(nN \cdot nm/rad)$
Mechanical compliance for actin and matrix arm	$[0.5,0.5](nm)$	[0, 0.5]-[0.5, 0] (nm)

Effect of matrix fiber diameter

The focal adhesion building phenomenon is strongly influenced by the geometrical properties of the ECM. One of the most important factors to consider is the diameter of the matrix fiber since this regulates the geometrical limits for the adhesion. In Fig. 3.6B, we show the same case of section 3.3.2 (Fig. 3.6A), but with a diameter reduced to 150 nm. The results show that when the fiber crosslinkings are stiffer, it gets more difficult to reorient them. The fiber

diameter strongly influences the adhesion size since it regulates the limits for the formation of new adhesions.

Effect of the unfolding

In this case, we aim to observe the influence of the unfolding on the adhesion size. For this purpose the ACs unfolding event is blocked. The results shown in Fig. 3.6C establish a general drop in the size of the adhesion compared to the reference case (Fig. 3.6A). Unfolding allows the ACs to elongate further for the same force values. This gives stability to the bonds allowing them to last longer.

Analysis for catch bond law

In order to assess the different responses of the system for the two unbinding laws, we change the classic slip bond law for a catch bond one (Fig. 3.6D). We see that the size of the adhesion generally drops with the catch bond law. This depletion is provoked by the higher probability of unbinding that this law exhibits for low force cases. At the beginning, the ACs disengage faster than they bind, causing a lower density of unions. When the ACs starts to transmit force, they become more stable, but the load is shared by less ACs than in the slip bond case. Therefore, even though they can bear higher forces, they are not able to compensate this lack of bonds.

Effect of the ligand concentration

The ligand concentration is a determining regulator of cell matrix adhesions. This variable, relatively easy to change experimentally, has a huge impact on this phenomenon. To analyze its effect on the proposed model, we have carried out numerical simulations with four different concentration of ligands: $1.5 \cdot 10^{-3}, 1.2 \cdot 10^{-3}, 0.9 \cdot 10^{-3}$ and $0.6 \cdot 10^{-3} ligand/(nm^2)$. These concentration values correspond to the reference value and to its 80%, 60% and 40% value, respectively. The obtained results are shown in Fig. 3.8. When reducing the ligand concentration, the adhesion size also decreases. Ligands serve as anchoring points for the ACs, therefore a depletion in their number makes the formation of new adhesions more difficult.

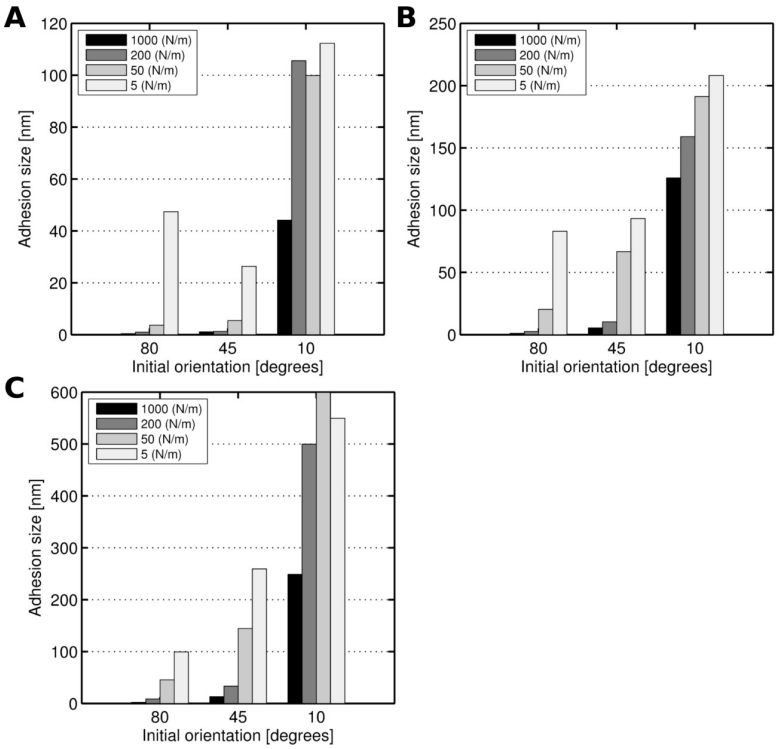

Fig. 3.8 Sensitivity analysis of ligand concentration. In each graph the adhesion size depending on the initial level of alignment for different fiber crosslinking stiffness is shown. By reducing the ligand concentration, smaller adhesions are obtained, since it is more difficult for the ACs to bind. (A) $1.2 \cdot 10^{-3}(ligands/nm^2)$ (B) $0.9 \cdot 10^{-3}(ligands/nm^2)$ (C) $0.6 \cdot 10^{-3} ligands/(nm^2)$.

Effect of the unbinding rate

In the proposed model, ACs bound to both sides can unbind from actin filament or from ligands on the matrix fiber. However, phenomenologically it is not clear whether it unbinds more from one side or another. In order to address this question, we have conducted some tests forbidding the unbinding in one side and maintaining it on the other side. The considered parameters are the given in Section 3.3.2 and the obtained results are shown in Fig. 3.9. We observe that, when the ACs only separate from the actin filament, the adhesion size is larger than when the AC only unbinds from the ligands on the matrix fiber. This results can be explained from a geometric point of view: finding the actin filament is easier than finding a free ligand to bind since the actin filament is considerably bigger; therefore, when an AC

separates from a ligand on the matrix fiber, it is more difficult for the AC to bind again, which ultimately provokes a smaller adhesion. In addition, we can see that in both cases the adhesion size is higher than in the case when unbinding phenomenon is permitted from both sides, since in the latter case, the adhesion has higher possibilities of breaking.

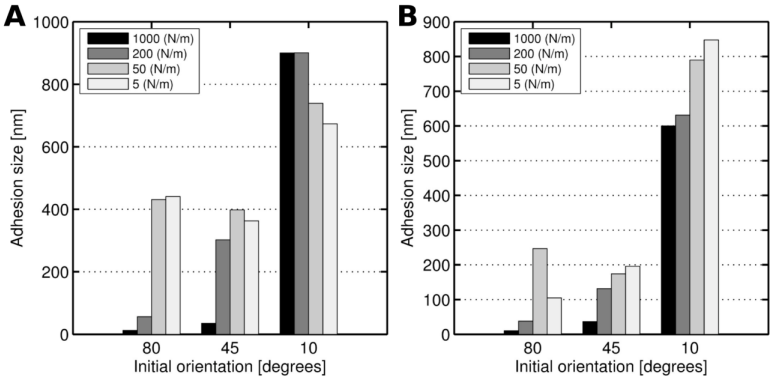

Fig. 3.9 Adhesion size for different unbinding places. In each graph the adhesion size depending on the initial alignment between actin filament and matrix fiber for different fiber crosslinking stiffness is shown. Since the actin filament is bigger and easier to find than a free ligand, when the ACs only separate from the actin filament, the adhesion size is larger. When the ACs only unbind from the ligand on the matrix fiber, the adhesion size is reduced. (A) Only unbinding from actin is permitted. (B) Only unbinding from ligand is permitted.

3.4 Discussion

Computational works in biology help us to unravel fundamental mechanisms that are observed in experiments, but that require further analysis for a better understanding. Here, we have presented some particle-based numerical simulations providing an insight of the role that different components play on the cell-matrix adhesions. In particular, the proposed model reproduces the building of adhesion complexes between a filopodium and a single matrix fiber during actin retrograde flow.

To our knowledge, this model for cell-matrix adhesions in a 3D environment, considering a matrix-fiber approach, is novel and original. We have observed that the alignment between the myosin retraction and the matrix fiber is crucial for the maturation of the focal adhesions and therefore essential for cell migration. Due to this, it is worth to analyze how different conditions or scenarios may regulate this process. In this case, we have considered that ACs

are flexible elements with a non-linear behavior and they present some important properties, such as binding-unbinding or unfolding-refolding. We have also considered the spatial distribution of the ligands on the ECM, that determines the pattern of how the traction forces are transmitted to the matrix fiber. This model offers the possibility of analyzing, individually, the influence of the different proteins involved in the mechano-biological process: the ligand concentration determining the adhesion size or the impact of the initial orientation between the filopodium and the matrix fiber. In addition, we also consider how the matrix fiber crosslinking stiffness influence the capacity of the ECM to reorganize itself under cell-generated forces.

Qualitatively, the tendency obtained between the relative orientation of the filopodia and the matrix fibers was already confirmed experimentally by Kubow *et al.* [108]. Moreover, they showed that the local fiber size also has a significant role in 3D adhesions, in such a way that the adhesive area in the fiber depends not only on the fiber orientation, but also in the fiber size. The model proposed here is also consistent with those experimental observations, as shown in the analysis of the matrix fiber diameter. Furthermore, this model allows us to study a wide range of conditions providing a lot of information of how local properties of both matrix and cell regulate the adhesion process. This could be a powerful tool that provides an interesting insight of how the phenomenon responds under those conditions.

It is true that some of the shown results are strongly influenced by the specific conditions set in this model. For the catch bond analysis, a different parameter adjustment would have cause a different outcome in the results as we show further in this thesis. Parameters are adjusted so numerical results are in a reasonable range according to the experimental data from the literature. However, it has been observed that the variability of the lifetime average depending on the force in catch bonds is very high. It depends on factors like integrin type or different concentrations of elements in the experiments [171, 106]. Also, the difference shown in the case where adhesion complexes are allowed to detach only from the ECM fiber or only from actin are influenced by the geometry of the problem. If the simulations were composed by various ECM fibers, instead of one, surrounding the cell protrusion, the ability of the ACs to bind to actin would have been increased. Therefore, it is expected that the size of the adhesion grows as the number of fibers increases. The effect is similar to increase the ligand density, but taking into consideration that more ECM fibers would probably imply the necessity of applying more force to reorient all of them. This sensitivity in some initial conditions is something inevitable; however, this model currently offers the possibility of adjusting some of them to the specific case of study (catch bond), and the possibility of simulating more ECM fibers as future work.

The formulation of some hypotheses and simplifications is a crucial and indispensable procedure when building a simulation model. It is essential that they are selected accordingly with the biology of the phenomenon. Here, we have assumed that locally, the property of one matrix fiber is more determining than the whole ECM properties. In addition, we have set the hypothesis that the fiber is pre-stressed and that the cell forces are not able to deform it. Due to this, we assume that the fiber deformability is mainly due to the deformation of the crosslinkers that links the different fibers. Moreover, referring to the fiber crosslinkers, we have assumed, as a first approach, that they have a linear behavior and they cannot break.

In vivo, ECM fibers are usually loose and they tighten and deform when cells exert forces over them, in fact, until they are not tight, cells are not able to move over them. For example, collagen type I exhibits a viscoelastic behavior, they store elastic energy and partially relax internal stress through dissipative process [135]. The fiber crosslinkers exhibit a complex behavior and when they are subjected to a high level of force, they can break down. Despite all these differences, the proposed model reproduces reliably the addressed phenomenon. In the same ECM, at a local level, properties can change within a certain range depending on the zone. With the proposed hypotheses, and based on the experimental data found in literature, we have shown that the size of the adhesion (depending on the relative orientation between protrusion and matrix fiber) presents a real behavior pattern that fits in that range.

Crucial phenomena in cell adhesion process are addressed in this chapter. The relevant process of how cells exert forces over the ECM, provoking its reorganization, is studied. The role of matrix fiber stiffness in this process is analyzed through numerical simulations, observing that the stiffer the crosslinkings are, the more difficult to reorganize the ECM by the cell is. A tendency to always try to obtain the largest adhesion size is remarked. This helps the cells to regulate their migration. To conclude, the discrete modeling presented here is a relevant tool to improve the understanding of cell matrix-adhesions and to go deeper on the biological knowledge of these processes.

Chapter 4

A hybrid computational model for collective cell durotaxis

In this chapter, we improve the model from Chapter 2 to simulate single and collective cell durotaxis. This chapter is published as [67]:

Escribano, J., Sunyer, R., Sánchez, M. T., Trepat, X., Roca-Cusachs, P., and García-Aznar, J. M. (2018). A hybrid computational model for collective cell durotaxis. Biomechanics and Modeling in Mechanobiology.

4.1 Introduction

Cell migration is crucial in a great number of biological processes, such as angiogenesis, wound healing, and cancer metastasis [8, 124, 211]. In these processes, cell movement is determined by a complex assessment of environmental cues that include soluble factors, extracellular matrix (ECM) composition, anisotropy, and stiffness. Gradients related with these different cues might result in directional migration [85]. The most studied condition of directional cell migration is chemotaxis, which is the ability of cells to follow a gradient of soluble chemical cues [122, 132, 164, 189]. It is also known that cells are able to sense and respond to the mechanical properties of their surrounding environment. Cell morphology and motility [39, 45, 94] are critically influenced by ECM stiffness. Cells placed in substrates

with a spatial stiffness gradient move towards the stiffer part. This process is known as durotaxis and it is implicated in development, fibrosis and cancer [118, 189, 195].

The mechanisms guiding single cell migration in 2D are well understood, and they could be applied to collective migration. However, collective cell motility is not just the outcome of several cells moving independently. Collective movement also involves integration of guiding signals between cells in order to maintain the migration of cells as a group [84, 166]. Cells move together in a coordinated way with a behavior that cannot be seen in individual cells. Recently, Merkher and Weihs [128] observed how single cells exhibit less invasiveness when they are isolated than when they are surrounded by other cells. To understand how this collective behavior emerges is a current research topic that is been thoughtfully investigated [28, 126, 127].

In order to understand the mechanism guiding both single and collective cell migration, computational modeling has been a powerful tool over these last years. Models can help us to determine whether a mechanism would be feasible and to make predictions that can be tested in experiments. They allow us to have much more control over any proposed mechanism, which we rarely have on experiments. During the last few years there have been many attempts to model cell collective behavior and motility in order to obtain a deeper insight of the mechanisms that regulate this process and to understand how cells interact with each other to produce this collective behavior. Rappel *et al*. [28] have presented an interesting review of different works focusing on collective motility. In their work, they have divided the models in three main groups based on the number of cells that they have simulated: motion in micropatterned substrates, chemotaxis and cell sheets models. Leong [115] studied the dynamics of a pair of cells using a dissipative particle dynamics model that takes into account the acto-myosin forcing, viscous dissipation, and cortical tension. Later, Camley *et al*. [29] simulated the same effect using the phase field model, including cell nucleus and polarity and considering the forces between the substrate and the other cell. Kulawiak [109] also used a computational phase field model of collective cell motility that includes the mechanics of cell shape and a minimal chemical model for CIL (contact inhibition for locomotion). They simulated a large number of cell-cell collisions on narrow micropatterned stripes, with the aim to probe which properties in the cell-cell interactions are responsible for the different outcomes.

There are different numerical approaches to simulate large amounts of cells: Cellular Potts models can simulate cells in large confluent sheets [95] whereas vertex models are often used to simulate collective cell behavior in monolayer sheets. Both models could integrate

feedback mechanisms between cell migration and motile forces. Hybrid models have also been used to predict the morphology of epithelial cells moving collectively [79]. Lin *et al.* [117] have used a vertex model to study the effect on cancer cell invasion on the collective dynamics of a tumor monolayer. Peng *et al.* [150] presented a two scale moving boundary model of cancer invasion. Particle-based methods [180] and continuum approaches [44, 190] have also been used to model monolayer expansion. In chemotaxis different behavior between single and collective migration has also been reported and different models have been used to simulate this phenomenon [123, 192]. Different cell-based models have been used to simulate large cell populations behavior in different scenarios: growing monolayers [60], epithelial monolayers in tumor initiation stages and progression [201], wound contraction where the immune reaction, fibroblasts and myofibroblasts are considered [22]. Vermolen *et al.* [200] used a cell based model for epithelial wound healing that incorporates processes like cell proliferation and death, cell–cell contacts, random walk, chemotaxis, paralysation of constituent cells by pathogen secreted lactates. Chen et al, [36] used this kind of models to describe cell migration in non-isotropic fibrin networks around pancreatic tumor islets.

Models simulating durotaxis are not usual in literature and most of them correspond to single cell motion in 2D surfaces. Different approaches have been used to model single cell durotaxis. Stefanoni *et al.* [185] proposed a 2D approach based on Langevin equation with some modifications to consider mechanical properties of the substrate to simulate single cell paths. Dokukina and Gracheva [55] developed a model of a fibroblast with viscoelastic behavior using a Delaunay triangulation. Allena *et al.* [6] used the previous mentioned Cellular Potts Model to reproduce single cell migration over flat substrates with different rigidity. More recently, Novikova *et al.* [140] used a Random Walk model varying persistence time with substrate rigidity. Kim *et al.* [100] built a force-based computational model in order to predict the cell invasion into a 3D ECM in response to chemotaxis and durotaxis cues. Collective durotaxis was studied previously by [189]. In that work, it was observed how emergent collective behavior is more efficient than single cell behavior. A discrete clutch model which was able to predict experimental results was proposed.

Durotaxis in this model emerges as a consequence of a force balance. The combination of cell-cell interactions with a spatial-temporal analysis of discrete cell-ECM adhesions allows the system to respond to mechanical changes in the substrate. The model contains a monolayer formed by several discrete cells. Cells are bound to each other by cadherin proteins and each cell contracts and polymerizes. They also adhere to the extracellular matrix through adhesion complexes (ACs). These ACs are dynamic structures that are constantly binding and unbinding. The ECM is simulated as a set of truss elements with a variable

stiffness which allows us to reproduce different rigidity gradients. Displacements of the monolayer are considered only in one dimension, along the rigidity gradient direction. The contribution of this model to the literature is considerable since it offers the possibility of simulating both single and collective cell durotaxis. We are able to analyze mechanisms that are crucial to understand how collective behavior emerges and compare it to single cell migration.

That previous work [189] was focused on the experimental findings on how collective behavior emerges from supracellular transmission of contractile physical forces. The model explained the physics behind this phenomenon and was able to reproduce the main experimental results shown there. However, due to the main focus on the experimental findings, the implications and regulation of the proposed model were not explored. Here, we provide an in-depth analysis of the proposed molecular clutch model of collective durotaxis. We incorporate improvements and adjustments to simulate larger time ranges, and we present novel results of the model such as the analysis of the effect of adhesion size or actin velocity. Crucial aspects such as myosin activity, adhesion density and substrate stiffness sensing are analyzed through a sensitivity analysis. We conclude that collective migration is much more efficient than single cell migration. Force transmission, adhesions size as well as the substrate stiffness difference between adhesive areas are crucial to regulate stiffness directed migration, and we show qualitative predictions of the emergent behavior in each case.

4.2 Durotaxis model

We develop a generalized model for simulating single cell or collective cell migration considering the dynamics of cell-matrix adhesions. The model methodology is an expanded version of the one previously presented in [189]. These interactions are modeled using a discrete approach based on a local clutch at the corresponding edges of the cell. Fundamental aspects of the mathematical approach are based on previous chapters. The model consists of three main parts to simulate the dynamics of cell population and to analyze their behavior during migration: the cell monolayer, the ECM and the adhesion complexes, which are a conglomerate of adaptor proteins that connect the other two parts (Fig. 4.1). The entire model is composed by truss elements with different properties in order to simulate the different parts. Cell monolayer contains several cells bound to each other by cadherins, which are simulated as springs.

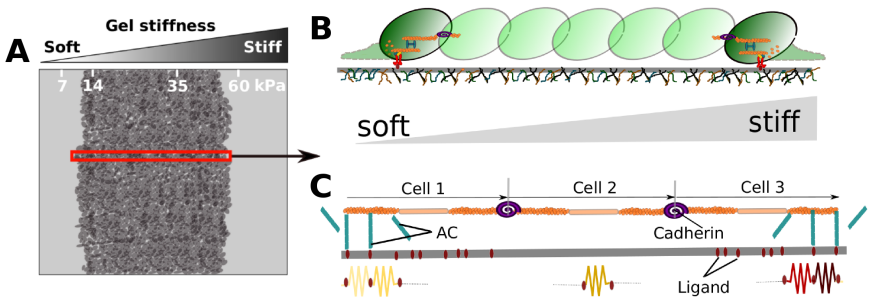

Fig. 4.1 Cell monolayer model. (A) Schematic of the cell monolayer (dark grey) expanding over a gel with stiffness gradient, based on experiments performed in [189]. Model approximation only considers displacements in the direction of the stiffness gradient (red rectangle). (B) The monolayer is composed by several bound cells placed in a substrate with a rigidity gradient. (C) Cells are bound to each other with cadherins. Adhesion complexes (ACs) bind the monolayer with the ligands in the extracellular matrix transmitting the forces and causing the substrate deformation. The ECM, simulated as a set of springs with a variable Young modulus, presents a stiffness gradient, which guides migration direction and speed.

Each individual cell is divided in three different parts (Fig 4.2): The first part is a central contractile rod where myosin molecular motors apply forces to contract the actin filaments. The second part consists of two adhesive zones flanking the contractile part, which binds to the ECM through discrete particles called adhesion complexes (ACs). Those represent the different adapter proteins (such as talin, vinculin, paxillin, and integrins) that bind the actin to the ECM [46, 96]. Finally, there is a protrusive part at each monolayer edge, where the actin monomers polymerize. Due to the high number of elements involved in this kind of process and to the lack of knowledge that there still exists in some of the involved phenomena, some simplifications in the system are necessary when building the model. Thus, this approach simplifies the system by considering only the spatial direction along the stiffness gradient. In the following sections, we describe the mathematical formulation of the model and its corresponding numerical implementation.

The cell monolayer consists of a set of cells, n_{cell}, bound to each other with cadherins. As we have described previously in Fig. 4.2, each cell is composed by three main parts. The central contractile part of the monolayer is modeled as a long truss element with variable length on which myosin exerts a constant contraction, pulling on the adhesive and protrusive parts. This contraction is included by means of a gradient deformation tensor, $\mathbf{F}_c$. This tensor provokes a contraction in the contractile part which generates no residual internal stress. However the presence of other cells or the adhesion complexes binding to the substrate might

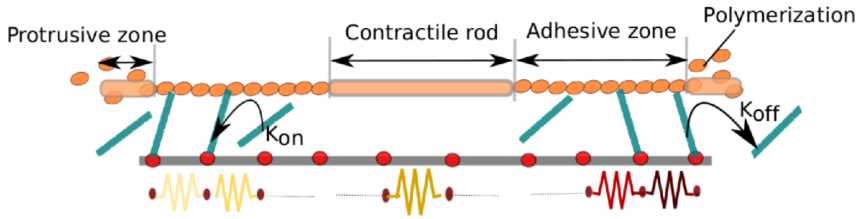

Fig. 4.2 Schematic of a single cell. Cell (upper horizontal bar) is connected to the substrate (lower black bar) by the adhesion complexes (ACs, blue bars). Contractile forces generated in the cell are transmitted through these ACs to the substrate. The cell consists of a contractile part, an adhesive part and a protrusive part. The contractile part contracts and pulls the rest of the monolayer. The adhesive part is formed by actin monomers and allows the cell to adhere to the substrate through the ACs. The protrusive part enables the monolayer to expand, adding new actin monomers to the adhesive part.

generate residual internal stress which makes $\mathbf{F}_c$ incompatible. The total deformation gradient due to contraction $\mathbf{F}^{cont}$ needs to warrant compatibility in the mechanical equilibrium. To make $\mathbf{F}^{cont}$ compatible, an auxiliary tensor $\mathbf{F}_0^{cont}$ is needed. This tensor incorporates the internal residual stress of the system caused by the presence of other cells or adhesions to the substrate. Thus, the total deformation is described by the deformation gradient [158, 165] (see Fig. 4.3):

$$\mathbf{F}^{cont} = \mathbf{F}_0^{cont} \cdot \mathbf{F}_c \tag{4.1}$$

In general, kinematics of the deformation gradient tensor is expressed [20] as:

$$\mathbf{F} = \frac{\partial \Phi}{\partial X}, \tag{4.2}$$

where the motion is described by a mapping Φ between initial and current particle positions as: $\Phi = x(\mathbf{X},t)$. If we consider a small displacement $u(x)$ from the current configuration $\Phi = x(\mathbf{X},t)$, we can express the displacement gradient tensor $\mathbf{L}$ as:

$$\mathbf{L} = \frac{\partial u(\mathbf{x},t)}{\partial X}, \tag{4.3}$$

where the displacement gradient tensor corresponds to the linearized deformation ε and rotation tensors ω:

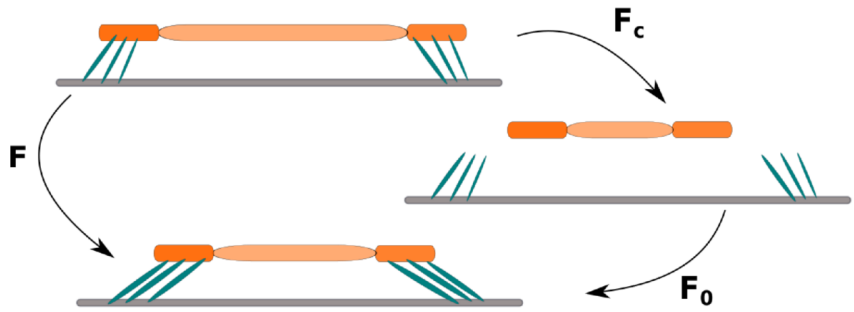

Fig. 4.3 Explanation of the deformation tensor for contraction. Deformation tensor, $\mathbf{F}_c$ is the consequence of myosin activity and it contracts the central part of the cell (orange). If there is no adhesion to the substrate (grey) or the presence of other cells no residual stress is generated and therefore, this deformation is compatible: $\mathbf{F}^{cont} = \mathbf{F}_c$. If there are adhesion complexes binding the cell with the ECM an internal residual stress is generated by these parts and the deformation tensor is not compatible. In this case, an auxiliary compatibility tensor $\mathbf{F}_0$, that englobes this internal residual stress is necessary to reach an equilibrium state: $\mathbf{F}^{cont} = \mathbf{F}_0^{cont}\mathbf{F}_c$.

$$\mathbf{L} = \frac{1}{2}(\mathbf{L}+\mathbf{L}^T) + \frac{1}{2}(\mathbf{L}-\mathbf{L}^T) = \varepsilon + \omega \tag{4.4}$$

Deformation gradient tensor can be written in terms of the displacement gradient tensor $\mathbf{L}$ using the expression $\mathbf{F} = \mathbf{1}+\mathbf{L}$, ($\mathbf{1}$ being the unity second order tensor). Then, if we expand equation 4.1, we obtain:

$$\mathbf{F}^{cont} = (\mathbf{1}+\mathbf{L}_0^{cont})(\mathbf{1}+\mathbf{L}_c) \tag{4.5}$$

If we develop this formulation under the small deformation assumption we have that:

$$\mathbf{F}^{cont} \simeq \mathbf{1}+\mathbf{L}_c+\mathbf{L}_0^{cont} \tag{4.6}$$

Therefore, myosin creates a strain rate on this contractile segment that is regulated by the forces associated to the adhesive complexes, $\mathbf{F}_0^{cont}$. Hence, if there are no ACs connected to the substrate, the contraction from the myosin only occurs in the cell and it is not transmitted to the substrate, then $\mathbf{F}_0^{cont} = \mathbf{1}$, and the total strain rate of the contractile segment $\mathbf{F}^{cont} = \mathbf{1}+\mathbf{L}_c$ is maximum. If there exist ACs connecting the cell to the ECM,

the transmitted force increases and opposes contraction, stalling myosin and cell movement when it reaches $\mathbf{F}_c$, and then $\mathbf{F}^{cont} = -\mathbf{L}_0^{cont}$, obtaining: $\mathbf{F}^{cont} = \mathbf{1}$.

The adhesive part is composed of a set of actin monomers, each of them allowing the dynamic binding and unbinding of adhesion complexes. This part has a length $L_{adhesive}$ that depends on the initial number of actin monomers, n_{am}, which are separated a distance d_{am}. n_{am} is kept constant throughout the simulation by balancing polymerization and depolymerization at both ends of the adhesive part.

In a similar way, the polymerization part is located at the cell edges in order to simulate the protrusion phenomenon due to actin polymerization and depolymerization. This part is also modeled as a long truss element with variable length, with a constant growth $\mathbf{F}_p$, pushing the other cells. Analogously to the contractile part, the total deformation in the polymerization part can be divided in two terms and it is described by:

$$\mathbf{F}^{poli} = \mathbf{F}_0^{poli} \cdot \mathbf{F}_p \tag{4.7}$$

Under the small deformations assumption we obtain:

$$\mathbf{F}^{poli} = \mathbf{1} + \mathbf{L}_0^{poli} + \mathbf{L}_p \tag{4.8}$$

where $\mathbf{F}^{poli}$ is the deformation gradient of the polymerization part, $\mathbf{L}_p$ is the maximal strain rate associated to the cell growth and $\mathbf{L}_0^{poli}$ is the strain rate due to the resistance that adjacent cells exert on the current cell. Hence, if there are no surrounding cells and both cell edges are free, there is no constraint strain due to surrounding cells ($\mathbf{F}_0^{poli} = \mathbf{1}$), and the total strain rate of the polymerization segment is maximum and equal to $\mathbf{F}^{poli} = \mathbf{1} + \mathbf{L}_p$. However, if there are surrounding cells close to the studied cell, these cells can regulate polymerization growth.

4.2.1 Particularization to 1D cell monolayer

Although the model is implemented in 2D, the mechanical resolution of the whole system is one-dimensional (1D), considering all the elements as trusses. Here we present the model described previously in the particular case of the 1D approach. We simulate the myosin retrograde flow applying a constant deformation to the contractile part, $\varepsilon_c(t)$. The displacement gradient tensor is therefore:

$$\mathbf{L}_c(t) = \begin{bmatrix} \varepsilon_c(t) & 0 & 0 \\ 0 & 0 & 0 \\ 0 & 0 & 0 \end{bmatrix}. \tag{4.9}$$

$\varepsilon_c(t)$ is related with the maximum velocity of contraction for the unloaded case (that is, without bound ACs) $v_{c,max}$:

$$\varepsilon_c(t) = \frac{L_{cell,c}(t) - v_{c,max} \cdot \Delta t}{L_{cell,c}(t)}, \tag{4.10}$$

where $L_{cell,c}(t)$ is the length of the contractile part of the monolayer and Δt is the simulation step time. The elastic modulus of the contractile part , $E_{cell,c}(t)$, is updated at each time increment to reproduce the known inverse relationship between actin retrograde speed and maximum force exerted by myosin, f_m [34].

$$v_c(t) = v_{c,max}(1 - \frac{f_{AC}(t)}{f_m}), \tag{4.11}$$

where $f_{AC}(t)$ is the force exerted by the adhesion complexes and $v_c(t)$ is the real contraction velocity for each time step. $f_{AC}(t)$ is determined by the deformation of the compatibility tensor $\mathbf{F}_0^{cont}$, necessary to obtain the actual deformation of the contractile part that corresponds to the total deformation gradient due to contraction, $\mathbf{F}^{cont}$. To this end, $E_{cell,c}(t)$ is updated so that the contraction $\varepsilon_c(t)$ produced by f_m results in the maximum myosin contraction speed $v_{c,max}$ when divided by the duration of each time step of the model, that is:

$$E_{cell,c}(t) = \frac{f_m \cdot L_{cell,c}(t)}{v_{c,max} \cdot A_{cell} \Delta t}, \tag{4.12}$$

where A_{cell} is the cell area.

In a similar way, we propose the following formulation for the polymerization. Polymerization only occurs in the protrusive zones provoking their and, therefore, the growth of the cell. The maximum polymerization elongation is defined as

$$\mathbf{L}_c(t) = \begin{bmatrix} \varepsilon_p(t) & 0 & 0 \\ 0 & 0 & 0 \\ 0 & 0 & 0 \end{bmatrix} \tag{4.13}$$

with $\varepsilon_p(t)$ related with the maximum polymerization velocity $v_{p,max}$ (when there are no surrounding cells):

$$\varepsilon_p(t) = \frac{L_{cell,p}(t) - v_{p,max} \cdot \Delta t}{L_{cell,p}(t)}. \tag{4.14}$$

This elongation produces a maximum polymerization force, f_p exerted over the surrounding cells. In order to conserve a linear relation between f_p and the polymerization velocity, the elastic modulus of this part is also updated at each time step to ensure this relation:

$$E_{cell,p}(t) = \frac{f_p \cdot L_{cell,p}(t)}{v_{p,max} \cdot A_{cell} \Delta t}. \tag{4.15}$$

The surrounding cells provoke a deformation corresponding to the compatibility tensor $\mathbf{F}_0^{poli}$. So, the actual deformation of the polymerization part is given by the total deformation gradient due to polymerization $\mathbf{F}^{poli}$. Therefore, equation 4.14 defines the kinematics associated to the polymerization part of the cell. Hence, after computing $\mathbf{F}^{poli}$ by means of numerical simulations, the length of the contractile part of the cell is updated at each time increment. Depolymerization is also considered by means of updating the length; when the protrusive part length increment is higher than the distance between two actins (d_{am}), a new monomer is added provoking the growth (of d_{am}) of the adhesion zone and the corresponding shrink of the protrusive part. In order to keep the length of the adhesive zone constant at each time that polymerization occurs, depolymerization is forced at the other end of the adhesive zone, which ultimately provokes a growth of d_{am} in the contractile part. In this way, the cell is growing as a consequence of actin polymerization whereas adhesion zone length is kept constant. The elastic moduli of the contractile and protrusive parts are recalculated at each time step in order to ensure the same linear relation between the contraction or protrusion velocity and the force that opposes to it.

It is important to remark that polymerization is what causes the general cell/monolayer growth. There are no other effects included in the model that causes the growth of the monolayer. In fact, the cell growth is determined by a competition between contraction and polymerization. Both phenomena have been considered independent from each other. Contraction total velocity depends not only on the contraction itself but also on the adhesion with the ECM. Polymerization depends on the actual polymerization velocity and the existence of other cells surrounding the part that is polymerizing.

Finally, we note that the elastic moduli of the different parts of the cell $E_{cell,c}$, $E_{cell,p}$ and $E_{cell,a}$ (contractile, polymerization and adhesive) merely serve to reproduce a contractile, stiff actin filament and they are not meant to represent actual values of cell stiffness. In fact, the elastic modulus of the contractile and protrusive part varies throughout the simulation in order to ensure the same linear relation (equations 4.12 and 4.15) between maximum force and maximum contraction independently of the current length of each part.

4.2.2 Substrate

The substrate is simulated as a set of truss elements with total length L_{sub}, and a cross-sectional area A_{sub}. Note that A_{sub} does not coincide with the gel section in experiments since the displacements observed in experiments do not occur through the entire gel substrate depth, but only near the surface. The substrate contains a set of ligand points, which serve as anchoring points for the ACs and are separated a fixed distance, d_{lig}. To model the different stiffness gradient conditions, the stiffness of each truss element E_{sub} (between ligands) is different depending on its spatial location. We assume that the substrate behaves as a linear elastic material where its elastic modulus is defined by E_{sub}.

4.2.3 Adhesion complexes (ACs)

ACs are modeled as a bar in which one end binds to the actin monomers and the other one to the ligands. Thus ACs can be completely free and moving according to Brownian dynamics, bound only at one edge, or bound at both edges. Force transmission between cells and substrate only occurs in the latter case. Brownian dynamics of free ACs are governed by the Langevin equation [101], in which inertial effects are neglected. If we consider the i-th AC,

$$\frac{d\mathbf{r}_i}{dt} = \frac{1}{\zeta_i}\mathbf{F}_i^B. \tag{4.16}$$

where $\mathbf{r}_i$ corresponds to the current position of the AC, ζ_i is the drag coefficient, and $\mathbf{F}_i^B$ is a stochastic force. In order to model the Brownian behavior of the adhesion complexes, we consider that these complexes are subjected to stochastic forces approximated as white-noise processes fulfilling the hypothesis of the fluctuation-dissipation theorem [59], that is, they must satisfy the following relations:

$$\left\langle \mathbf{F}_i^B(t) \right\rangle = 0, \qquad \left\langle \mathbf{F}_i^B(t)\mathbf{F}_j^B(t') \right\rangle = 2k_B T \zeta_i \delta_{ij} \boldsymbol{\delta}(t-t'), \tag{4.17}$$

where k_B is the Boltzmann constant, T the absolute temperature, ζ_i the drag coefficient, δ_{ij} the Kronecker delta, and $\boldsymbol{\delta}$ the Dirac delta function (it means that when $t \simeq t^{'}$ then $\delta \longrightarrow \infty$). In order to simulate these forces numerically, an equivalent discrete form of the previous equations during an individual time step, beginning at time t and ending at time $t + \Delta t$, are considered:

$$\left\langle \mathbf{F}_i^B(t) \right\rangle = 0, \qquad \left\langle \mathbf{F}_i^B(t)\mathbf{F}_j^B(t) \right\rangle = \frac{2k_B T \zeta_i \delta_{ij}}{\Delta t}\boldsymbol{\delta}, \tag{4.18}$$

where Δt the time increment considered in the simulation and $\boldsymbol{\delta}$ the second-order unit tensor. We considered for simplicity that the geometry of the AC corresponds to a sphere with drag coefficient $\zeta_i = 3\pi\eta r_A C$, being r_{AC} the radius of the sphere and η the viscosity of the medium [66].

Binding and unbinding of ACs to the actin filaments and to the substrate are modeled through binding rates k_{bind} and unbinding rates k_{ub}^{cb}. Binding rates are modeled according to the Bell equation as a function of the distance between them:

$$k_{bind} = \begin{cases} k_{bind}^0 exp(-\lambda_{bind} \cdot d_b) & \text{if } d_b \leq d_{bind}^{max}, \\ \\ 0 & \text{if } d_b > d_{bind}^{max}, \end{cases} \tag{4.19}$$

where λ_{bind} is the mechanical compliance for creating the bond, k_{bind}^0 is the zero-distance binding coefficient, d_b is the distance between the adhesion complex and the closest ligand or actin binding site and d_{bind}^{max} is the maximum distance for binding.

Unbinding is modeled as a catch/slip bond law, experimentally proved in different integrins [141]:

$$k_{ub}^{cb} = exp(\Phi_c - \Phi) + exp(\Phi - \Phi_s), \tag{4.20}$$

with $\Phi = F_b/F^*$, where Φ_c, Φ_s are the parameters of the catch and slip bond regimes respectively, F^* is used to normalize the force and F_b is the modulus of the current force for the specific adhesion complex (modulus of the local force transmitted from the cell to the substrate).

4.2.4 Model implementation

Computational simulations are implemented using the Finite Element Method (FEM), under the assumption of small deformations and considering that all the mechanical components present a linear elastic behavior. Nevertheless, a dissipative analysis is required due to the friction between the cell monolayer and the surrounding medium. All equations are implemented in a C++ code. Simulations start with all the ACs unbound and free, and the monolayer expanding symmetrically at both edges in such a way that the speed of actin polymerization dominates over contraction. Fig 4.4 shows the algorithm that is carried out after initialization at each time step increment. The parameters used in the model can be found in Table 4.1.

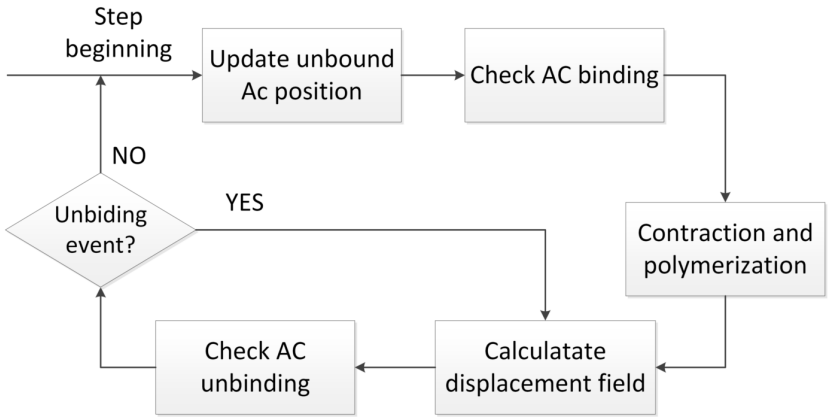

Fig. 4.4 Computational algorithm for each time step. First we calculate unbound AC locations through Langevin equation and then check if a binding event occurs. Binding depends on AC distance to ligand or actin monomer. After we apply cell contraction and actin polymerization and compute the resulting displacement field. Then, from the displacement field we calculate bound AC forces to determine whether they unbind or not. If any unbinding event occurs we recalculate the displacement field and this process is repeated until no unbinding occurs and the system is in equilibrium.

We have made a 1D approximation of a 3D problem where we analyze the system in one direction (the one along the gradient). Since we assume that this direction is much longer than the other two, we can simulate all the elements as a set of rods with a given length, area and Young modulus. The behavior of the system can be expressed in terms of the global stiffness matrix, $\mathbf{K}$ [90]. The displacement field $\mathbf{d}$ at the cell monolayer and the substrate are

Table 4.1 Model parameters. These parameters could be found in the literature and their values are maintained within a range. Myosin force and unloaded contraction velocity have been selected within the ranges observed in previous works [62, 63]. Parameters of the catch bond law are according to average lifetime reported for $FN-\alpha5\beta1$ [106]. Actin polymerization velocities are obtained from values reported for actin flow after myosin inhibition [75]. Binding properties have been selected in order to ensure a strong adhesion which allows a better force transmission, values are within the range used in [62]. Size of the adhesion complexes is within the range of experimental observations of focal adhesion architecture [96]. Polymerization velocity is set so total growth of the monolayer correlates with experimental observation [189]. Polymerization force is set within values reported in [9] .

Parameter	**Symbol**	**Value**
Boltzman energy	k_BT	$4.142\cdot10^{-21}(J)$
Myosin force	f_m	$630(pN)$
Unloaded contraction velocity	$v_{c,max}$	$80(nm/s)$
Polymerization force	f_p	$15(pN)$
Maximum polymerization velocity	$v_{p,max}$	$12(nm/s)$
AC radius	r_{AC}	$40(nm)$
Force to normalize parameters in catch bond law	F^*	$3(pN)$
Nondimensionalized force of catch curve in catch bond law	Φ_c	0.6025
Nondimensionalized force of slip curve in catch bond law	Φ_s	10.2112
Medium viscosity for the AC arm	η	$8.59\cdot10^{-4}(Pa\cdot s)$
Friction between cell and the surrounding medium	ς	$3.5\cdot10^{4}(Pa\cdot s)$
Mechanical compliance of the AC for creating the bond	λ_{bind}	$0.1(nN-1)$
Zero-force binding coefficient	k^0_{bind}	$100(s-1)$
Maximum distance for binding	d^{max}_{bind}	$15(nm)$
Cell adhesive part elastic modulus	$E_{cell,a}$	$5\cdot10^{7}(Pa)$
Monolayer total length	L_{cell}	$5\cdot10^{5}(nm)$
Cell area	A_{cell}	$8\cdot10^{5}(nm^2)$
Cell adhesive part length	$L_{adhesive}$	$6\cdot10^{3}(nm)$
Distance between actin monomers	d_{am}	$25(nm)$
AC spring constant	K_{AC}	$0.1N/m$
Substrate length	L_{ub}	$2.5\cdot10^{6}(nm)$
Substrate area	A_{sub}	$2.2\cdot10^{7}(nm^2)$
Distance between ligands	d_{lig}	$100nm$
Simulation step time	Δt	$0.03s$
Total time of the simulation	T	$360s$

computed through the Finite Element Method, considering both elastic forces and a friction coefficient between the cell monolayer and the surrounding medium, that is:

$$\mathbf{C}\dot{\mathbf{d}} + \mathbf{K}\mathbf{d} = \mathbf{b}, \tag{4.21}$$

where $\mathbf{C}$ is the viscous damping matrix only associated to the cell monolayer (adhesive and protrusive parts) and $\mathbf{b}$ is the external global force vector. For this particular model, external global forces are zero ($\mathbf{b} = 0$) since cell contraction and polymerization are included as a deformation of the bar, and therefore, they are considered as internal forces. The global stiffness matrix $\mathbf{K}$ is built from the assembly of the local stiffness matrix at each element i:

$$\mathbf{K}^i = \begin{bmatrix} \frac{E^i A^i}{L^i} & \frac{-E^i A^i}{L^i} \\ \frac{-E^i A^i}{L^i} & \frac{E^i A^i}{L^i} \end{bmatrix} \tag{4.22}$$

where E_i is the elastic modulus of the element i (belonging either to the cell, the substrate or the adhesion complex), and A^i and L^i are the area of the rod section and length of the rod, respectively [90].

A particular convenient form of the viscous damping matrix associated to the degrees of freedom of the cell monolayer (in the adhesive and protrusive parts) is the Rayleigh damping matrix:

$$\mathbf{C}^i = \frac{\varsigma}{\rho}\mathbf{M}^i = \frac{1}{2}\varsigma L^i \begin{bmatrix} 1 & 0 \\ 0 & 1 \end{bmatrix} \tag{4.23}$$

where ς is the friction coefficient associated to the surrounding medium (this coefficient is fixed to be $Kg/(nm \cdot s)$ to assure adequate units of $\mathbf{C}^i$ as (Kg/s), ρ is the density of the cell monolayer and $\mathbf{M}^i$ is the diagonal mass matrix associated to the cell monolayer. Due to the time dependence of the model, in order to solve the mechanical problem at each time step, we use a backward Euler method, that is:

$$\mathbf{C}\mathbf{v}_{n+1} + \mathbf{K}\mathbf{d}_{n+1} = \mathbf{b}_{n+1} \tag{4.24}$$

$$\mathbf{v}_{n+1} = \frac{\mathbf{d}_{n+1} - \mathbf{d}_n}{\Delta t} \tag{4.25}$$

where $\mathbf{d}_{n+1}$ and $\mathbf{b}_{n+1}$ are the temporal approximations of $\mathbf{d}(t_{n+1})$ and $\mathbf{b}(t_{n+1})$, respectively. In particular, we have implemented the d-form proposed by Hughes [90]:

$$\frac{1}{\Delta t}(\mathbf{C}+\Delta t\mathbf{K})\mathbf{d}_{n+1}=\mathbf{b}_{n+1}+\frac{1}{\Delta t}\mathbf{C}\mathbf{d}_{n} \tag{4.26}$$

4.3 Results

We aim to test the ability of the model to predict the durotaxis event under different conditions according to experimental measurements. We use different types of substrates with different stiffness gradients: steep gel, shallow gel and uniform gel (constant rigidity). Steep gel possesses a higher gradient than the shallow gel (Fig. S4.1). We simulate a cell monolayer for a specific length placed in different initial position on the substrate (different initial stiffness) for each of the gradients. We refer to this initial position as stiffness offset. The only parameter tuned for the different conditions is the elasticity modulus of the substrate, in order to reproduce the corresponding stiffness gradient and the initial monolayer stiffness offset, that have been used in the experiments.

Durotaxis in the model is caused by two different processes. The first one is the mechanical balance between the forces transmitted through the adhesions at both ends of the cells. Force balance causes the deformation of the substrate, which is higher in the softer part than in the stiffer part. This generates a directional movement towards the stiffer part (see Fig. S4.2). The second one is cell growth. Two mechanisms affect cell growth: the actin retrograde flow that is originated by myosin activity and provokes the cell shrinking, and actin polymerization, which causes cell growth. Balance between these two effects results in the effective cell growth velocity.

We test our model under different conditions. First, we establish two behavior hypotheses in order to understand the difference between single and collective cell migration and observe how different stiffness offsets in the gel along the stiffness gradient influence the effectiveness of the directional movement. Moreover, we compare our numerical results with experimental data. Then, we study different aspects on both edges of the monolayer (low and high stiffness) for different offsets and different gels: their movement and the actin retrograde velocity. Finally, we perform a sensitivity analysis identifying different parameters that are relevant to the durotaxis processes.

Results shown in this chapter are based on experimental results obtained by the same authors in [189]. Here, we use the same stiffness gradients and similar stiffness offsets in order to validate the model output with the experiments. The validation of the results is carried out in terms of velocity. In order to compare displacement results with experimental

data, simulations are linearly extrapolated from 6 minutes to 10 hours to accelerate calculation time due to the great number of different offsets. Simulating ten hours is computationally expensive and the results do not change significantly (Fig. S4.3).

4.3.1 Collective cell durotaxis is more efficient than isolated cell durotaxis

First, we compare isolated and collective behavior (Fig. 4.5). In isolated behavior, each individual cell contracts and adheres to the ECM on both sides. Each cell behaves as if it is isolated, without showing any kind of collective behavior. Our simulations show that cells inside the monolayer exert peak forces over the ECM, Fig 4.5C. However, it has been observed experimentally [189, 190] that higher forces are more likely to concentrate in both ends of the monolayer than in the middle of it. This suggests the existence of a mechanism that regulates collective behavior where cells in the middle are driven by the cells on the monolayer border. Based on these observations, we make the assumption that only cells in the monolayer edges adhere to the substrate and that forces inside the monolayer are fully transmitted through cell-cell adhesion from one edge to edge. In order to simulate this collective cell behavior, for simplicity, we assume the monolayer as a long cell that only adheres at its border (Fig 4.5B). We can observe that for this case, forces concentrate on the monolayer borders (Fig 4.5D).

With the aim of testing the efficiency of both mechanisms in exhibiting durotaxis, we run a test where we place different monolayers in different initial stiffness offsets and we track the movement of the monolayer center (Fig 4.6). Simulations for both hypotheses are compared with experimental data [189]. Tests are done for two different rigidity gradients (steep gel and shallow gel) and a case with constant rigidity (uniform gel). Cell monolayers with isolated behavior exhibit considerably lower durotaxis than experimental results and barely show sensitivity to the stiffness offset. These results for isolated behavior also correlate with experimental observations where cell connections were altered by the depletion of $\alpha-$catenin in order to avoid collective behavior [189]. Force transmission between cells and ECM inside the monolayer critically reduces their ability to sense the stiffness gradient and provokes a reduction on the directional movement towards the stiffer part. Results for collective behavior assumption, where force accumulates at the borders of the monolayer, show a considerable higher ability to follow the stiffness gradient and more sensitivity to changes in the stiffness offset. In general, durotaxis is higher when the monolayer is initially placed in the softer substrate position. The ability of cells to migrate with directionality is coupled with the

rigidity gradient that they are able to sense. This is determined by the difference in the substrate stiffness between both sides where the cell monolayer is attached. When the cell monolayer is placed in the softer part of the gradient, the stiffness difference between both sides is higher than when it is placed in the stiffer part due to the exponential nature of the stiffness gradient. For gels without rigidity gradient (Fig 4.6C) directional movement is lost, and the monolayer grows symmetrically towards both sides.

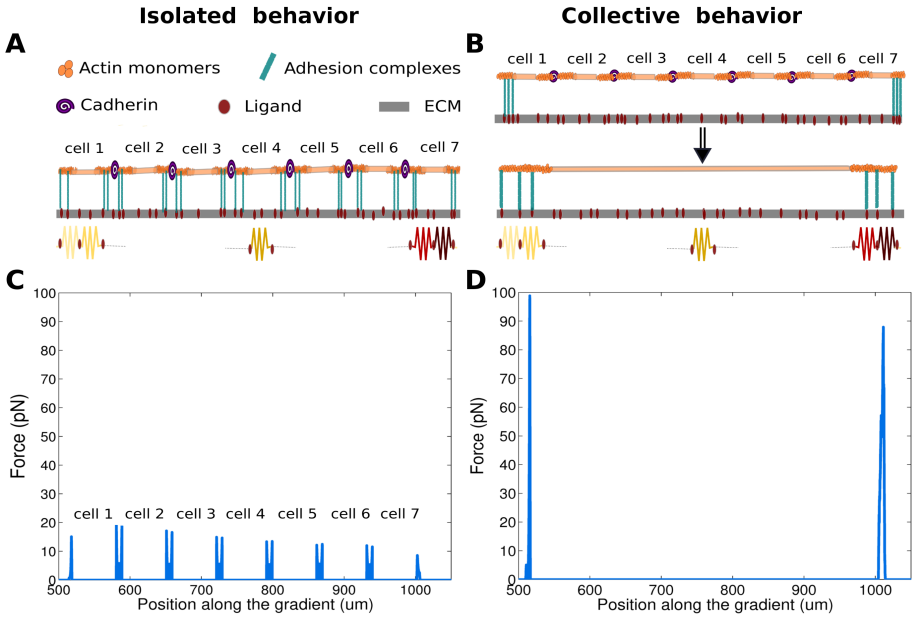

Fig. 4.5 Isolated vs collective cell behavior. Comparison between both hypotheses proposed for cell movement. Cell (orange) contraction forces, originated by myosin activity, are transmitted to the substrate by the adhesion complexes. These adhesion complexes adhere to the actin monomers in the cell and to the ligands in the ECM. The ECM is composed by a set of springs in series. Each spring has different stiffness in order to simulate the rigidity gradient. In isolated behavior each cell behaves in an independent way. Each of them adheres to the substrate transmitting the force. In collective behavior, cells inside the monolayer are driven by the cells in the border. Adhesion and therefore force is concentrated at the monolayer edges. (A) and (B). Schematic for each type of behavior. For collective behavior (B), since adhesion only occurs at both ends, the monolayer is simulated as a long single cell for simplicity. (C) Simulation results of force exerted by the monolayer over the substrate for isolated behavior at the final time step (monolayer composed by 7 cells). (D) Simulation results of force exerted by the monolayer over the substrate for collective behavior at the final time step.

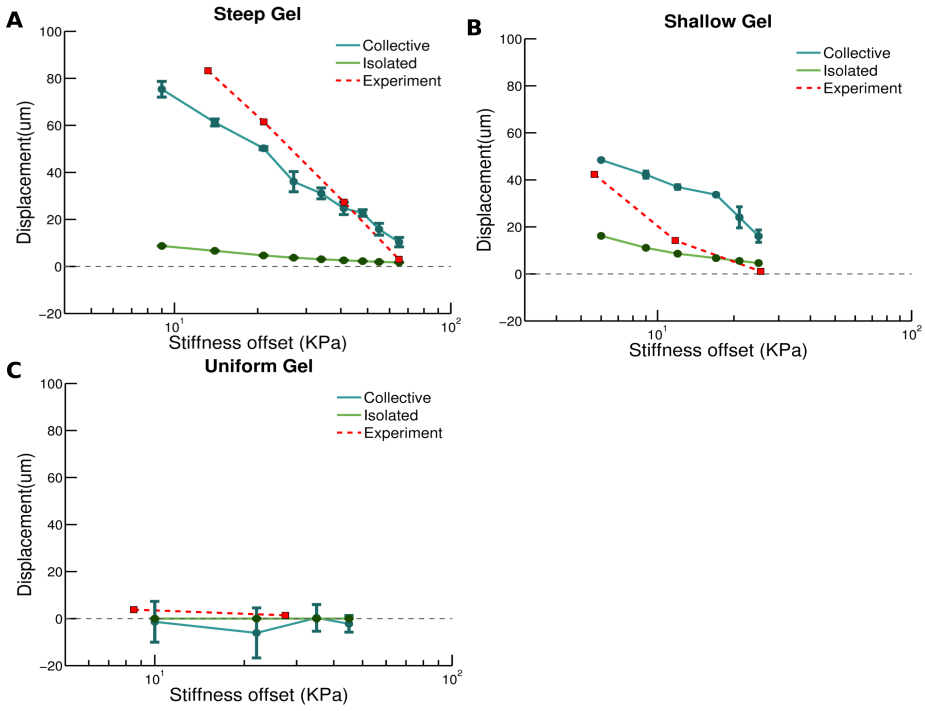

Fig. 4.6 Isolated vs collective durotaxis. Movement of the center of mass of different monolayers after 10 hours. Cell monolayers are placed in different initial positions of the substrate (stiffness offset). The horizontal axis represents the initial rigidity at which the monolayer center is placed in the substrate rigidity gradient. Color represents the two different hypotheses of behavior; isolated behavior (green) and collective behavior (blue). Red color corresponds to experimental measurements from [189]. Numerical results correspond to the mean of a sample with a population n=10. Error bars are the standard deviation. (A) Movement of the center of mass with a steep gel. (B) Movement of the center of mass with a shallow gel. (C) Movement of the center of mass in a uniform gel (without rigidity gradient).

4.3.2 Stiffer edge of the cell monolayer advances faster than the softer one

If we analyze both edges of the monolayer (Fig 4.7) we observe that the edge located in the stiffer part grows faster than the one located in the softer one. The growth of each part depends on the stiffness of the substrate where it is located. If we observe actin retrograde velocity of each side of the monolayer (Fig 4.8) we find that in the stiffer part retraction velocity is lower than in the softer part for both steep and shallow gels. This is consistent with previous experiments, where this same effect was described [189].

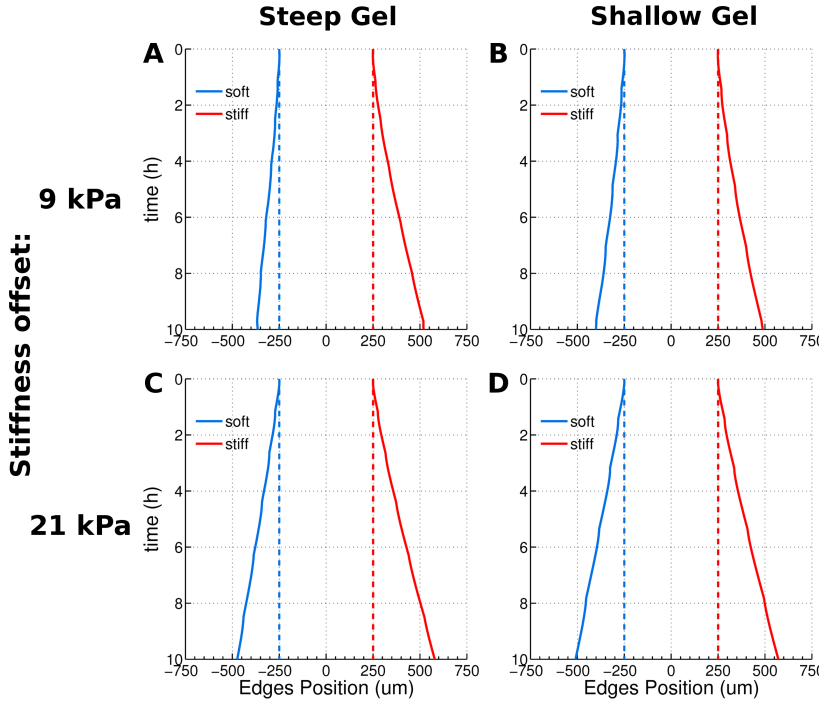

Fig. 4.7 Cell monolayer edges growth. Position of both edges of the cell monolayer (horizontal axes) during the simulation time (vertical axes). Left column corresponds to steep gel and right column to shallow gel. (A, B) Stiffness offset of 9 kPa. (C, D) Stiffness offset of 21 kPa.

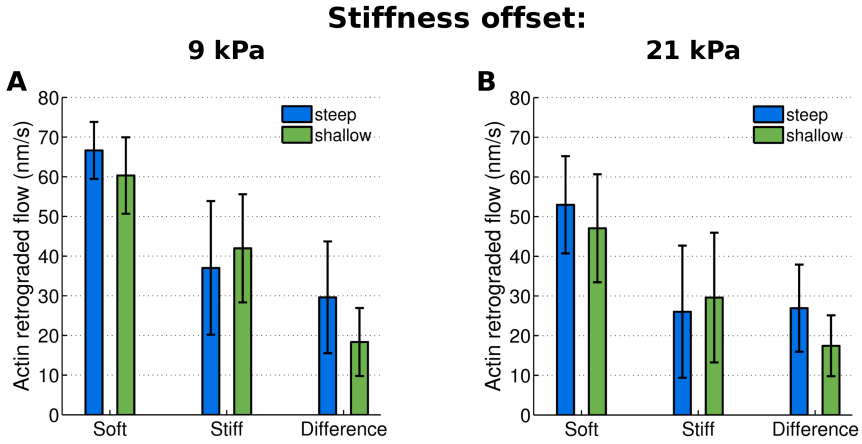

Fig. 4.8 Actin retrograde velocity comparison between both cell monolayer edges. Actin retrograde velocity average of one simulation case for the two different rigidity gradients. Velocity difference between stiff and soft edge is shown. Error bars correspond to the standard deviation. (A) Results for a 21 kPa stiffness offset. (B) Results for a 9 kPa stiffness.

A constant polymerization velocity with a lower retraction velocity means a higher growth. This higher growth of the stiffer part, coupled with the movement towards the stiffer part of the monolayer due to the force balance and the higher deformability of the softer part, provoke the higher growth in the stiffer part of the cell monolayer observed in the simulations.

4.3.3 Larger monolayers are more sensitive to stiffness gradients

In order to test the ability of cells to migrate with stiffness directionality depending on the rigidity gradient that they are able to sense, we change the monolayer length (Figs 4.9A and 4.9B) for steep and shallow gels respectively. We observe that a variation in the length, results in a variation of the rigidity gradient that the cell monolayer is able to sense, and it influences the ability of cells to move towards the stiffer part of the substrate. Increasing the monolayer length, and therefore the rigidity difference between both adhesive parts, increases directional migration.

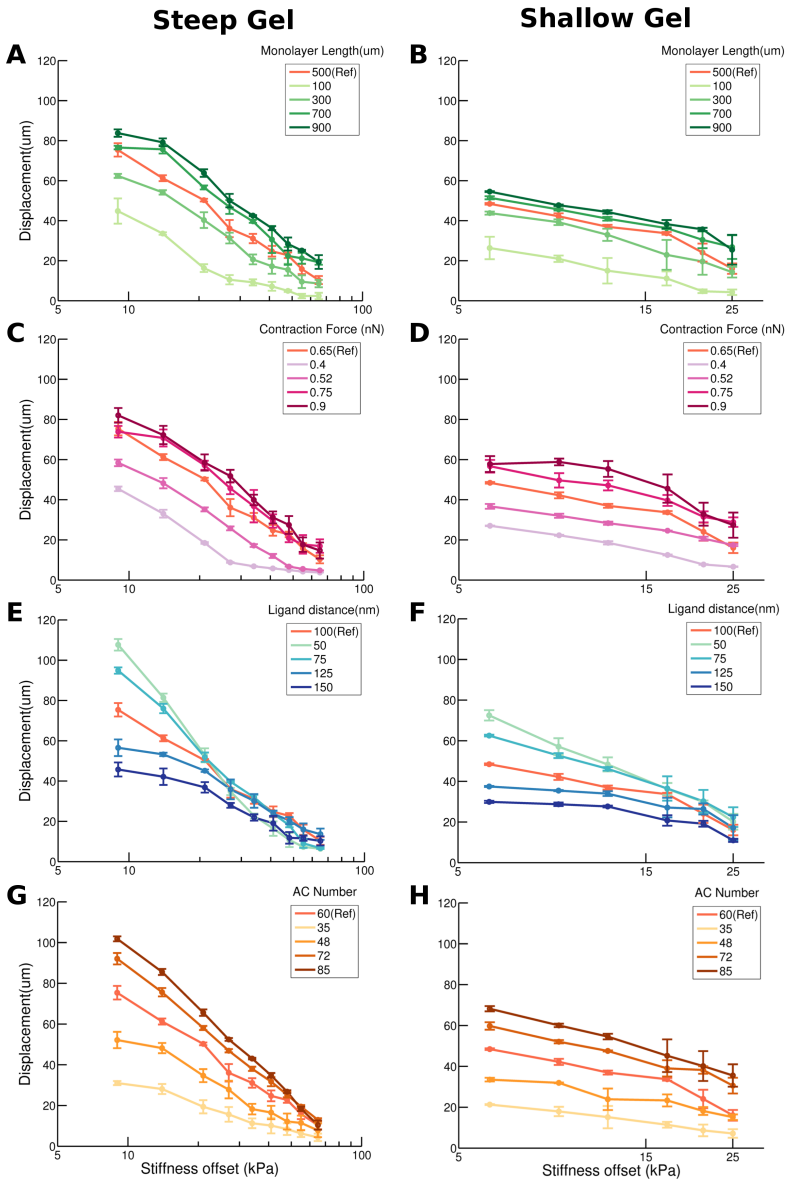

Fig. 4.9 Sensitivity analysis. Displacement of the cell monolayer center for different stiffness offset. Key parameters are changed and results are compared to the reference case. The first column corresponds to a steep gel and second column to a shallow gel. Results are the average of $n = 5$ simulations and error bars correspond to standard deviation. (A, B) Variation in the monolayer length. (C, D) Change in the contraction force of the monolayer. (E, F) Variation in the number of adhesion complexes available in each adhesion zone. (G, H) Ligand density, tuned by modifying the separation between the ligands in the substrate.

This correlates with experimental observations [189], and it also explains the mechanism by which collective migration is more effective than single cell migration. In our simulations, single cell would correspond to a monolayer of the size of a cell, which will show much less sensitivity to the gel gradient.

4.3.4 Myosin contractility promotes durotaxis

Cells are able to sense the rigidity gradient by means of force transmission from the cytoskeleton to the substrate through adhesion proteins. Therefore, we expect to obtain a reduction in the gradient sensitivity by means of decreasing this force transmission. To this end, we study the role of cell contraction on the cell monolayer migration. Figs 4.9C and 4.9D show that a reduction in myosin contractile force also reduces durotaxis. This effect correlates with experimental observations [189], where blebbistatin added to reduce myosin contractility provoked monolayers to grow more uniformly at both edges, therefore exhibiting less durotaxis.

4.3.5 Adhesion is crucial to regulate durotaxis

Cell-matrix adhesion has a relevant impact on force transmission. Therefore, we expect to obtain a significant impact on directional migration when we modify adhesion characteristics. We simulate this effect by changing AC density at each side of the monolayer. In Figs 4.9E and 4.9F we observe that a reduction in adhesion also reduces the ability of the monolayer to sense the stiffness gradient, provoking a more uniform growth at both edges which ultimately results in less durotaxis. A different way of tuning adhesion in the model is to change the ligand density in the substrate. This could be done by reducing or increasing the distance between them. Results are shown in Figs 4.9G and 4.9H where the same effect as the one observed with the change in AC density is obtained. Fig 4.10 shows how the average number of discrete adhesions for different cases, confirming that the number of adhesions is indeed responsible for the observed behavior.

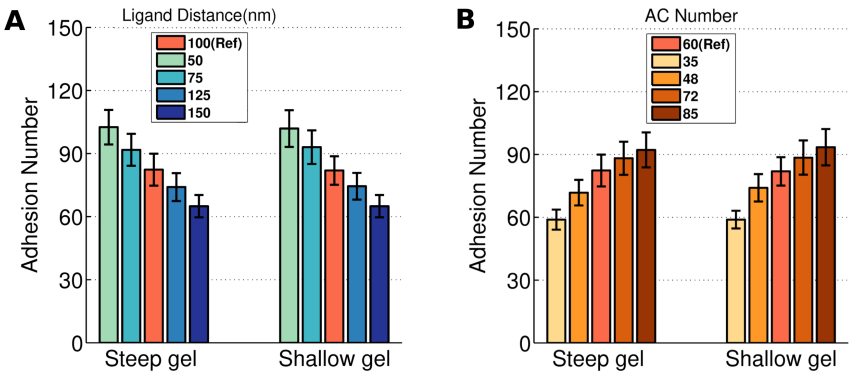

Fig. 4.10 Cell-ECM discrete adhesion number. Average number of adhesions (bound adhesion complexes) during the total simulation time. Simulations correspond to an offset of 9 kPa for both steep and shallow gel. (A) Variation in the number of adhesion complexes available in each adhesion zone. (B) Varying distance between the ligands in the substrate.

4.4 Discussion

We have proposed a computational approach that explains the well-known low to high stiffness motion in substrates with rigidity gradients as an emergent phenomenon caused by the force balance between cell-ECM adhesions. In our model, durotaxis occurs due to the ability of cells to deform the substrate more in the part of lower stiffness than in the stiffer part. Then, force balance results in preferential directional movement towards the stiffer part. Previous interesting approaches for modeling durotaxis [140] explained this phenomenon for single cells as a persistence driven process. The persistence time of cell motion was dependent on substrate rigidity, and based on experimental observations it was set higher for stiffer substrates. Our physical approach offers a different way of explaining durotaxis, although it is complementary to this previous explanation. In fact, we could observe how higher persistence movement for stiffer substrates emerges from our simulations (Fig S4.4). It is also worth to mention some other works where negative durotaxis was reported [21, 85, 182]. The fundamental physics of the durotaxis phenomenon presented in this work is not contrary to what it was observed in these other previous works. In fact, migration is the result of the competition between different mechanisms, not only durotaxis as we have considered in this chapter. If durotactant cues are not as strong as others, like chemotaxis, durotaxis is not going to be the main mechanism that regulates migration. This might result in migration towards softer parts of the matrix depending on these other potential

mechanisms activated by other stimuli [51]. Actually, even in the absence of other different factors regulating migration, in single cells or very shallow stiffness gradients cases, the mechanotransduction mechanism proposed here might not be strong enough to regulate migration. In such cases migration could be regulated by other force-sensing mechanism like sub-micrometre contractions that occur in a few seconds at the cell borders during the formation of nascent integrin adhesions [208].

Model is designed to reproduce experiments of 2D migration and it could also be valid for 3D migration. However, we have to keep in mind that although the physics that regulate our model are still valid in 3D migration, their contribution to the overall competition between the different mechanisms that regulates migration is going to be much less effective than in 2D migration. In 3D migration there are additional effects regulating migration that are not present or have less impact in 2D migration, such as pore size, porosity, permeability and matrix degradation. In fact, 3D migration is impaired by steric hindrance [51, 111, 133]. The model presented here allows us to compare single motility with collective cell migration and to understand the underlying mechanisms that make collective migration much more efficient than single cell migration. For this matter, we consider two main types of behavior for cell monolayers: collective or isolated. In isolated behavior all cells contract and adhere to the substrate as individual entities. As a consequence of this individual connection to the substrate, transmission of forces between cell-cell connections is not effective, impeding cell monolayer from sensing the gradient. All of this results in much less efficiency in durotaxis. This is in line with previous experimental results where cell-cell junctions were inhibited [189] and directional movement towards the stiffer part was critically reduced. For collective behavior, based on experimental observations [189, 190], we assume that forces exerted over the substrate accumulate at both edges of the monolayer. Cells inside the monolayer do not adhere to the substrate and are driven by the cells in the border. This provokes a more efficient transmission of forces through the monolayer, enabling a better stiffness gradient sensing which ultimately results in higher durotaxis. In order to simulate this behavior, for simplicity, we simulate all the monolayer as a long single cell that only adheres to the monolayer at their edges. The reason for this is that if passive cells inside the monolayer do not adhere to the substrate, then their contraction and polymerization in the model are formally equivalent to simply considering one big cell. For this case durotaxis is clearly observed.

Results are also in concordance with other previous works that showed that collective movement is more efficient than isolated cell movement [128]. Moreover results in both behavior hypotheses (isolated and collective) correlate with experimental data of [189], showing the same trend and adjusting with relative accuracy. We do not only validate results

in terms of final displacement of the monolayer, but we also observe how actin velocities and monolayer growth emergent behavior correlate with experimental measurements.

A sensitivity analysis shows interesting evidence on how durotaxis can be regulated by different mechanisms. Cell monolayer size regulates gradient sensing. Single cells sense a smaller range of the stiffness gradient than a cell monolayer. This difference increase as the monolayer becomes bigger. Force transmission from the cell to the substrate is also observed to play a major role in gradient sensing. By reducing myosin contractility, we also obtain a decrement in durotaxis. The same effect is reported when reducing the overall localized number of cell-substrate adhesions. In fact, substrate adhesions have been reported as a crucial factor in other works on durotaxis [153, 214]. Adhesion is known to be higher in the stiffer part than in the softer part. Here, adhesion properties are only modelled in terms of a catch-slip bond law, with no specific relation to stiffness. If we compare adhesion in different rigidities (Fig. S4.5), we observe that in the stiffer parts adhesion is slightly higher, although difference is not significant. Promoting this adhesion difference in terms of rigidity seems a complementary way of promoting durotaxis.

There are some aspects that have not been considered here and could also play an important role in durotaxis. For example, cell proliferation in the monolayer, adhesion spatial distribution on a 2D plane, or the previously mentioned more significant difference between overall adhesion number in softer parts of the gel than in stiffer parts of the gel (which could be modeled as the well-known adhesion reinforcement that occurs under higher force rates [62]. However, in summary, our model presents an intuitive approach to simulate durotaxis as the consequence of the cell's ability to deform the substrate more in its softer part than in the stiffer one. This explanation is compatible and consistent with other models proposed in the literature [140]. The possibility of simulating not only single cells but also collective migration under stiffness gradients adds a significant advance to the existing literature.

Suplementary Information

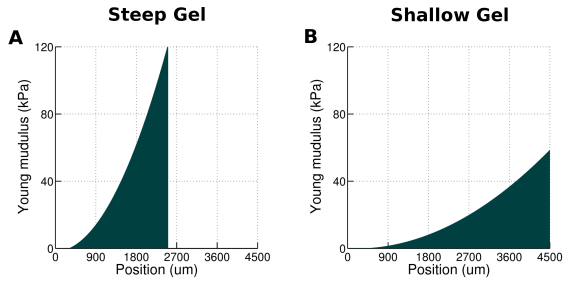

Fig. S4.1:Cell-Extracellular matrix adhesion schematic. Representation of the main components that define the cell-matrix attachment through actin cytoskeleton.

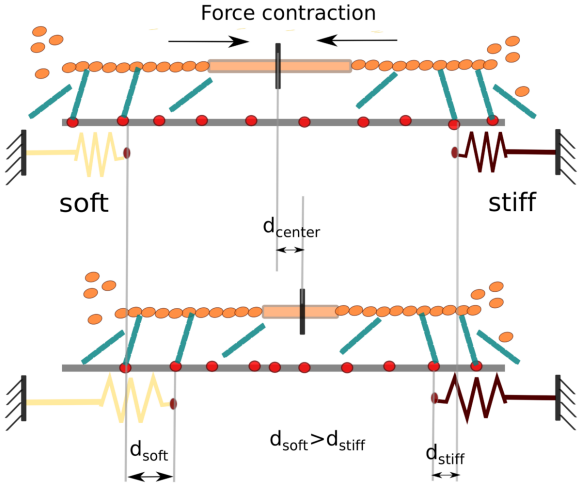

Fig. S4.2:Physical explanation behind durotaxis. Actomyosin-driven contraction of the monolayer causes substrate deformation. Velocity of such contraction is related to the binding/unbinding dynamics of focal adhesion and local substrate deformation. Substrate deformation is represented as a deformed discrete spring for simplicity, but the model is composed by a continuum set of springs with variable Young modulus. (Bottom) To maintain force balance across the monolayer after each myosin-driven contraction step, the substrate is pulled by a larger amount on the soft side (d_{soft}) than on the stiff side (d_{stiff}), which eventually causes overall movement toward the stiff side.

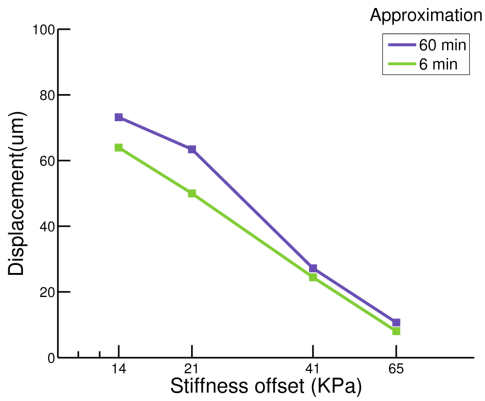

Fig. S4.3:Comparison between linear-time approximations. Movement of the monolayer center of mass depending on the initial stiffness offset. Approximation to 10 hours by linear extrapolation of 6 minutes (green) and 60 minutes (purple). As the simulation time approximates to real experimental time results are more accurate. The reason behind this is that when cell monolayer grows, the gradient that it is able to sense also increases resulting in higher velocities at the end of the simulation than at the beginning. However, difference between both approximations is not significant and results show the same qualitatively behavior.

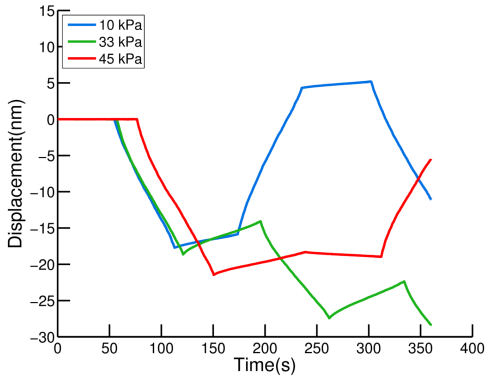

Fig. S4.4:Persistence movement of cell monolayers placed on uniform gels. A single cell is placed in three uniform gels with different stiffness (10, 30 and 45 kPa). We observe a higher persistence movement in stiffer gels.

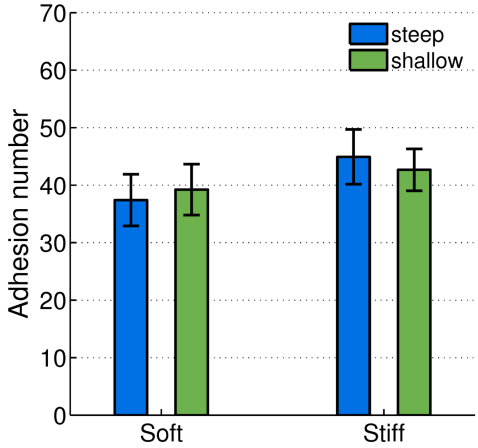

Fig. S4.5:Average number of discrete adhesion at both edges of the monolayer (stiff and soft). Results are shown for the two different rigidity gradients. Adhesion is always slightly higher in the stiffer part, where the forces exerted by the cell are divided more linearly between the adhesion complexes than in the softer part.

Chapter 5

Balance of mechanical forces drive endothelial gap formation

In this section, we present a new computational model to simulate an endothelial cell monolayer focusing on cell-cell junction dynamics. This section corresponds to a journal publication that is currently in preparation:

Escribano, J., Chen, M.B., Moeendarbary, E., Spill F., García-Aznar, J.M. and Kamm R.D. (2018). Balance of Mechanical Forces Drive Endothelial Gap Formation and Facilitate Cancer and Immune-Cell Extravasation.

5.1 Introduction

Immune and cancer cells alike are characterized by their ability to travel within the vasculature and then to leave the vasculature into different tissues. These processes are crucial for a functioning immune system to fight acute infections [202] or participate in wound healing [147]. However, chronic inflammation or tumor metastases are ultimately also initiated by extravasating immune or cancer cells, respectively [82, 136]. Hence, while extravasation is critical to clear communicable diseases, it is also a critical contributor to virtually all non-communicable diseases, ranging from cancer to asthma, atherosclerosis, rheumatoid arthritis and heart diseases [116, 136, 134].

Much of the research on extravasation, also termed diapedesis, has focused on the role of the extravasating cell during this process, and how it interacts with the endothelial cells of the vasculature through which it is transmigrating. First, the extravasating cell needs to adhere to the vasculature. This adhesion is mediated by molecules including P-and E-selectin, ICAM or VCAM [7]. Typically, the arrested cells are migrating further on top of the endothelium before they start the actual process of transmigration, which can occur both through a single endothelial cell (transcellular extravasation) or, more commonly, in between two or more endothelial cells (paracellular extravasation) [125].

During paracellular extravasation, it has been investigated how the extravasating cell signals to the endothelial cells, leading to weakening of VE-cadherin-mediated cell-cell junctions and subsequently gap formation, through which the cells can transmigrate [14, 160]. Gap formation may, for instance, be stimulated by thrombin [198]. As such, molecular signaling events are firmly established as important contributors to extravasation.

However, on a fundamental level, all the processes involved in extravasation are mechanical processes. Transmigration, like other forms of cell migration, involves the generation of mechanical forces through the actomyosin cytoskeleton [30]. Moreover, the mechanical properties of the endothelium provide passive mechanical resistance [30]. For instance, increased endothelial cell and junctional stiffness could reduce paracellular extravasation rates [174, 125]. Interestingly, recent research established that active mechanical properties of the endothelial cells are also critical during endothelial gap formation [173, 143], and the rearrangements of cytoskeletal structures are associated with changes in barrier function. For instance, a rich actin cortex parallel to cell-cell interfaces is associated with stabilized VE-cadherin junctions and thus tight barriers [10, 56], whereas actomyosin stress fibers pulling radially on junctions can lead to junctional remodeling [91]. Additionally, actin-rich pores can actively contract to prevent leakage during extravasation [88]. However, there is still a lack of understanding of the different roles of active and passive mechanical properties of the endothelium in the extravasation process.

Mathematical multiscale models are powerful tools to investigate the interplay of different physical drivers in biological processes. Many different approaches have been employed to model and understand the dynamics of epithelial monolayers. Agent-based models, where individual cells are explicitly taken into account, include center-based models (CBM)[73], vertex models [117] and deformable models (DFM)[92, 149]. However, these models do not explicitly model cell-cell adhesion dynamics in a way that leads to the experimentally

observed gap formation in monolayers of endothelial cells, and thus, they cannot easily be employed to study this problem so crucial for cancer and immune transmigration.

In this chapter, we introduce a mathematical model to simulate the mechanical behavior of an endothelial monolayer. Each endothelial cell contains contractile actin structures that may contract radially or in parallel to the plasma membrane. Then, cells are tethered to neighboring cells by cell-cell junctions that can dynamically form and break in a force-dependent manner. We employ this model to investigate the mechanisms of gap formation in an endothelial monolayer. Interestingly, we find that gaps open dynamically in the absence of extravasating cells. These gaps are formed preferentially at the vertices where three or more endothelial cells meet, as opposed to the edges in between two cells. This is in line with data obtained by our collaborators from quantifying gap formation of monolayers of HUVECs seeded on glass (not published yet). Moreover, we quantify the frequency of gap openings as well as the duration of gap openings. Then, through multi-dimensional parameter studies, the model is providing us insights into the physical and molecular driver of the gap formation and gap dynamics. The model predicts that active forces not only play an important role in the initial gap formation, but they are also even more important in controlling gap size and lifetime once they are initially formed. This is due to the catch-slip bond nature of the cell-cell adhesion complexes as well as the force-dependent reinforcement of adhesion clusters [113], both of which stabilize junctions in response to forces acting on them. However, while the catch-slip bonds ultimately weaken when force is increased beyond the maximal lifetime of a single molecular bond, the force-dependent reinforcement will always increase adhesion strength with increasing force. Although the slip-catch bond nature and the force dependence of the adhesion clustering processes both crucially influence gap opening frequencies, we find that gap lifetime and gap size are even more sensitive to the passive mechanical properties of the cell. Increased elasticity of the membrane/cortex and, even more notably, of the actin stress fibers will reduce gap lifetime and size, since the cells will mechanically resist opening gaps through counteracting forces.

Our model predictions of gap opening frequency and lifetime at both cell vertices and interfaces correlate with experiments showing such gaps in endothelial monolayers in the absence of any extravasating cell. Thus, our work challenges the paradigm that the extravasating cells primarily cause gap opening through interactions with the endothelium. Experimental observations show that cells indeed primarily extravasate at vertices [26]. In summary, the results presented in this chapter highlights the importance to take into account the dynamic and autonomous mechanical properties of the endothelium when trying

to understand gap formation and extravasation as well as when devising new strategies to overcome the adverse effects of these processes in chronic inflammations or cancer metastasis.

5.2 Computational model of endothelial monolayers

We design a computational model of a cell monolayer. Model contains several cell that are bound through cell-cell adhesion complex simply referred as cadherins. Each cell contains a number of radial contractile actin stress fibers modeled by viscoelastic springs and the cell membrane together with the cortex is also represented by viscoelastic springs (with different mechanical properties). Therefore,the whole cell is discretized into nodes, which represent the fundamental degrees of freedom of the resulting network of stress fibers, membrane elements and cell-cell junctions. Cell membrane is discretized into n_{nodes} nodes with a spacing, l_n between them. These membrane points are connected to the center by a stress fiber, which, for the hexagonal geometry shown in Fig. 5.1, are connected by a single node in the center. The actual model is independent of cellular initial geometry, since cells are able to dynamically adapt their geometry depending on the forces they bear. Both membrane and stress fiber bars are considered as viscoelastic elements and they are approximated by Kelvin-Voigt structures. Nodes dynamics can be expressed in terms of the Langevin equation assuming that inertial forces have no significant impact on the system and the forces exhibit inherent randomness, the dynamics of the nodes is described by the Langevin equation [101]:

$$\frac{d\mathbf{r}_i}{dt} = \frac{1}{\xi}\mathbf{F}_i. \tag{5.1}$$

Here, $\mathbf{r}_i$ corresponds to the current position of each membrane and cell center node i, ξ is the medium drag coefficient, and $\mathbf{F}_i$ represents the sum of all forces due to active, random contractions or due to passive mechanical interactions between node i and its neighboring nodes:

$$\mathbf{F}_i = \mathbf{F}_i^{sf} + \mathbf{F}_i^{memb} + \mathbf{F}_i^{cadh} + \mathbf{F}_i^{rep} + \mathbf{F}_i^{gen}, \tag{5.2}$$

where, $\mathbf{F}_i^{sf}$ is the force due to radial stress fibers, $\mathbf{F}_i^{memb}$ is the force due to the membrane and cortex, $\mathbf{F}_i^{rep}$ is the repulsion force due to contact between different cells and, $\mathbf{F}_i^{gen}$ is the cell generated force of the contractile/protrusive element in membrane and stress fibers. $\mathbf{F}_i^{cadh}$ is the force originating through cell-cell adhesions, represented by cadherin in our stochastic adhesion model described in Section 5.2.2.

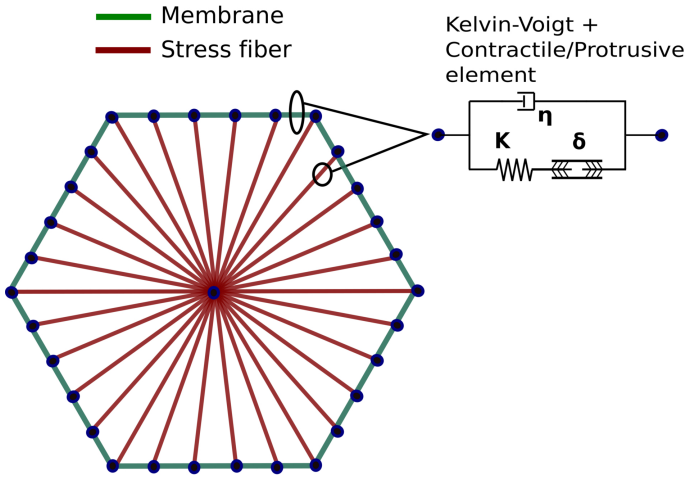

Fig. 5.1 Schematic of the cell model. Cells present an initial hexagonal form, where the membrane is divided into a discrete number of membrane points. Physically, our membrane elements connecting the nodes represent the combined lipid bilayer with the actin cortex. Moreover, the nodes are connected to the center by stress fiber structure. Both of them behave as a Kelvin-Voigt structure with a contractile/protrusive element but with different properties.

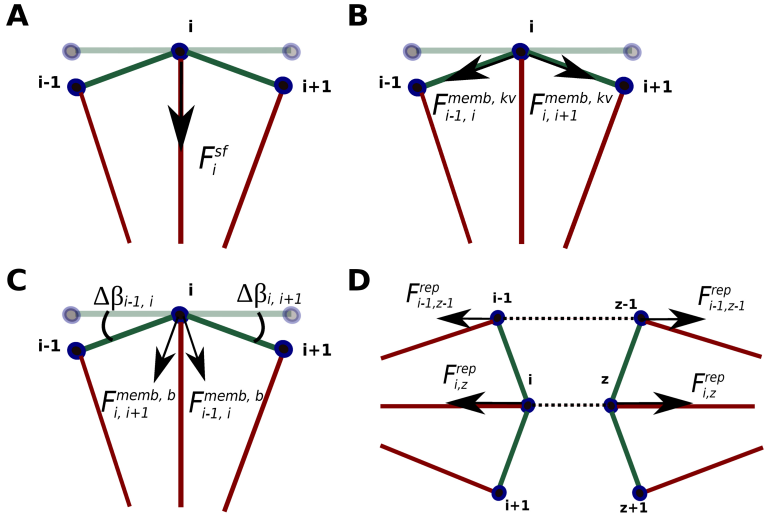

Fig. 5.2 Different cell forces acting on membrane points and cell center. (A) Force due to stress fiber structures. (B) Force due to membrane structures. (C) Force due to membrane bending stiffness. (D) Force due to repulsion between membrane points of different cells.

5.2.1 Model of passive intracellular mechanics

In this section we introduce the mechanical model for a single cell describing the passive forces due to the stress fibers and membrane. Both radial stress fibers and tangential membrane/cortex segments are modeled with Kelvin-Voigt elements (Fig. 5.1). For simplicity, we consider hexagonal cells as a starting point, even though the actual modeling framework is independent of the cell geometry. Stress fibers connect the node in the center of the cell with a node on the membrane. Additional to the Kelvin-Voigt force arising due to deformations in parallel with two membrane points $\mathbf{F}_i^{memb,kv}$ (Fig. 5.2B), the membrane/cortex exhibits bending stiffness resulting in forces due to deformations perpendicular to the membrane, $\mathbf{F}_i^{memb,b}$ (Fig 5.2C). The total force on a membrane node due to deformations of neighboring membrane nodes is thus given by:

$$\mathbf{F}_i^{memb} = \mathbf{F}_{i-1,i}^{memb,kv} + \mathbf{F}_{i+1,i}^{memb,kv} + \mathbf{F}_{i-1,i}^{memb,b} + \mathbf{F}_{i+1,i}^{memb,b}, \tag{5.3}$$

where $i-1$ and $i+1$ are the neighboring points of i, $\beta_{i-1,i}$ is the angle denoting deviations from the balance position (Fig. 5.2C). For the forces derived from the Kelvin-Voigt structures, $\mathbf{F}_i^{memb,kv}$ and $\mathbf{F}_i^{sf,kv}$, the direction corresponds to the vector $\vec{\mathbf{k}}$ formed by the corresponding nodes indicated in the sub-index ($i-1$ or $i+1$, i). ($\mathbf{F}_i^{memb,b}$) is the bending stiffness component:

$$|\mathbf{F}_{i-1,i}^{memb,b}| = K_{bend} \cdot (\beta_{i-1,i} - \beta_{i-1,i}^0), \tag{5.4}$$

where the direction of the force is perpendicular to $\vec{\mathbf{k}}$ (unit vector of the membrane segment), $d_{i-1,i}$ is the distance between the two points and K_{bend} is the bending stiffness constant.

Kelvin-Voigt structures consist of a parallel arrangement of a purely elastic spring and a purely viscous damper:

$$F(t) = EA\varepsilon(t) + \frac{d\varepsilon(t)}{dt} A\eta, \tag{5.5}$$

where E is the elastic modulus, A is the area of the section and η is the viscosity of the material (membrane or stress fiber). Forces are implemented for both stress fibers and membrane structures as:

$$\mathbf{F}_i^{sf} = [K_{sf}(l_n - l_n^0) - \eta_{sf} v_n] \cdot \vec{\mathbf{k}}, \tag{5.6}$$

$$\mathbf{F}_i^{memb,kv} = [K_{memb}(l_n - l_n^0) - \eta_{memb} v_n] \cdot \vec{\mathbf{k}}, \tag{5.7}$$

where K_{sf} and K_{memb} are the stiffness of stress fiber and membrane and η_{sf} and η_{memb} are the drag coefficients of stress fibers and membrane bar. n is the bar that bind the point i and $i-1$ which could correspond to a stress fiber or a membrane bar. l_n is the current length of the bar and l_n^0 is the rest length. v_n corresponds to the velocity at which the bar is varying its length and $\vec{\mathbf{k}}$ is the unit vector in the bar direction.

A repulsion force is included to avoid different cells from occupying the same space at the same time. This force occurs when two membrane points of two different cells are within a certain distance range (L_{rep}). The magnitude of this force grows with the distance between two membrane points, i and z of different cells (Fig. 5.2D):

$$\mathbf{F}_{i,z}^{rep} = K_{rep} \cdot (L_{rep} - d_{i,z}) \cdot \vec{\mathbf{j}}. \tag{5.8}$$

Here, K_{rep} is a constant parameter, $d_{i,z}$ is the distance between the two membrane points of a different cell and L_{rep} is the maximum distance at which repulsion is applied. The direction of the force, $\vec{\mathbf{j}}$, is the unit vector in the opposite direction of the straight line that binds both points (i and z), as explained in (Fig. 5.2D).

5.2.2 Model of cell-cell adhesions

Endothelial cells are mechanically coupled to neighboring cells through cell-cell adhesions. VE-Cadherin is the major protein in endothelial cell adherent junctions and it is known to cluster on the membrane [91]. We assume that each membrane point is a binding site for cadherin clusters. Cadherin clusters thus connect two membrane points of two different cells. In order to model their mechanical behavior, we assume that the cadherin clusters are connected as linear springs, that is,

$$|\mathbf{F}_i^{cadh}| = |\mathbf{F}_z^{cadh}| = K_{cadh} \cdot (d_{i,z} - L_{cadh}^0). \tag{5.9}$$

Here, $d_{i,z}$ is the distance between the points that the cadherin cluster binds (i and z), K_{cadh} is the stiffness constant for the cadherin cluster and L_{cadh}^0 is the cadherin equilibrium length. The direction of the force corresponds to the vector formed by the two points of the cadherin i and z. From now on, we refer to the cadherin cluster that binds points i and z with the subindex p.

The probability of binding two membrane points depends on the distance between them by means of the following rate:

$$k_{bind,p} = \begin{cases} k_{on}^{o} \cdot \rho_{cadh} \cdot (1 - \frac{d_{i,z}}{L_{bind}^{limit}}) & \text{if } L_{bind}^{limit} \leq 0, \\ \\ 0 & \text{if } L_{bind}^{limit} > 0, \end{cases} \tag{5.10}$$

where k_{on}^{o} is the binding rate constant, L_{bind}^{limit} is the maximal distance at which a cadherin could bind, and ρ_{cadh} is the cadherin density available for binding in the monolayer. In this equation, the probability is based on distance and we only employ it for initial binding.

A reinforcement event is also included in the cell-cell junctions in order to strengthen the adhesion between different cells. It is known that VE-Cadherins recruit vinculin to prevent junction from opening during force-dependent remodeling [91]. Here we include force dependent reinforcement by designing each discrete union as a conglomerate of individual cadherins. Each conglomerate can contain several cadherins up to a maximum value n_{reinf}^{max}. Depending on the current number of single cadherins in each clutch, n_{reinf}, the resulting stiffness of the spring may change in a linear way:

$$K_p = n_{reinf} \cdot K_{cadh}^{0}, \tag{5.11}$$

where K_{cadh}^{0} is the stiffness for a single cadherin.

Once a union is formed (following equation 5.10), the number of single cadherins in a clutch can vary stochastically following a force dependent law:

$$k_{reinf,p} = \begin{cases} k_{reinf}^{o} \cdot \rho_{cadh} \cdot (1 - \dfrac{\lambda_{reinf} - F_p^{cadh}}{\lambda_{reinf}}) & \text{if } F_p^{cadh} \leq F_{reinf}^{limit}, \\ \\ 0 & \text{if } F_p^{cadh} > F_{reinf}^{limit}, \end{cases} \tag{5.12}$$

where k_{reinf}^{o} is the binding rate constant for the reinforcement and λ_{reinf} is a force constant for adjusting the reinforcement curve. F_{reinf}^{limit} is a force threshold to stop applying reinforcement. This threshold is set to ensure that, at high forces rates, unbinding is predominant over binding. This value is considerably higher than the peak of stability of the catch bond considered to model unbinding to ensure that this happens when unbinding rate is already high.

Unbinding is modeled as a catch-slip bond law [141]:

$$k_{ub,p} = k_c^0 \cdot exp(\Phi_c - \Phi) + k_s^0 \cdot exp(\Phi - \Phi_s), \tag{5.13}$$

where $\theta = |F_p^{cadh}|/F^*$ and Φ_c, Φ_s are the parameters of the catch and slip bond regimes respectively. F^* is used to normalize the force, $|F_p^{cadh}|$ is the modulus of the current force for the specific cadherin and k_c^0 and k_s^0 are the unbinding rate at zero force for the catch and slip curves respectively.

Each time that a reinforcement process occurs n_{reinf} is increased by one and each time an unbinding event occurs n_{reinf} is decreased by one.

5.2.3 Cell generated forces

Cell generated forces are the responsible of cell adhesion rupture. These forces correpond to myosin forces ($\mathbf{F}_i^{myo}$), acting in the stress fibers and the cortex membrane, and protrusive forces ($\mathbf{F}_i^{prot}$), generated by actin polymerization and cell outward directed. Thus,

$$\mathbf{F}_i^{gen} = \mathbf{F}_i^{myo} + \mathbf{F}_i^{prot}. \tag{5.14}$$

Myosin forces are the result of the combination of two types of forces. First one is radial contraction which is generated by the myosin activity in the stress fibers and it has a radial direction. The second one is tangential forces that occur due to contractions of the cortical actin filaments and are directed parallel to the membrane. Both forces have a magnitude of F_{Radial}^{max} and F_{Cortex}^{max} for each stress fiber and membrane segment respectively. Both types of forces are not homogeneously distributed throughout all the stress fibers and membrane segments of the cell and are not acting during the whole simulation time. Spatial distribution of the forces is controlled by n_{Radial}^{Force} and n_{Cortex}^{Force}, which represents the number of consecutive stress fibers or membrane segments respectively that has the same force. Each one of this set of segments has a probability of activating the force of p_{Radial}^{Force} and p_{Cortex}^{Force}. Depending on this probability, the force for each segment of the different sets could be the magnitude indicated by F_{Radial}^{max} or a baseline contraction of a random number between [0, $0.1 \cdot F_{Radial}^{max}$] for the radial force case. For cortex force, depending on the probability value, the force could be the magnitude indicated by F_{Cortex}^{max} or it could be zero. This probability is calculated for each of the stress fibers and membrane sets every given time indicated by t_{Radial}^{Force} and t_{Cortex}^{Force}. These values indicate the time between each activation force probability is recalculated (see Fig. 5.3A and B). When, following previous explanation, there is a change in the force for stress fiber or membrane segment, force does not change abruptly in one time step. Force magnitude changes linearly in time from the previous value to the new one in a given total time, $t_{Transition}^{Force}$. In this way, cell forces are not homogeneously distributed

in time and space. Vasoactive agents like thrombin increase intracellular levels of Ca+2 leading to myosin activation [198]. This induces rapid changes in traction forces, leading to heterogeneously force distribution which causes the formation of inter-cellular gaps.

Protrusive forces are caused due to cell polymerization at the leading edge. They are modeled exactly the same as the radial forces but in the opposite direction (outward the cell) and with its own parameters (n_{Prot}^{Force},p_{Prot}^{Force} and t_{Prot}^{Force}) (see Fig. 5.3C).

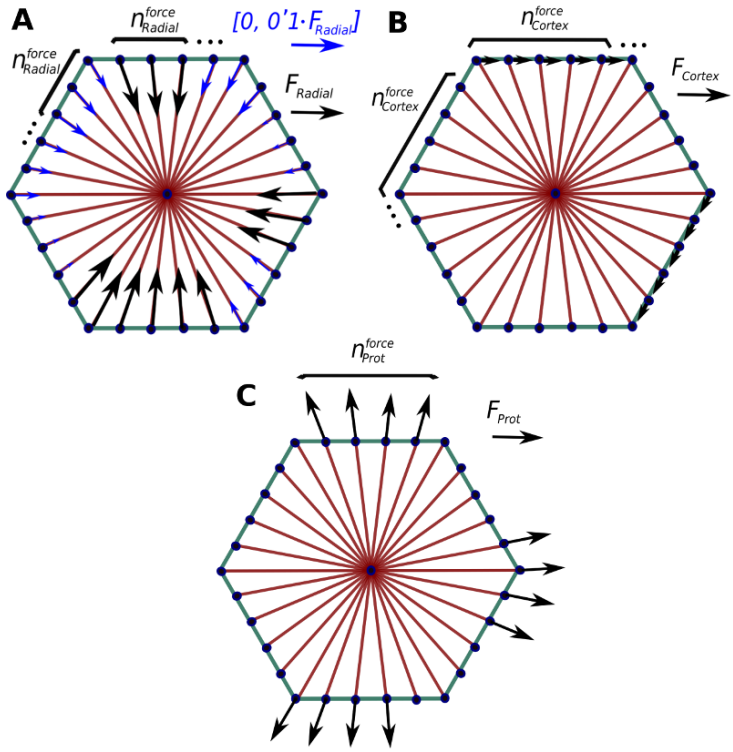

Fig. 5.3 Cell generated forces. (A) and (B) correspond to myosin forces: Radial force and Cortex force respectively. (C) Protrusive forces.

5.2.4 Actin remodeling

Our model incorporates the dynamical remodeling of stress fibers. This can be done due to the polymerization of existing fibers, leading to protrusions, or the shrinking of existing fibers due to severing or buckling and the subsequent breakage. For simplicity, we do not consider total depolymerization of a fiber or de novo polymerization of new fibers in response

to nucleation. Moreover, we assume that the total amount of F-actin is conserved, i.e. the G-actin available after depolymerization is assumed to quickly polymerize in other fibers.

We describe the remodeling of the stress fibers through a change in the rest length of the spring in the Kelvin-Voigt element. Stress fibers dynamically remodel by adapting their balance length to their current length at a certain velocity:

$$\dot{L_s^0} = v_s^{remodel} = K_{remodel} \cdot (L_s - L_s^0), \tag{5.15}$$

where s is the index of the stress fiber, L_s is the current length of the stress fiber, L_s^0 is the current balance rest length of the stress fiber and $K_{remodel}$ is a constant describing the rate of length adaptation.

Since we assume total conservation of actin, we maintain constant the total length of the fibers, that is:

$$\sum_{s=1}^{S} L_s^0 = const, \tag{5.16}$$

where S is the total number stress fibers in a cell. In order to fulfill this equation, length balance of all the stress fiber in a cell is modified in a proportional way (see Fig. 5.4).

5.2.5 Gap formation

Gaps are formed between the cell's membranes as a consequence of the cadherin bond rupture. They are limited by the membrane and bound cadherins (see Fig. 5.5). We only quantify the gaps generated around the cell in the center of the monolayer. The minimum area to consider the formation of a gap is $A_{GAP,F}$. When the gap area drops below a threshold $A_{GAP,C}$, that area is no longer considered as a gap. We differentiate between gaps formed at a two cell interface and gaps formed in the vertex shared by three or more cells.

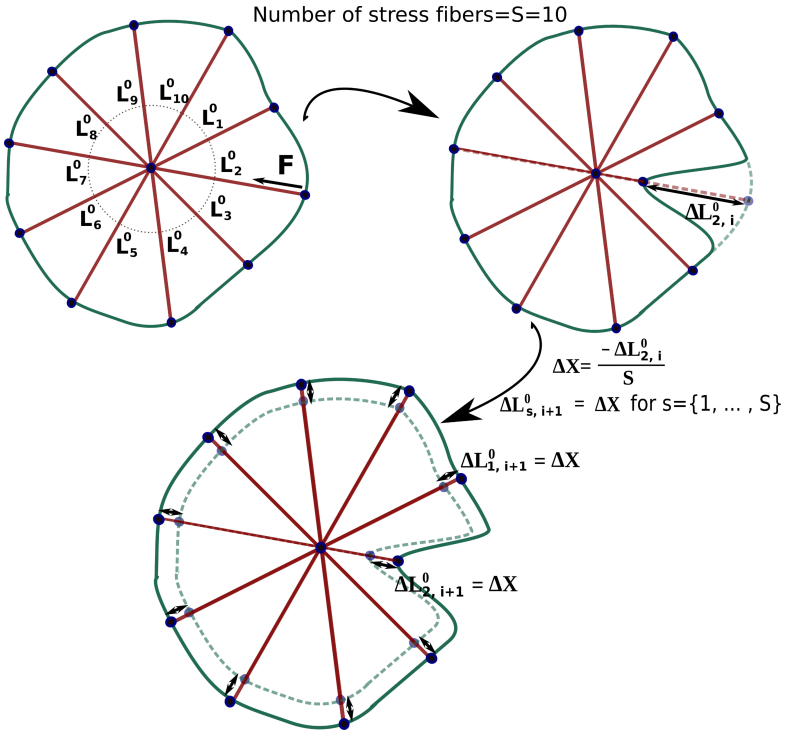

Fig. 5.4 Stress fiber remodeling. Due to myosin contractility a change in the rest length of the stress fiber occurs. This change in rest length is compensated by all the stress fibers in a proportional way.

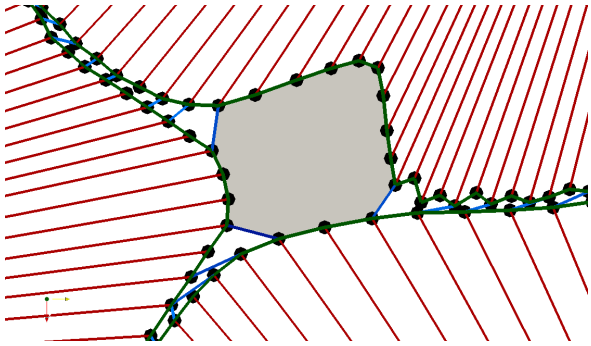

Fig. 5.5 Paracellular gap. Gap (grey) is delimited by the cell membrane (green) and the cadherins binding the cell (blue). Red: cell stress fibers. Black dots: Membrane points

5.3 Implementation

The cell monolayer is formed by placing cell interfaces at a fixed initial distance in a way that the whole monolayer has a rhombus geometry. The monolayer is fully bound at its initial state and cells present a hexagonal form in such a way that the distance between them is the same throughout the whole monolayer (see Fig. 5.6). Initial configuration is at balance; when simulation starts, membrane points at the edge of the monolayer are encastred so that limits of the monolayer are fixed. The aim of the simulation is to study the mechanisms behind gap formation. For that matter, we focus on the gaps that are formed around the cell in the center of the monolayer and in that way avoid the influence of the boundary conditions. The simulation starts by myosin forces activation.

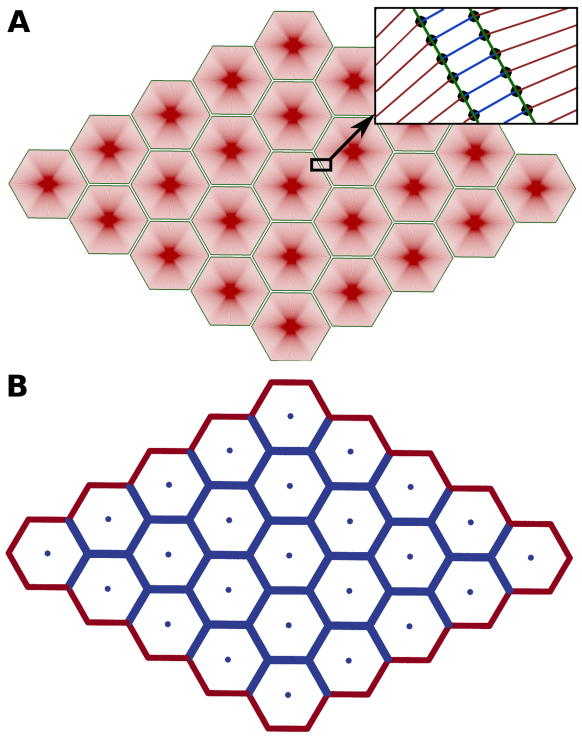

Fig. 5.6 Initial state of the monolayer. (A) Cells with a hexagonal form are in a rest state and fully bound with their neighboring cells. Cell membrane (green), stress fibers (red), cadherin complexes (blue), membrane points (black). (B) Boundary conditions: Points in the border of the monolayer (red) are fixed and act as a wall. In blue are membrane points, where cadherin adheres and the cell centers.

Actions performed during each simulation step are as follow:

1- Check Binding: First we analyze the position between membrane points of different cells and see if a new union is formed (equation 5.10). At the same time, we analyze reinforcement of cadherins that are already bound to check if the adhesion becomes more stable (5.12).

2- Point displacement: We analyze the force balance in each node ,i of the system and update their position. Forces considered are detailed in equation 5.2.

3- Stress fiber remodeling: Based on the new positions the new rest length of the different stress fibers is calculated (equation 5.16).

4- Check unbinding: We update cadherin force and check unbinding phenomenon in each cadherin cluster following equation 5.13.

5- Gap formation: We analyze the new gaps that have been formed and update the position, size and lifetime of the ones that are already bound.

Table 5.1 Model parameters used in the simulation.

Parameter	Symbol	Value	Source
Medium drag coefficient	ξ	$7.709 \cdot 10^{-4}$ (kg/s)	[149]
Membrane stiffness	K_{memb}	$2.5 \cdot 10^{-3}$ (kg/s^2)	[57]
Stress fiber stiffness	K_{sf}	$1.25 \cdot 10^{-4}$ (kg/s^2)	[149]
Bending stiffness constant	K_{bend}	$2.2 \cdot 10^{-17}$ (Nm)	[57]
Membrane viscosity	η_{memb}	$3.709 \cdot 10^{-3}$ (kg/s)	[57]
Stress fiber viscosity	η_{sf}	$3.709 \cdot 10^{-3}$ (kg/s)	[57]
Force to normalize parameters in unbinding law	F^*	0.008 (nN)	Adjusted from [146]
Non-dimensionalized force of catch curve in unbinding law	Φ_c	0.01	Adjusted from [146]
Non-dimensionalized force of slip curve in unbinding law	Φ_s	4	Adjusted from [146]
Unbinding cadherin rate for minimum force for catch curve	k_c^0	0.23 s^{-1}	Adjusted from [146]
Unbinding cadherin rate for minimum force for slip curve	k_s^0	0.23 s^{-1}	Adjusted from [146]
Binding rate for cadherin at maximum distance	k_{on}^0	15.3 $(\mu m^2/(mol \cdot s))$	Adjusted from unbinding law
Binding rate for cadherin reinforcement at zero force	k_{reinf}^0	11.5 $(\mu m^2/(mol \cdot s))$	Adjusted from unbinding law
Cadherin density	ρ_{cadh}	21 $(mol/\mu m^2)$	[35]

Parameter	Symbol	Value	Source
Limit distance for cadherin binding	L_{bind}^{limit}	0.95 (μm)	Estimated
Constant for reinforcement curve	λ_{reinf}	10 nN)	Estimated
Force threshold to stop applying reinforcement	F_{reinf}^{limit}	0.06 (nN)	Adjusted from unbinding law
Single cadherin stiffness constant	K_{cadh}^{0}	$2 \cdot 10^{-4}$ (kg/s)	Estimated
Cadherin equilibrium length	L_{cadh}^{0}	0.1 (μm)	[42]
Maximum number of cadherins per clutch	n_c^{max}	8	Estimated
Maximum force due to radial contraction	F_{Radial}	0.775 (nN)	Adjusted from [157]
Maximum force due to cortical tension	F_{cortex}	0.025 (nN)	[87]
Maximum force due to protrusion	F_{Prot}	0.14 (nN)	Estimated
Force recalculation time for radial force	t_{Radial}^{Force}	25 min	Estimated
Force recalculation time for cortical force	t_{Cortex}^{Force}	25 min	Estimated
Force recalculation time for protrusive force	t_{Prot}^{Force}	25 min	Estimated
Force transition time	$t_{Transition}^{Force}$	2 min	Estimated
Number of nodes with similar radial force	n_{Radial}^{Force}	5	Estimated
Number of nodes with similar cortical force	n_{Cortex}^{Force}	10	Estimated
Number of nodes with similar force for protrusive forces	n_{Prot}^{Force}	20	Estimated
Force activation probability for radial force	p_{Radial}^{Force}	0.01	Estimated
Force activation probability for cortical force	p_{Cortex}^{Force}	0.01	Estimated
Force activation probability for protrusive force	p_{Prot}^{Force}	0.1	Estimated
Constant for repulsion	K_{rep}	10^{-3} (kg/s^2)	Estimated
Maximum distance to apply repulsion	L_{rep}	0.05 (μm)	Estimated
Remodel rate constant	$k_{remodel}$	$0.025s^{-1}$	Estimated
Hexagon side length	$l_{hexagon}$	$25(\mu m)$	Estimated
Distance between membrane points	l_n	$625(nm)$	Estimated
Minimum area for gap formation	$A_{GAP,F}$	$2(\mu m^2)$	Estimated
Area for gap closing	$A_{GAP,C}$	$1.5(\mu m^2)$	Estimated
Time step	Δt	$1.26(s)$	

5.3.1 Parameter Justification

Parameters for the unbinding law are adjusted to match data from [146] where distributions of forces required to break single VE-cadherin/VE-cadherin bonds in HUVECs were measured. Binding and binding reinforcement values have been adjusted accordingly to the unbinding rates; at low loading rates binding and unbinding rates are within the same range and which one is higher depends on the binding distance or force, respectively. For intermedium load rates binding is predominant due to reinforcement phenomenon. For high load rates unbinding is predominant. Radial forces in the monolayer are within values reported by [157]. For protrusive forces, we have selected values lower than the ones chosen for radial forces. Geometrical parameters of the model are estimated based on experimental images and cadherin geometrical values are extracted from [42]. Stress fiber stiffness corresponds to the value used in the model for cytoskeleton stiffness in epithelial cells introduced in [149]. Membrane stiffness is within the range of values reported for two neighboring membrane ring segments in [57] and similar to measurements of cellular cortex stiffness in endothelial cells [80]. Membrane and stress fiber viscosities are within one order of magnitude of values reported for viscous drag coefficient for filament shrinkage [57]. Value for the bending stiffness is within one order of magnitude of values reported by [57]. Medium drag coefficient is also within one order of magnitude of values used in another model for epithelial cell monolayers [149]. Typical values reported for cortical tension are $400 pN/\mu m$ [179] if we assume that membrane thickness is $50nm$ we have force values around $20pN$ which are considerably smaller than contraction forces.

5.4 Results

We employ our endothelial monolayer model to explore the dynamics of endothelial cell junctions. We predict the frequency, size and duration of gaps, as well as the preferred geometrical locations of the gap formation. These results are in line with experimental results made by our collaborators that are not published yet. The parameters used in the simulations are detailed in Table 5.1. Moreover, we perform sensitivity analyses to investigate how cell mechanical properties, cell-cell adhesion characteristics and myosin generated forces regulate the formation, lifetime and size of gaps in the endothelium.

5.4.1 Gaps open preferentially at vertices

Figure 5.7A and B show typical simulations of the monolayer dynamics obtained by using the computational model. We observe that gaps open preferentially at vertices, i.e. the intersections of three or more cells, as opposed to the edges between two cells. We have quantified this behavior by counting the total number of gaps formed at edges and vertices of the cell in the center of the monolayer (see Fig. 5.7 C). Vertices are points where more than two cells exert forces and where tangential force components naturally propagate to. Therefore, it is expected that stress concentrates at the three cell vertex rather than at the two cells interfaces, and the simulations confirm this hypothesis (see Fig. S5.1). The forces on cadherin clusters at the vertices are thus more likely to exceed the corresponding force of maximal lifetime of the bonds, as will be discussed in more detail below.

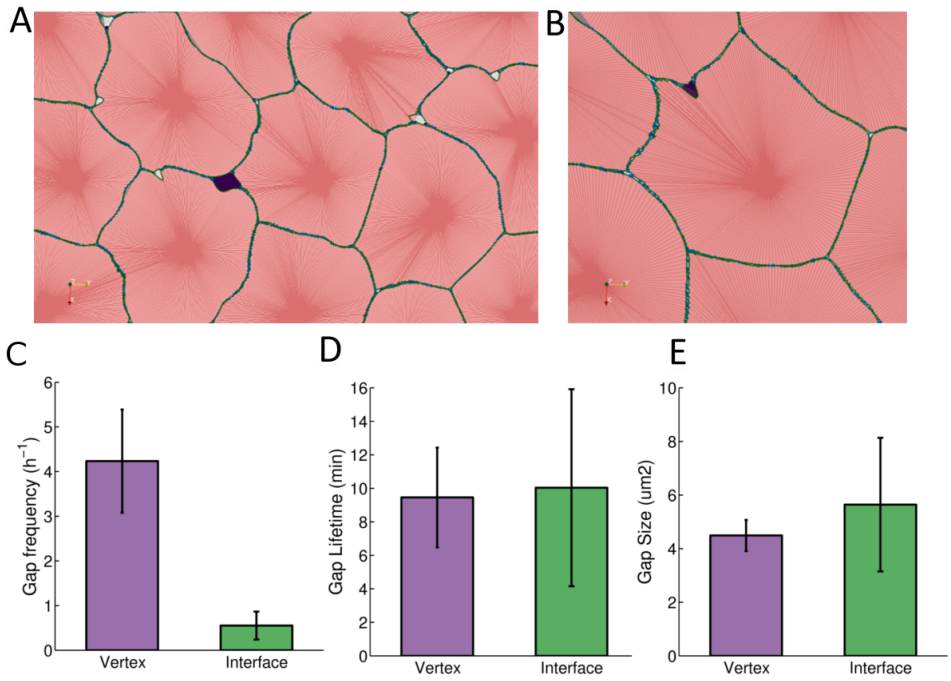

Fig. 5.7 Endothelial Gaps open preferentially at vertices. (A, B) Simulation of endothelial monolayer. Cell membrane corresponds to green lines. Cell body are represented in red (stress fibers composing the cell in darker red). A detected gap is coloured in dark purple. (A) A gap at a vertex. (B) A gap at the cell edge. (C) Quantification of the number of gaps at vertices or two cell interfaces, respectively, observed at a given time. Quantification of the lifetime (D) and size (E) of gaps at vertices or two cell interfaces.

5.4.2 Mechanical properties of cadherin adhesions and intracellular forces dictate endothelial gap opening frequency

We study how variations in the mechanical properties of the cells, the cadherin adhesions or force variations affect the rate of gap formation. Fig. 5.8A,B shows how passive mechanical properties of the cell affect both the frequency (Fig. 5.8A) and the location of the gap openings (Fig. 5.8B). Increasing stiffness of either the membrane or the stress fibers provokes a decrement of the gap generation frequency (Fig. 5.8A). This is intuitive, since increasing stiffness stabilizes the movements of cells and makes the monolayer less dynamic. On the other hand, the location of the gap openings (i.e. whether they occur at a vertex or interface) is less affected by membrane stiffness, but very stiff stress fibers prevent gaps from opening at the interfaces (Fig. 5.8B).

Interestingly, bending stiffness induces gap generation up to a maximum point. Above that stiffness, gaps start to appear less frequently (Fig. 5.8A). For small to intermediate bending stiffness, the frequency of gap openings increases, since bending stiffness is critical for effective force propagation between neighboring adhesion sites at vertices. When a single adhesion complex ruptures, bending stiffness leads to increased forces on neighboring adhesions. After a peak in gap opening frequency at intermediate bending stiffness, a drop in the gap formation is observed for higher bending stiffness. This is caused by the resulting stabilization of the existing gaps at vertices. This high bending stiffness opposes sharp corners of the membrane at vertices and thus favors stable gaps that are permanently open, implying no new gaps are formed. On the other hand, at cell interfaces, a high bending stiffness implies that if a single adhesion cluster is ruptured, the forces on it are redistributed across many neighboring adhesion sites and this stabilizes the interfaces (Fig. 5.8B).

Turning to the role of cadherin properties, our model shows that as the cadherins become more stable, gaps open less frequently 5.8C. To increase cell-cell adhesion stability, we increase the mechanical stiffness of individual cadherins, or the density of avilable cadherins for binding. These results are in line with previous experimental work [125], which reported that more stable cell-cell adhesion result in less transmigrating cells. Figure 5.8D shows that as the cell-cell adhesion become more stable, gaps are more likely to be generated at the vertices. While the total number of gaps at either vertex or interface decreases with increasing cadherin stiffness or cadherin density available for binding, we see that there are no significant differences between gaps generated at the vertex and gaps generated at the interfaces.

Fig. 5.8E and F show the impact of the cortical and radial forces, where the total force is kept constant (when the radial force decreases, the cortical force is incremented by the same magnitude). This is biologically relevant since cells are known to shift their cytoskeletal compartments in a context dependent manner [188]. In fact, cell monolayers subjected to shear flow have been reported to increase cortical actin while decreasing stress fibers [125]. Endothelial cells in particular, are known to exhibit both radial and tangential stress fibers with a vastly different effect on gap opening dynamics [143]. As the force shifts from radial to cortical forces, gap formation slightly fluctuates with a final increment (Fig. 5.8E) and the gaps, clearly, tend to localize more at the vertices (Fig. 5.8F) since contractions parallel to the membrane result in force concentrations at the vertices. For very high cortex forces, the typical stresses on adhesion clusters at the vertices may thus be higher than the force where the lifetime of catch-slip bonds peaks (Fig. S5.2), explaining the small increase in the number of gaps formed (Fig. 5.8E). On the other hand, we will later show that these gaps formed at high cortical forces are typically small and have a short lifetime, limiting their potential for extravasation (see Figs. 5.10 E, F).

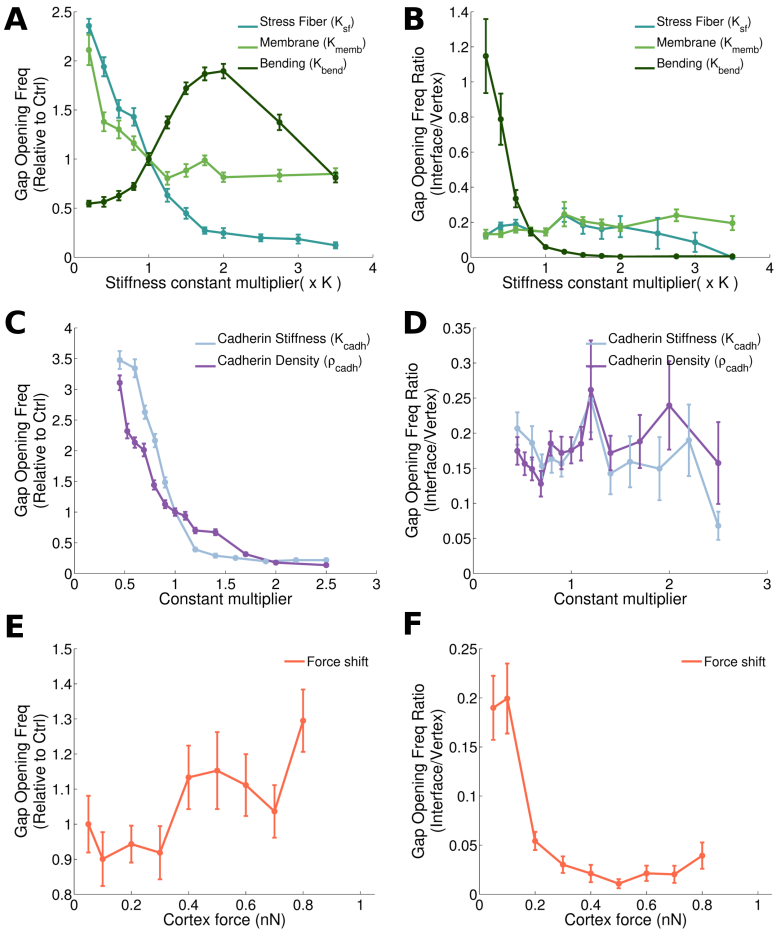

Fig. 5.8 Cell and cell-cell junctions mechanical properties dictate gap opening dynamics. The first column corresponds to the total number of gaps generated compared to the reference case. The second column shows the ratio between gaps occurring at a two cell interface and gaps originated at a three cell vertex. First row (A and B) shows results varying cell mechanical properties such as stress fiber, membrane and bending stiffness. In the second row (C and D) properties of cell-cell junction are changed: stiffness and cadherin density (which affects the binding probability). Third row (E and F) shows results for increasing cortical force, keeping the total force constant. Results are the average value of a sample with $n = 30$ and error bars correspond to standard error.

To take into account that molecular or physical perturbations may simultaneously affect multiple parameters, we now study how variations of two of these parameters at the same time may influence the monolayer integrity and the localization of the gap formation. In Fig.

5.9A we observe how variations in the membrane and stress fiber stiffness have a similar effect on the gap opening frequency, in line with Fig. 5.8A. However the effect of the stress fiber stiffness is clearly predominant over the membrane effect. Interestingly, the combined effect of increasing membrane and stress fiber stiffness is synergistic in suppressing gap formation, due to synergies in stabilizing the overall dynamic movements of the cells that is sensitive to the weakest components. Moreover, the ratio of the gap opening frequency at the interface to vertex indicates a regime with a high ratio for intermediate stress fiber stiffness, whereas the ratio increases monotonically with the membrane stiffness (Fig. 5.9B).

Figs. 5.9C and D shows the impact of varying cadherin stiffness and cadherin density available for binding. We see how both parameters have a similar effect on gap opening, although it appears that for high values of adhesion complex stiffness, adhesion complex density has a less significant impact on the system. This could indicate that for high adhesion stiffness a plateau of maximal stability is reached. We also observe that adhesion cadherin density barely influence the localization of the gaps 5.9D.

In Figs. 5.9E and F we show the role of cortex and radial forces, thus not keeping total force fixed as in Figs. 5.8E,F. Interestingly, we see that total force is what mainly drives gap opening frequency (Fig. 5.9E) whereas radial force mainly drives gap opening location, with higher radial force resulting in proportionally more gaps at the interface. This is, as we argued before, cortical forces naturally propagate to and thus accumulate at the vertices, so radial forces are necessary for gaps at the interfaces.

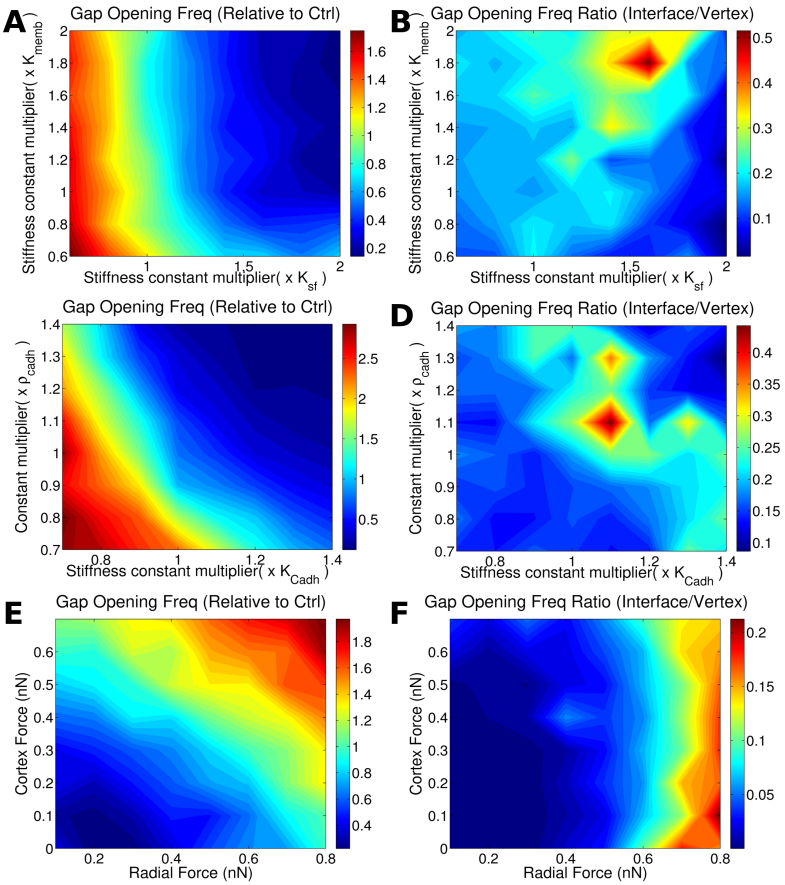

Fig. 5.9 Effect of two parameter variation on gap opening frequency. The first column corresponds to the number of total gaps generated compared to the reference case. The second column shows the ratio of gaps that occur at a two cell interface divided by the gaps that originate at a three cell vertex. First row (A and B) shows results varying membrane and stress fiber stiffness. In the second row (C and D) properties of cell-cell junction are changed: cadherin stiffness versus cadherin density (binding rate). Third row (E and F) shows results for varying cortical and radial force. Results are the average value of a sample with $n = 30$

5.4.3 Passive cell-mechanical properties limit endothelial gap lifetime and size

The lifetime and size of a gap are physical parameters that may also limit a cancer or immune cell's potential to extravasate through the monolayer. Here, we show how the lifetime and size of a gap are also influenced by cell mechanical and junction properties, without the

presence of extravasating cells (Fig. 5.10). We observe that membrane stiffness has a marginal influence on the life of the gap whereas increasing stress fiber stiffness clearly reduces the time that a gap is open and the gap size (Fig. 5.10A and B). Indeed, higher stress fiber stiffness will result in mechanical resistance to an opening gap and thus inhibit the propagation of the defect in the cell-cell junctions, leading to a stabilization of the gaps. The dominance of stress fiber stiffness over membrane stiffness in regulating lifetime remains valid in a broad range of parameter space (Fig. 5.11A). On the other hand, the regulation of size is dominated by stress fiber stiffness only in the regime of high stiffness, whereas for low stress fiber stiffness we see that membrane stiffness has a comparable effect (Fig. 5.11B). Interestingly, bending stiffness critically increases the lifetime of the gaps while slightly decreasing their size. Increasing bending stiffness may increase gap lifetime (Fig. 5.10A). This is because higher bending stiffness will resist deviations from straight membranes. Thus, at straight interfaces, higher bending stiffness will resist gap openings whereas at pointed vertices, cells are less likely to adapt their shape in order to close the gaps.

Figs. 5.10C and 5.11C shows that cadherin stiffness and density at low values do not have a big impact on lifetime, however as they increase, lifetime starts to clearly decreases. Both stiffness and density have a similar effect since the total stiffness of a bond depends on both density and single bond stiffness. The maximum is due to two competing mechanisms: higher cadherin stiffness lead to higher forces on the bonds, which may stabilize or destabilize the bond depending on weather the force is lower or higher than the peak of the catch-slip bond lifetime (Supplementary Fig. S5.2). On the other hand, higher cadherin stiffness leads to more passive mechanical resistance to gap openings, and this effect dominates for high stiffness. For the gap size, the stabilizing effect of both adhesion complex stiffness and density dominates and leads to a reduction in gap size (Figs. 5.10D and 5.11D). However, the effect of increasing density is stronger than that of increasing stiffness, suggesting that cadherin density available for binding is more important in avoiding the gap propagation (once the gap is opened) and it also helps in the gap closing process.

Earlier, we have shown that a shift in the force (from radial to cortical) produces an increment in gap formation (Fig. 5.8E). Fig. 5.10E and F show that this shift in the force critically reduces gap lifetime and size. This indicates that, although the frequency of opening is increased, these gaps are smaller and last shorter in time which may reduce paracellular extravasation, as suggested in previous experimental work [125]. Combined changes of cortical and radial force show that although both kind of forces are needed to increases gap size and lifetime, radial force impact is clearly predominant over cortex force (Figs. 5.11E and F). This intuitive, since radial forces clearly separate cells interfaces generating bigger

gaps and harder to close, whereas cortical forces distribute forces to vertex regions stabilizing the interfaces. This does not provoke large cell deformations which reflects in the low impact on the gap size and lifetime observed.

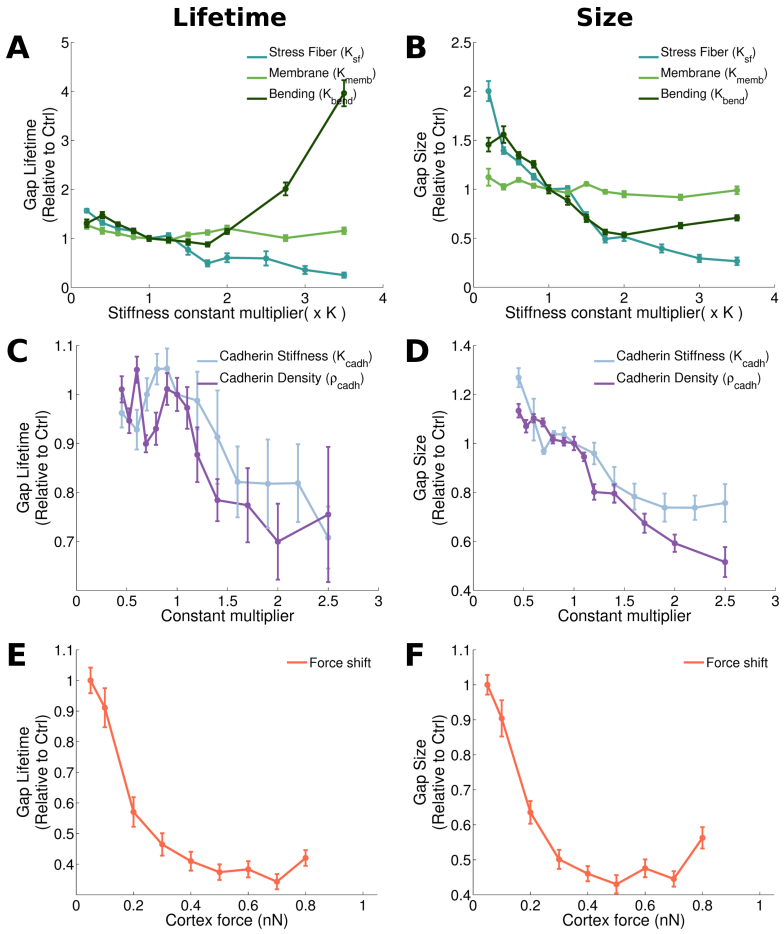

Fig. 5.10 Cell mechanics and cell-cell junctions properties dictate lifetime and size of gaps. Average lifetime of gaps ratio (divided by control case) in the left column and average size in the right column. A, B: Impact of the membrane, stress fiber and bending stiffness. C, D: Impact of cadherin properties: cadherin stiffness and density (which affects the binding probability). E, F: Increasing cortical force, keeping the total force constant. Results are the average value of a sample with $n = 30$ and error bars correspond to standard error.

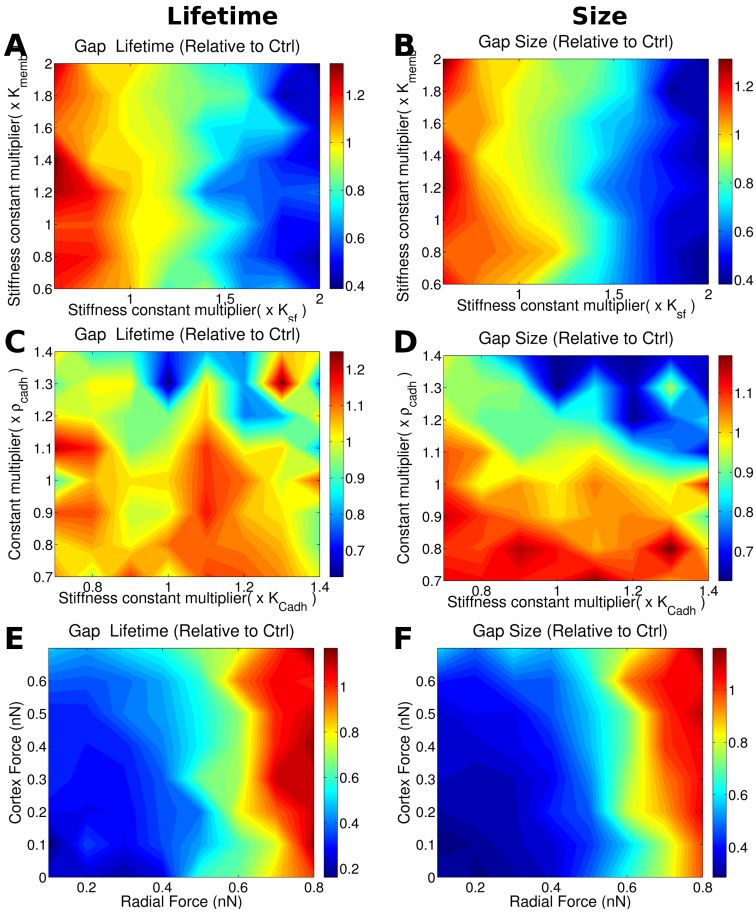

Fig. 5.11 Effect of two parameter variation on gap lifetime and size. The first column corresponds to average lifetime and the second column corresponds to gap size. First row (A and B) shows results varying membrane and stress fiber stiffness. In the second row (C and D) properties of cell-cell junction are changed: cadherin stiffness versus catch bond unbinding constant. Third row (E and F) shows results for varying cortical and radial force. Results are the average value of a sample with $n = 30$.

5.4.4 Force fluctuations regulate gap opening dynamics

We have shown that both the magnitude of forces and the cytoskeletal compartment that generates the forces (stress fibers or cortex) affect gap opening frequency, size and and lifetime. Besides these broad compartments, many other biological and physical parameters affect how forces ultimately act on cell-cell junctions: Forces may act in a directed manner

due to larger parallel actin bundles and synchronous myosin activation, e.g. initiated through waves of activators [198]), or may act more random in branched networks. We do test such scenarios through parameters that affect the transition time when forces change ($t^{Force}_{Transition}$), through spatial force distributions and through the velocity at which forces are modified. In Fig. 5.12A we observe how increasing the force transition time $t^{Force}_{Transition}$ slowly reduces the gap opening. This is due to the fact that a slower, persistent application of forces leads to a redistribution of the forces through rearrangement and remodeling of the cell. It is consistent with experimental works that showed that force fluctuation influence gap opening dynamics [198].

Then, distributing the same radial forces over several adjacent stress fibers reduces gap opening frequency (Fig. 5.12B). More spatially distributed forces are less capable of damaging cell-cell junctions than localized peak forces, since such high peak forces are required to overcome the catch-slip bond maximal lifetime.

Next we observe the effect of force persistence in time. We vary the force recalculation time parameter (equally for all forces) in Fig. 5.12C. Results show that the time that forces are applied does not have a big influence on gap formation. This suggests that cells are able to adapt to forces in longer time scales and therefore it is not the time that forces are applied what regulates gap formation but force fluctuations as suggested above.

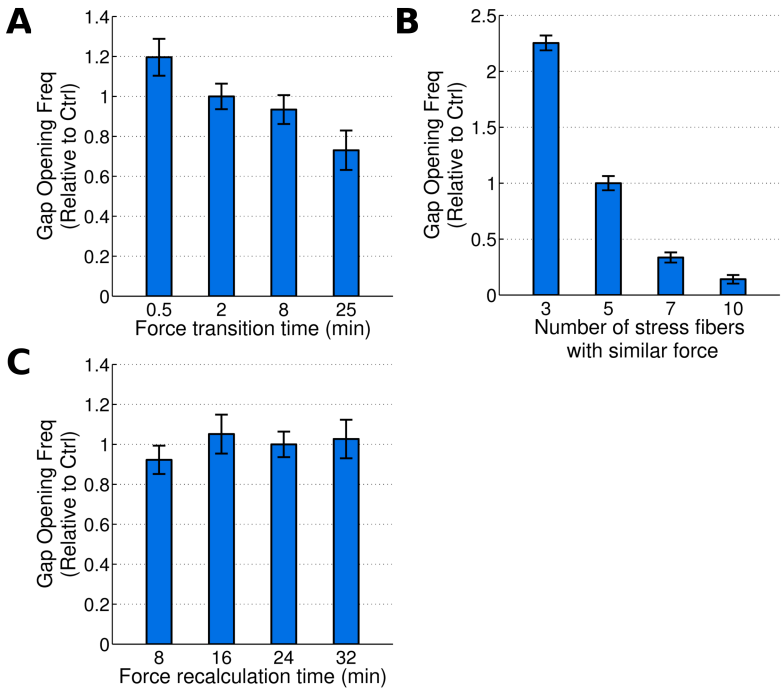

Fig. 5.12 Effect of force application on total gap opening frequency. (A) Total gap opening frequency depending on the time for the force transition. Longer time means smoother force changes. (B) Total gap opening frequency depending on the number of stress fibers at which the same force is distributed. (C) Variation in force fluctuation time for all types of forces considered in the model. Results are the average value of a sample with $n = 30$ and error bars correspond to standard error

5.4.5 Catch-slip bonds facilitate regimes of maximal endothelial stability

In Fig. 5.13A, we show the impact of varying the catch-bond unbinding parameter k_c^0 that shifts the location of the peak of maximal lifetime of a single catch-slip bond, while we maintain the actual maximum value through simultaneously shifting the slip-bond unbinding parameter k_s^0 (Eqn. 5.13 and Fig. S5.2). We observe that for a pure slip bond (corresponding to $k_c^0 = 0$), gaps occur at a higher rates than for small nonzero values of k_c^0. Increasing k_c^0 further leads to a minimum in gap opening frequency, from which the frequency increases again. This minimum corresponds to a maximum of stability, where forces on the adhesions are similar in magnitude to the peak of stability of the catch-slip bond. Consequently, shifting

the location of that peak even further towards higher forces (by increasing k_c^0 even further) means we destabilize the catch-slip bonds again. Note that the gap lifetime and size of gaps are much less influenced by the location of the catch-slip bond maximum than the gap opening frequency.

In Supplementary Fig. S5.3, we show histograms of the forces on adhesions comparing the number of bound clutches, the number of unbinding events at each cluster, and the ratio of unbound to total bonds for slip bonds ($k_c^0 = 0$) to the catch-slip bond with reference values ($k_c^0 = 0.23s^{-1}$). We see that adhesions in the catch-slip bond case bear and disengage at higher forces than for the slip bond case, confirming that the typical forces on bonds are of such magnitude that the catch-slip bond nature stabilizes the junctions. Obviously, shifting to even higher values of k_c^0 would result in the unbinding of most bonds (not shown).

In Fig. 5.13B,D,F, we modify the reinforcement binding rate k_{reinf}^0 to check the influence of the reinforcement. This is different from the previous analysis where the adhesion complex density available for binding was changed, since now the binding probability based on distance is not affected (equation 5.12). However, we see the same trend of increasing stability with increasing k_{reinf}^0 (Fig. 5.13B), in line with the result obtained from varying cadherin density (Fig. 5.8C), suggesting that binding is mainly regulated by this reinforcement process. Similar to the catch/slip bond, we see that cadherin reinforcement is less important in determining gap size or lifetime (Figs. 5.13D,F) than in regulating gap opening frequency.

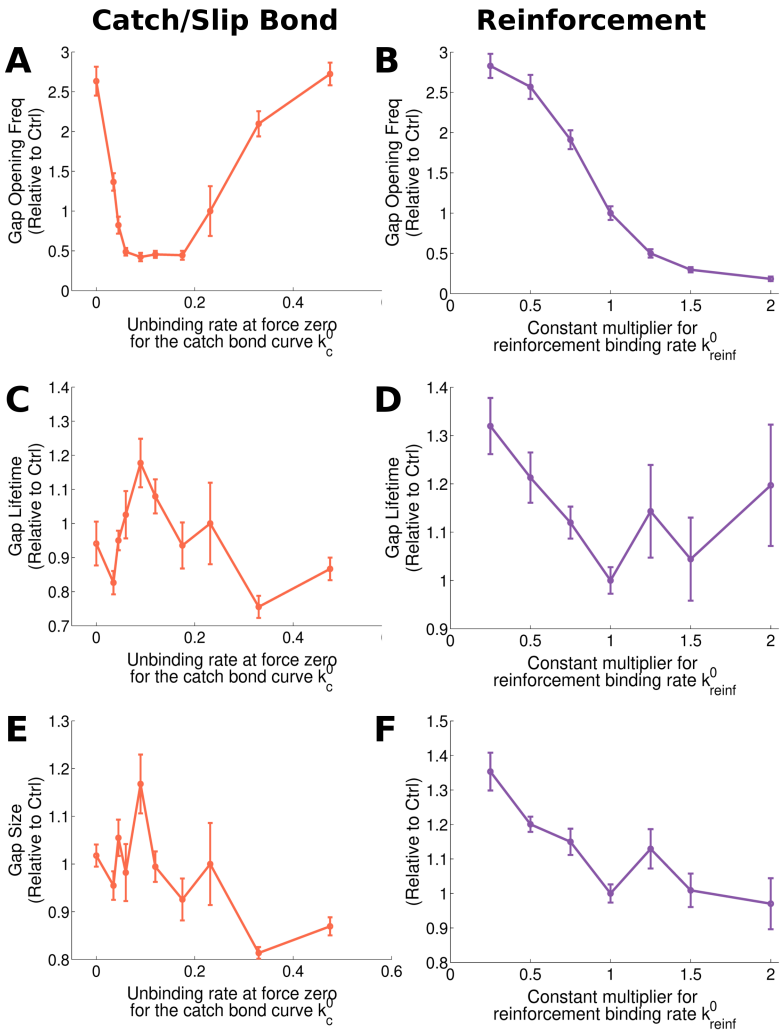

Fig. 5.13 Effect of the catch-slip vs slip bond and the cadherin reinforcement. First column shows the impact of shifting from a pure slip bond ($k_c^0 = 0$) to a catch bond. As k_c^0 increases the peak of stability moves to higher force but keeping its magnitude. Right column shows reinforcement analysis varying k_{reinf}^0. Results are normalized with reference case values and are shown for gap opening frequency (A, B), gap lifetime (C, D) and gap size(E, F). Results are the average value of a sample with $n = 30$ and error bars correspond to standard error.

5.4.6 Cell monolayer stability

Fig. 5.14 summarized some of our key conclusions: By comparing our reference case with extreme variations of very low stress fibers or membrane stiffness (more than one order of magnitude of the reference case), we see that these passive mechanical properties only slightly increase gap opening frequency (Fig. 5.14A). On the other hand, the lifetime and size of gaps increases significantly, since the softer cells are more likely to deform and adapt in response to the opened gap (Fig. 5.14B,C). In contrast, properties of the cell-cell adhesions affect the frequency of the gap openings, but less so their lifetime or size. Indeed, changing the catch-slip bond to a pure slip bond, or decreasing the density of adhesion bonds, likewise strongly increase the frequency of forming gaps (Fig. 5.14A) while only marginally affecting the size or lifetime of the gaps (Figs. 5.14B,C). This data thus summarizes our biological model where adhesion properties control the initial formation of gaps, while cell mechanical properties are critical in limiting the size and duration of opened gaps.

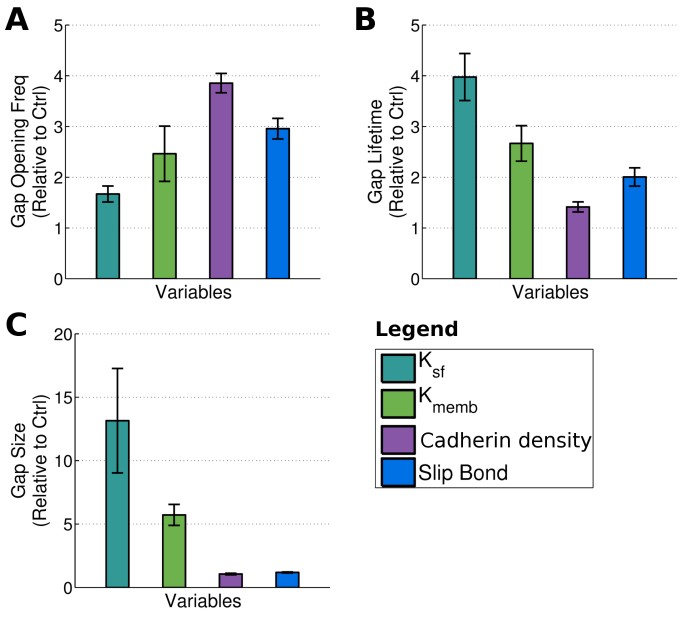

Fig. 5.14 Effect of critical variation in key parameters. Values for different parameters are highly modified to get extreme behaviors. Stiffness ($K_{sf} = 2.5 \cdot 10^{-7}$ (kg/s^2)), membrane stiffness ($K_{memb} = 5 \cdot 10^{-6}$ (kg/s^2)) and cadherin density ($\rho_{cadh} = 0.21$ $(mol/\mu m^2)$). Unbinding law is modified to show slip bond behavior ($k_c^0 = 0$ and $k_s^0 = 3.5$). (A) Gap opening frequency. (B) Average lifetime of the gaps. (C) Average size of the gaps. Results are the average value of a sample with $n = 30$ and error bars correspond to standard error.

5.5 Discussion

Extravasation is a multistage process, involving the adhesion of extravasating cells to the endothelium, the transmigration through endothelial gaps and the subsequent invasion of the underlying tissue [187]. Some works have shown intricate molecular factors that tumor or immune cells use to signal to the endothelium, enabling gap formation, here we provide evidence that the highly dynamic nature of the endothelium may play an active role in this process. We show that the endothelium dynamically generates gaps without the presence of extravasating cells, and these preferentially occur at the vertices.

The analysis made in this chapter has let us identify how the gap opening process occurs and how different cell or cell-cell adhesion properties influence it. By studying how gaps initially open, grow, stabilize and finally close, we identify which properties are important at each stage. Initial break in the cadherins binding the cells occurs as a consequence of the balance between the effect of unbinding and binding laws. When a bond ruptures, the force on that bond will be redistributed on neighboring bonds. The resulting higher force on neighboring bonds provokes the reinforcement of that bond due to the catch-bond nature, and the force-dependent cadherin clustering, leading to further active stabilization of the bonds. For the initial gap opening, a sufficiently large myosin-generated force fluctuation is thus required to provoke breakage of the union. When a region with broken adhesions appears, cell deformation starts to increase. this deformation is a consequence of the mechanical balance between the force applied and the mechanical properties of the cell. If cells are very stiff, deformation is going to be small, and therefore, the gap is not going to be able to grow. Thus, high stiffness could lead to a fast closure of the gap. If the cell is softer, the gap might grow, until the stress and the mechanical properties of the cell are balanced. As the force fluctuation disappears, the cell starts to close the gap. When the cell has recovered from the deformation caused by the force fluctuation and the membranes of two different cells are close enough, the gap finally closes.

The results presented in this chapter are consistent with previous experiments: it was observed that an increment in cell-cell junction integrity leads to less paracellular transmigration [125] and an increment of the stiffness and density of cadherins lead to less gap generation. Moreover, it is shown that changes in actin activity from the cell body to the cortex compartments resulted in higher cell-cell junction integrity and, therefore, provoked a reduction in paracellular transmigration [125]. Here, we show how a shift in contractile force from the stress fibers to the cortex results in much smaller and unstable gaps. We have also

shown that heterogeneous peak force fluctuations are crucial for gap generation. This was also in line with previous experimental observations [198].

Microvasculature is a 3D object where vessels are strongly curved and exposed to shear stresses due to the flow. That, in turn, may be affected by extravasating cells that may obstruct blood flow. Modeling of epithelial sheets in 3D has proved challenging, with some recent interesting progress after decades of mainly focusing on epithelial monolayers. Given these challenges, it was paramount to establish a 2D model of an endothelial monolayer to conduct new predictions about gap formation, which plays a critical role during cancer and inmune extravasation.

Suplementary Information

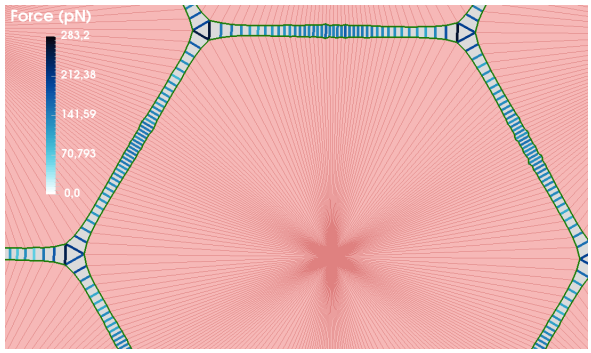

Fig. S5.1: Stress accumulates at the the vertex. This stress distribution promotes cell-cell junction failure and consequently the gap opening in the vertex positions. Color map indicates the force at the cell-cell junctions.

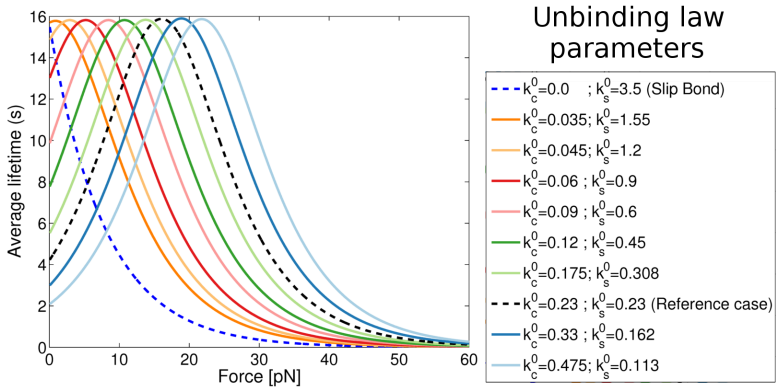

Fig. S5.2:Shift from slip to catch bond law. Lifetime average for the bond depending on the force for different unbinding laws. Legend shows the parameter variation to obtain the different curves.

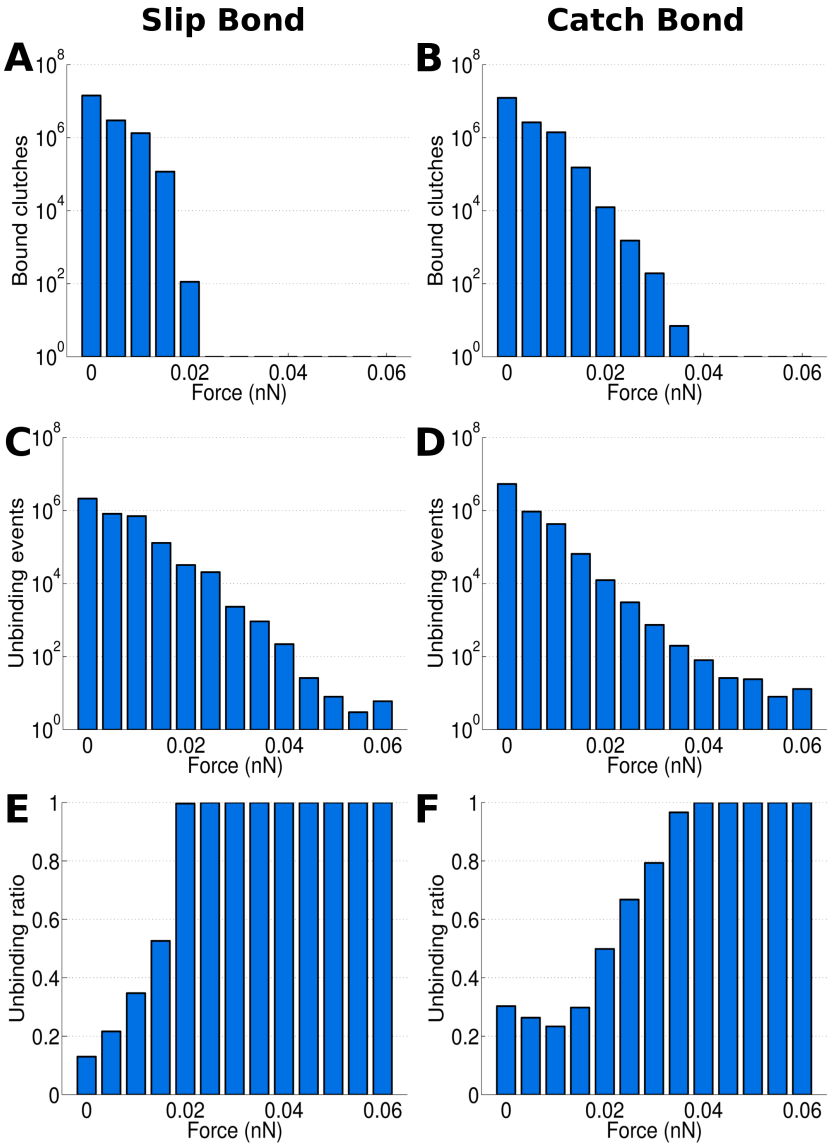

Fig. S5.3:Histogram of cadherin forces for a pure slip bond and the catch-slip bond law used as reference. First row shows force histogram of bound cadherins. Second row shows cadherins force at which cadherins unbind. Third row shows the ratio obtained by dividing unbound cadheins by the sum of unbound cadherins and bound cadherins $(ub/(ub+b))$, where ub and b corresponds to unbound and bound cadherins, respectively.

Chapter 6

Summary, conclusions and future work

In this chapter, we present a brief summary and the general conclusions of this thesis. In addition, we propose some lines for further research as a continuation of the work started in this thesis.

6.1 Summary

According to the main objectives mentioned in the first chapter of this thesis, we have developed four different computational models to investigate both cell-cell and cell-ECM interactions and to analyze the role these interactions play in different biological processes.

In Chapter 2, we have proposed a discrete computational model to simulate cell-ECM adhesions in flat substrates during filopodium retraction. This model includes an actin filament, adhesive proteins and an extracellular matrix with a spatial distribution of binding sites known as ligands. The actin filament is simulated as a rigid bar and the substrate and adhesive proteins (adhesion complexes) as deformable bars. The adhesive proteins can dynamically bind, unbind and unfold in a force-dependent manner. They bind actin monomers in the actin filament and the ligands in the substrate. Brownian dynamics are used to reproduce the free movement of the adhesion proteins in the medium when they are completely free.

We analyze how different mechanical properties of the substrate influence force transmission, actin velocity, and adhesion size. We expand the model in the Supplementary Information and add the possibility of simulating adhesion force reinforcement phenomenon.

In the third chapter, we adapt the model introduced in Chapter 2 to simulate how filopodia pull from a three-dimensional fiber. Actin filament and adhesion complexes approximations are simulated with the models described there. However, the extracellular matrix is simulated as a rigid 3D fiber able to rotate and move depending on the forces. This model allows us to study how initial orientation between the cell and matrix fiber and properties of the crosslinking proteins of the matrix fibers are crucial for the cell to be able to attach to the ECM. The model gives also insight on the importance of different aspects such as protein unfolding, ligand concentration or diameter density in the cell-ECM adhesion.

In Chapter 4, we modify the model from Chapter 2 to simulate a whole cell and to measure the level of durotaxis that one single cell or a group of cells express in different scenarios. This model combines both cell-ECM and cell-cell interactions. All the elements in the model are simulated as truss elements. Cells are bars that have a contractile part in the center, and two adhesive zones at both sides of the contractile zone where the actin monomers are placed. Finally, they have two protrusive zones at both ends of the cell where the cell grows and polymerizes. We implement substrates with different rigidity gradients in order to simulate durotaxis phenomenon. Cells can also be placed alone or bound to each other with cadherin proteins forming a monolayer. In this way, we can simulate both single and collective cell migration. We propose a force balance mechanism between both ends of the cell to explain durotaxis. We employ the model to observe the differences between single and collective cell migration and show how different conditions like myosin forces, monolayer size or adhesion level influence durotaxis.

In the fifth chapter, we develop a different discrete model to simulate cell-cell adhesion failure and the consequent gap generation in an endothelial monolayer. We propose an agent-based model where cells are simulated as 2D objects formed by membrane and stress fibers bars. We employ Kelvin-Voigt elements to simulate both stress fibers and membrane structures. Cells bind to each other through cadherin complexes. These cadherins dynamically bind and unbind, in the same way that adhesions complexes did in the previous models. This model allows us to identify the frequency, location, size and lifetime of gaps that are generated as a consequence of adhesion rupture. Morover, it offers the possibility of identifying how different parameters such as cell mechanical properties, myosin generated

forces, unbinding characteristics and cadherin density influence gap generation, propagation, stabilization, and seal.

6.2 General conclusions

Here we summarize the main conclusions extracted from this thesis for the different scenarios studied with the proposed models:

- Mechanical properties of the substrate critically influence cell-ECM adhesion and force transmission.
- Adhesion reinforcement is critical for force transmission and adhesion maturation at high stiffness gradients.
- Orientation between the cell actin filaments and the matrix fiber is crucial for establishing strong adhesions.
- Different aspects like deformable crosslinking proteins, higher ligand densities or protein unfolding are crucial in promoting the alignment between the cell and the matrix fiber.
- Collective cell durotaxis is more effective than single cell durotaxis. Cells establish a collaboration when they move collectively that allows them to sense higher rigidity changes than when they move isolated. In the same way, gels with steeper gradients exhibit higher levels of durotaxis, whereas cells placed in gels without stiffness gradients do not show durotaxis.
- Cells exhibit higher levels of durotaxis when force transmission is promoted by increasing ligand density or myosin activity.
- Cells open gaps preferably at a three cell vertex than at a two cell interface.
- Mechanical properties of the cell are crucial in regulating gap propagation and size.
- Balance between binding and unbinding rates regulate initial gap formation.
- Large myosin force fluctuations are needed to promote unbinding over binding and initially generate the gap. These forces fluctuations also cause cell deformation leading to larger gap generation.

6.3 Future work

Here, we propose some lines of future work to continue with the work started in this thesis.

- Simulate a full 2D substrate with the finite element method with the aim of reproducing with high accuracy how forces are distributed between the adhesion complexes during actin retraction. Incorporate actin filament and adhesion complexes that dynamically bind and unbind with the 2D substrate to simulate the same process of Chapter 2 (see Fig. 6.1).

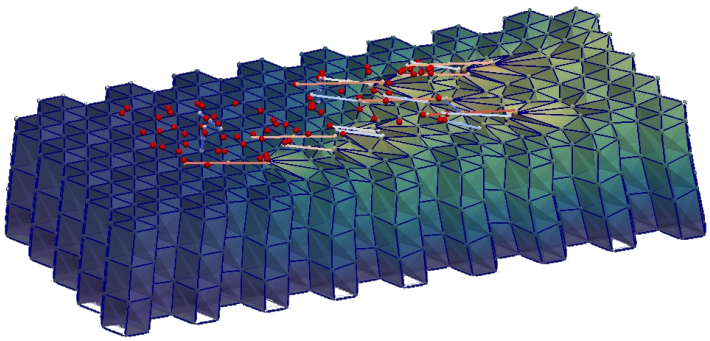

Fig. 6.1 Cell-ECM adhesion formation during actin retrograde flow. Model proposed for cell-ECM adhesion formation over a 2D substrate simulated with finite element method. Actin monomers are in red. ACs bind to the the ECM and pull from the substrate causinng its deformation.

- Include more matrix fibers and simulate how a cell would adhere to them. This improvement would offer the possibility of analyzing the role of different parameters that define the matrix architecture (fiber density and orientation, pore confinement and connectivity) in 3D cell migration.

- Study the effect of the extracellular matrix in the gap generation formation.

- Include cells that extravasate the monolayer. Cells could also exert some force to help in the gap opening process and migrate through it.

- Include a third dimension to the model to simulate a 3D vascular vein to study how curvature may influence monolayer integrity (Fig. 6.2).

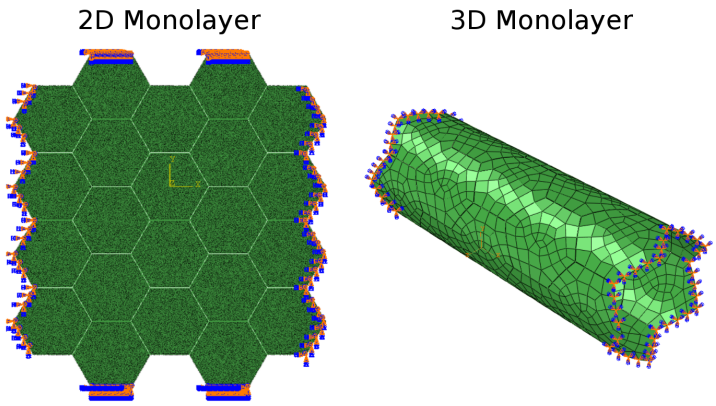

Fig. 6.2 Cell monolayer forming a vascular vein. 2D monolayer (left) and the same monolayer forming a vascular vein in 3D (right).

Appendix A

Contributions and funding

A.1 Articles in peer-review journals

Published work:

- Escribano, J., Sunyer, R., Sánchez, M.T., Trepat, X., Roca-Cusachs, P., and García-Aznar, J.M. (2018). A hybrid computational model for collective cell durotaxis. Biomechanics and Modeling in Mechanobiology. doi: 10.1007/s10237-018-1010-2
- Oria, R., Wiegand, T., Escribano, J., Elosegui-Artola, A., Uriarte, J.J., Moreno-Pulido, C., Platzman, I., Delcanale, P., Albertazzi, L., Navajas, D., Trepat, X., García-Aznar, J. M., Cavalcanti-Adam, E.A., and Roca-Cusachs, P. (2017). Force loading explains spatial sensing of ligands by cells. Nature. doi: 10.1038/nature24662
- Sunyer, R., Conte, V., Escribano, J., Elosegui-Artola, A., Labernadie, A., Valon, L., Navajas, D., Garcia-Aznar, J. M., Munoz, J. J., Roca-Cusachs, P., and Trepat, X. (2016). Collective cell durotaxis emerges from long-range intercellular force transmission. Science, 353(6304):1157–1161. doi: 10.5061/dryad.r8h3n
- Escribano J., Sanchez M.T., Garcıa-Aznar J.M. (2015) Modeling the formation of cell-matrix adhesions in 3D matrices. J Theor Biol 384:84–94. doi: 10.1016/j.jtbi.2015.07.015

- Escribano J., Sánchez M.T., García-Aznar J.M. (2014) A discrete approach for modeling cell–matrix adhesions. Comput Part Mech 1:117–130. doi: 10.1007/s40571-014-0006-7

In preparation:

- Escribano, J., Chen, M.B., Moeendarbary, E., Spill F., García-Aznar, J.M. and Kamm R.D. (2018). Balance of Mechanical Forces Drive Endothelial Gap Formation and Facilitate Cancer and Immune-Cell Extravasation.

A.2 Conferences

A.2.1 Oral presentation

- Discrete modeling of focal adhesions under different substrate conditions.III National Spanish chapter of the European Society of Biomechanics. J. Escribano, MT Sánchez, J.M. García Aznar. October 2013. Barcelona
- Modeling cell-matrix adhesions at different scales. VII World Congress of Biomechanics (WCB). J.M. García Aznar, J. Escribano, M. Cóndor, MT Sánchez. July 2014. Boston.
- Modeling the mechanics of cell locomotion.XI Congreso Mundial en Mecánica Computacional (WCCM). J.M. García Aznar, C. Borao, T. Rüberg, J. Escribano, M. Cóndor, MT Sánchez, R.D. Kamm. July 2014. Barcelona.
- 3D discrete modeling of cell-ECM adhesion.6th European Cell Mechanics Meeting "CellMech 2015". Jorge Escribano, Roger Oria, M.T. Sánchez, Pere Roca-Cusachs and JM García-Aznar. May 2015. Barcelona
- Discrete modeling of focal adhesions during filopodium retraction. 4th International Conference on Particle-Based Methods. J.M. García-Aznar, Jorge Escribano, Roger Oria, MT Sánchez and Pere Roca-Cusach. September 2015. Barcelona

A.2.2 Poster presentation

- Hybrid computational modeling of collective cell durotaxis. Jorge Escribano, Raimon Sunyer, María Teresa Sánchez, Xavier Trepat, Pere Roca-Cusachs, José Manuel García-

Aznar. The American Society for Cell Biology (ASCB) Annual meeting . December 2016. San Francisco, California (EEUU).

- Discrete modeling of collective migration under ECM stiffness gradients. Jorge Escribano, Raimon Sunyer, María Teresa Sánchez, Xavier Trepat, Pere Roca-Cusachs, José Manuel García-Aznar. The 7th European Meeting on Cellular Mechanics. June 2017. Lake Windermere (UK)

A.3 Collaborations

We have made collaborations with different groups during this thesis. With Xavier Trepat and Pere Roca Cusachs from the Institute for Bioengineering of Catalonia (IBEC), with Taeyoon Kim from Purdue University and Roger D. Kamm and Fabian Spill from the Massachusetts Institute of Technology (MIT).

With Pere Roca and Xavier Trepat we have collaborated throughout the full duration of this thesis. We have developed different models of cell-ECM adhesion and cell migration under stiffness gradients to reproduce experimental results that have been made in their laboratories. Three of the publications mentioned above were made as a consequence of this collaboration. I also did a short stay (for one week) in Pere Roca´s Lab at the IBEC founded by Spanish Mechanobiology Network.

I did a research stay during four months at Purdue University at Taeyoon Kim´s lab. During this stay, I studied 3D cell migration using a complex agent-based model developed in that lab. Although, the work I did there has not been directly included in this thesis, everything I learned there has helped to improve the quality of this thesis.

I did the last research stay for another four months at Roger Kamm´s Lab in the Massachusetts Institute of Technology (MIT). Chapter 5 of this thesis corresponds to the work done during that stay. A journal article that includes the model and some experimental results made in Kamm´s lab by other researchers is currently in preparation.

A.4 Funding

This thesis is supported by the Spanish Ministry of Economy and Competitiveness/FEDER. Proyect code: DPI2012-38090-C03-01. Reference FPI: BES-2013-063684.

Appendix B

Resumen y conclusiones

B.1 Resumen

Las propiedades químicas y físicas del medio ambiente regulan diversos procesos como la diferenciación celular, la proliferación o la apoptosis. Las células necesitan adaptarse rápidamente a las características ambientales para poder moverse. Éstas son capaces de sentir las propiedades de su entorno mediante la formación de adhesiones y la transmisión de fuerza a través de ellas. La interacción entre la célula y la matriz extracelular (ECM) está mediada por adhesiones focales (FA) o complejos focales que presentan una alta concentración de los receptores de adhesión de la familia de las integrinas. Las células también interactúan con otras células a través de diferentes estructuras adhesivas como uniones adherentes, que también contienen altos niveles de otros receptores transmembrana conocidos como cadherinas. Estas adhesiones de células-ECM y célula-célula son cruciales en los procesos mecano sensores, siendo responsables de la transmisión de las fuerzas generadas por las células a su entorno y participando en la transducción de señales mecánicas en señales bioquímicas. La influencia de estas estructuras adhesivas en el movimiento celular es crucial. Las células las utilizan para sentir su entorno, reorganizar su estructura y ejercer las fuerzas necesarias para su movimiento. Además, el movimiento y la forma de las células varían significativamente dependiendo de la rigidez de los sustratos o de si la migración ocurre en sustratos planos o matrices tridimensionales. La presencia de otras células también tiene un impacto importante en la migración. Cuando las células se mueven colectivamente, se

forma una colaboración entre ellas (a través de las adhesiones célula-célula) para lograr una migración más eficiente. La estabilidad de la unión célula-célula en algunas monocapas celulares, como el endotelio, es crucial durante diversos procesos, incluyendo la inflamación y la metástasis del cáncer. La ruptura de las adhesiones provoca la formación de huecos que pueden permitir que las células inmunes o cancerosas transmigren a través del endotelio.

En esta tesis, se estudia, desde un punto de vista mecánico, el papel de estas diferentes estructuras de adhesión en diversos procesos como la migración celular o la integridad de la unión de células endoteliales. Este trabajo se centra en cómo las propiedades mecánicas del entorno influyen en la formación de la adhesión y la transmisión de fuerzas. Para lograr este objetivo, se diseñan cuatro modelos computacionales diferentes para simular el proceso de transmisión de fuerza a través de las adhesiones célula-matriz o célula-célula en diferentes escenarios y estudiar el comportamiento emergente del sistema en cada caso.

En el capítulo 2, se ha propuesto un modelo computacional discreto para simular las adhesiones de ECM-célula en sustratos planos durante la retracción de un filopodio. Este modelo incluye un filamento de actina, proteínas adhesivas y una matriz extracelular con una distribución espacial de los sitios de unión, también conocidos como ligandos. El filamento de actina se simula como una barra rígida, y el sustrato y las proteínas adhesivas (complejos de adhesión) como barras deformables. Los complejos de adhesión se pueden unir, desacoplar y desplegar de forma dinámica dependiendo de la fuerza que soportan. Son ellos los que unen los monómeros del filamento de actina con los ligandos en el sustrato. Para reproducir el movimiento por el medio de los complejos de adhesión que se encuentran completamente libres se utiliza dinámica Browniana. El objetivo de este modelo es estudiar cómo las diferentes propiedades mecánicas del sustrato influyen en la transmisión de fuerza, la velocidad de actina y el tamaño de adhesión. A su vez, este modelo se amplía en el material suplementario añadiendo la posibilidad de simular el fenómeno de refuerzo de la adhesión.

En el tercer capítulo, se adapta el modelo del capítulo anterior para simular el proceso de retracción de una protusión adherida a una fibra tridimensional de la matriz extracelular. La simulación de las protusiones de actina y de los complejos de adhesión se realizan con los modelos del capítulo 2. Sin embargo, la matriz extracelular se simula como una fibra en tres dimensiones, rígida y que es capaz de rotar y moverse en función de las fuerzas a las que está sujeta y de las propiedades mecánicas de la unión entre distintas fibras. Este modelo permite estudiar cómo la orientación inicial entre la célula y la fibra matricial y las propiedades de las proteínas reticuladas de las fibras matriciales son cruciales para que la célula pueda unirse a la matriz. El modelo también pone de manifiesto la importancia de diferentes aspectos como

el despliegue de proteínas, la concentración o densidad de ligandos y el diámetro de la fibra en la adhesión célula-matriz.

En el capítulo 4, se modifica el modelo del capítulo 2 y se simula una célula completa para medir el nivel de durotaxis que una sola célula o un grupo de células muestran en diferentes condiciones. Este modelo combina ambas interacciones: célula-ECM y célula-célula. Todos los elementos del modelo se simulan como elementos barra con propiedades elástico lineales. Las células son barras que tienen una parte contráctil en el centro de la célula y dos zonas adhesivas a ambos lados de la zona contráctil donde se colocan los monómeros de actina. Finalmente, tienen dos zonas protrusivas en ambos extremos de la célula donde la célula crece y polimeriza. Se implementan sustratos con diferentes gradientes de rigidez para simular el fenómeno de durotaxis. Las células también pueden colocarse solas o unidas entre sí formando una monocapa con proteínas de cadherina. De esta manera, se puede simular tanto la migración celular individual como la colectiva. Se propone un mecanismo de equilibrio de fuerza entre ambos extremos de la célula para explicar el fenómeno de durotaxis. Posteriormente, el modelo se emplea para observar las diferencias entre la migración celular individual y colectiva y para observar cómo diferentes condiciones como las fuerzas de la miosina, el tamaño de la monocapa o el nivel de adhesión influyen en el proceso de durotaxis.

En el quinto capítulo, se propone un modelo discreto, diferente a los anteriores, para simular la ruptura de la adhesión célula-célula y la consiguiente generación de huecos en una monocapa endotelial. Se propone un modelo basado en agentes donde las células son simuladas como objetos 2D formados por dos tipos de barras que representan la membrana y las fibras de esfuerzo. Se utilizan elementos Kelvin-Voigt para simular tanto fibras de esfuerzo como estructuras de membrana. Las células se unen entre sí a través de complejos de cadherina. Estas cadherinas se unen y separan dinámicamente, de la misma manera que lo hacían los complejos de adhesión en los modelos anteriores. Este modelo permite identificar la frecuencia, ubicación, tamaño y vida de los huecos que se generan como consecuencia de la ruptura las adhesiones. Además, ofrece la posibilidad de identificar cómo diferentes factores como las propiedades mecánicas de las células, las fuerzas generadas por la miosina, las características de las uniones y la densidad de cadherinas influyen en la generación de los huecos, su propagación, estabilización y finalmente sellado de los mismos.

B.2 Conclusiones

Se ha demostrado cómo las propiedades mecánicas del sustrato influyen de forma crítica en la adhesión célula-ECM. Para sustratos blandos, las fuerzas transmitidas son menores y, por lo tanto, la velocidad de retroceso de actina es alta. A medida que el sustrato se vuelve más rígido, los complejos de adhesión comienzan a soportar más carga y el tamaño de adhesión y las fuerzas aumentan. Todo esto se refleja en la caída de la velocidad de actina. Hay un punto en el que, si la rigidez del sustrato sigue aumentando, debido a las altas cargas, las adhesiones se separan más rápido de lo que se unen. Esto causa un fallo general en la adhesión que resulta en un incremento en la velocidad de actina. Se sabe a través de otros trabajos que a altas rigideces del sustrato, esta caída en la velocidad no ocurre. De hecho, el tamaño de adhesión y las fuerzas crecen provocando el efecto contrario. Esto está relacionado con un fenómeno de refuerzo de la adhesión que sólo ocurre en sustratos rígidos. Al incluir este refuerzo como un incremento de la probabilidad de unión provocada al traspasar un umbral de fuerza y se observa cómo el modelo es capaz de reproducir los resultados encontrados en la bibliografía. A pesar de las mejoras, el modelo presenta algunas limitaciones en cómo se distribuyen las fuerzas entre los diferentes complejos de adhesión. Dichas limitaciones son causadas por la naturaleza unidimensional del sustrato. A pesar de estas limitaciones, el modelo es capaz de simular la respuesta global del sistema a las diferentes condiciones de rigidez del sustrato. El modelo no sólo es capaz de predecir el nivel de fuerza en la adhesión célula-ECM, sino que también nos sirve de base para crear algunos de los modelos propuestos en esta tesis.

Posteriormente se ha reproducido el mismo fenómeno descrito anteriormente, pero en una matriz 3D en lugar de sobre un sustrato plano. Este nuevo modelo permite conocer los diferentes aspectos que son importantes para la formación de la adhesión en estas condiciones. Se estudia cómo la orientación entre los filamentos de actina celular y la fibra matricial es crucial para establecer adhesiones fuertes. Además, se observa cómo diferentes aspectos como las propiedades de las proteínas reticulares que unen distintas fibras, la densidad de ligandos, el despliegue de los complejos de adhesión son cruciales para establecer la adhesión y favorecer el alineamiento entre la célula y la fibra de la matriz.

También se ha estudiado la durotaxis celular en sustratos 2D para la migración celular individual y colectiva. El modelo muestra que las células se mueven preferiblemente hacia la parte más rígida de los geles y que la migración colectiva es más efectiva que la migración unicelular. Cuando las células se mueven colectivamente, unen sus fuerzas y sólo las que se encuentran en los bordes de la monocapa establecen adhesiones y ejercen fuerzas sobre

el sustrato. Esto permite que la monocapa detecte una mayor diferencia de rigidez. El movimiento está regulado por la diferencia de rigidez del sustrato en ambos extremos de la monocapa, que se detecta por la transmisión de fuerza a través de las adhesiones célula-ECM. Las células individuales son capaces de sentir menos parte del gradiente que varias células juntas, de modo que a medida que la monocapa se hace más grande, el movimiento es más eficiente. De la misma manera, los geles con gradientes menos pronunciados presentan menos migración que los geles con gradientes más marcados, y en los geles sin gradiente de rigidez, las células no muestran durotaxis. Además, se demuestra que al favorecer la transmisión de fuerzas, bien incrementando la densidad de ligandos o promoviendo la actividad de la miosina, las células exhiben niveles más altos de durotaxis.

En el último modelo propuesto, se analiza la formación de huecos en una monocapa endotelial. El modelo permite observar que los huecos se generan en los vértices entre tres o más células con más frecuencia que entre dos células. Posteriormente se estudia cómo los huecos se abren, crecen, estabilizan y finalmente se cierran, analizando qué propiedades son importantes en cada una de estas etapas. Se observa que la ruptura inicial en la unión de las células se produce como consecuencia del equilibrio entre la velocidad de formación y la velocidad de ruptura de adhesiones. Cuando una unión se rompe, la fuerza de esa unión se redistribuirá entre las uniones vecinas. El incremento de fuerza resultante sobre las uniones vecinas reforzará dichas uniones, y la agrupación de cadherinas, que depende de la fuerza conducirá al refuerzo y estabilización de las uniones. Para la apertura inicial del hueco, se requiere una fluctuación de la fuerza generada por la miosina lo suficientemente grande como para provocar la rotura de la unión. Una vez que hay una región donde las uniones se rompen, la deformación de la célula comienza a aumentar. La deformación es consecuencia del equilibrio mecánico entre la fuerza aplicada y las propiedades mecánicas de la célula. Si las células son muy rígidas, la deformación va a ser pequeña, y por lo tanto, la brecha no va a poder crecer. Por lo tanto, una alta rigidez puede llevar a un rápido cierre del hueco. Si la célula es menos rígida, el espacio puede crecer más, hasta que se aplica una fuerza y se equilibran las propiedades mecánicas de la célula. A medida que la fluctuación de la fuerza desaparece, la célula comienza a cerrar el hueco. Cuando la célula se ha recuperado de la deformación causada por la fluctuación de la fuerza y la membrana entre las dos células se acerca lo suficiente, el espacio finalmente se cierra.

References

[1] Abbey, C. a. and Bayless, K. J. (2014). Matrix density alters zyxin phosphorylation, which limits peripheral process formation and extension in endothelial cells invading 3D collagen matrices. *Matrix biology : journal of the International Society for Matrix Biology*, 38:36–47.

[2] Abe, K. and Takeichi, M. (2008). EPLIN mediates linkage of the cadherin–catenin complex to F-actin and stabilizes the circumferential actin belt. *Proceedings of the National Academy of Sciences*, 105(1):13–19.

[3] Abu Taha, A. and Schnittler, H.-J. (2014). Dynamics between actin and the VE-cadherin/catenin complex. *Cell Adhesion & Migration*, 8(2):125–135.

[4] Alberts, B., Johnson, A., Lewis, J., Raff, M., Roberts, K., and Walter, P. (2008). *Molecular Biology of the Cell, Fifth Edition*.

[5] Alessandri, K., Sarangi, B. R., Gurchenkov, V. V., Sinha, B., Kießling, T. R., Fetler, L., Rico, F., Scheuring, S., Lamaze, C., Simon, A., Geraldo, S., Vignjevic, D., Doméjean, H., Rolland, L., Funfak, A., Bibette, J., Bremond, N., and Nassoy, P. (2013). Cellular capsules as a tool for multicellular spheroid production and for investigating the mechanics of tumor progression in vitro. *Proceedings of the National Academy of Sciences of the United States of America*, 110(37):14843–8.

[6] Allena, R., Scianna, M., and Preziosi, L. (2016). A Cellular Potts Model of single cell migration in presence of durotaxis. *Mathematical Biosciences*, 275:57–70.

[7] Allingham, M. J., van Buul, J. D., and Burridge, K. (2007). ICAM-1-Mediated, Src- and Pyk2-Dependent Vascular Endothelial Cadherin Tyrosine Phosphorylation Is Required for Leukocyte Transendothelial Migration. *The Journal of Immunology*, 179(6):4053–4064.

[8] Aman, A. and Piotrowski, T. (2010). Cell migration during morphogenesis. *Developmental Biology*, 341(1):20–33.

[9] Ananthakrishnan, R. and Ehrlicher, A. (2007). The forces behind cell movement. *International Journal of Biological Sciences*, 3(5):303–317.

[10] Ando, K., Fukuhara, S., Moriya, T., Obara, Y., Nakahata, N., and Mochizuki, N. (2013). Rap1 potentiates endothelial cell junctions by spatially controlling myosin ii activity and actin organization. *J Cell Biol*, pages jcb–201301115.

[11] Balaban, N. Q., Schwarz, U. S., Riveline, D., Goichberg, P., Tzur, G., Sabanay, I., Mahalu, D., Safran, S., Bershadsky, A., Addadi, L., and Geiger, B. (2001). Force and focal adhesion assembly: a close relationship studied using elastic micropatterened substrates. *Nature Cell Biol.*, 3(May):466–472.

[12] Baluk, P., Hashizume, H., and McDonald, D. M. (2005). Cellular abnormalities of blood vessels as targets in cancer. *Current Opinion in Genetics & Development*, 15(1):102–111.

[13] Bao, G. (2002). Mechanics of biomolecules. *Journal of the Mechanics and Physics of Solids*, 50(11):2237–2274.

[14] Barry, A. K., Wang, N., and Leckband, D. E. (2015). Local VE-cadherin mechanotransduction triggers long-ranged remodeling of endothelial monolayers. *Journal of Cell Science*, 128(7):1341–1351.

[15] Bausch, A. R. and Schwarz, U. S. (2013). Cellular mechanosensing: Sharing the force. *Nature materials*, 12(11):948–9.

[16] Bazzoni, G. (2004). Endothelial Cell-to-Cell Junctions: Molecular Organization and Role in Vascular Homeostasis. *Physiological Reviews*, 84(3):869–901.

[17] Bechara, A., Nawabi, H., Moret, F., Yaron, A., Weaver, E., Bozon, M., Abouzid, K., Guan, J.-L., Tessier-Lavigne, M., Lemmon, V., and Castellani, V. (2008). FAK-MAPK-dependent adhesion disassembly downstream of L1 contributes to semaphorin3A-induced collapse. *The EMBO journal*, 27(11):1549–62.

[18] Bell, G. (1978). Models for the specific adhesion of cells to cells. *Science*, 200(4342):618–627.

[19] Boal, D. (2012). *Mechanics of the Cell*. Cambridge University Press, 2 edition.

[20] Bonet, J. and Wood, R. D. (2008). *Nonlinear Continuum Mechanics for Finite Element Analysis*. Cambridge University Press.

[21] Bookholt, F. D., Monsuur, H. N., Gibbs, S., and Vermolen, F. J. (2016). Mathematical modelling of angiogenesis using continuous cell-based models. *Biomechanics and Modeling in Mechanobiology*, 15(6):1577–1600.

[22] Boon, W. M., Koppenol, D. C., and Vermolen, F. J. (2016). A multi-agent cell-based model for wound contraction. *Journal of Biomechanics*, 49(8):1388–1401.

[23] Borm, B., Requardt, R. P., Herzog, V., and Kirfel, G. (2005). Membrane ruffles in cell migration: indicators of inefficient lamellipodia adhesion and compartments of actin filament reorganization. *Experimental cell research*, 302(1):83–95.

[24] Brandt, A. (1977). Multi-Level Adaptive Solutions to Boundary-Value Problems. *Mathematics of Computation*, 31(138):333.

[25] Brieher, W. M. and Yap, A. S. (2013). Cadherin junctions and their cytoskeleton(s). *Current Opinion in Cell Biology*, 25(1):39–46.

[26] Burns, A. R., Walker, D. C., Brown, E. S., Thurmon, L. T., Bowden, R. A., Keese, C. R., Simon, S. I., Entman, M. L., and Smith, C. W. (1997). Neutrophil transendothelial migration is independent of tight junctions and occurs preferentially at tricellular corners. *The Journal of Immunology*, 159(6):2893–2903.

[27] Caflisch, A. and Paci, E. (2005). Molecular dynamics simulations to study protein folding and unfolding. In Buchner, J. and Kiefhaber, T., editors, *Protein Folding Handbook*, volume 05, chapter 32, pages 1143–1169. Wiley-VCH.

[28] Camley, B. and Rappel, W.-J. (2017). Physical models of collective cell motility: from cell to tissue. *Journal of Physics D: Applied Physics*, at press:h.

[29] Camley, B. A., Zhang, Y., Zhao, Y., Li, B., Ben-Jacob, E., Levine, H., and Rappel, W.-J. (2014). Polarity mechanisms such as contact inhibition of locomotion regulate persistent rotational motion of mammalian cells on micropatterns. *Proceedings of the National Academy of Sciences*, 111(41):14770–14775.

[30] Cao, X., Moeendarbary, E., Isermann, P., Davidson, P. M., Wang, X., Chen, M. B., Burkart, A. K., Lammerding, J., Kamm, R. D., and Shenoy, V. B. (2016). A chemomechanical model for nuclear morphology and stresses during cell transendothelial migration. *Biophysical Journal*, 111(7):1541 – 1552.

[31] Carlsson, A. E. (2003). Growth velocities of branched actin networks. *Biophysical journal*, 84(5):2907–18.

[32] Case, L. B., Baird, M. a., Shtengel, G., Campbell, S. L., Hess, H. F., Davidson, M. W., and Waterman, C. M. (2015). Molecular mechanism of vinculin activation and nanoscale spatial organization in focal adhesions. *Nature cell biology*, (April).

[33] Case, L. B. and Waterman, C. M. (2015). Integration of actin dynamics and cell adhesion by a three-dimensional, mechanosensitive molecular clutch. *Nature Cell Biology*, 17(8):955–963.

[34] Chan, C. E. and Odde, D. J. (2008). Traction Dynamics of Filopodia on Compliant Substrates. *Science (New York, N.Y.)*, 322(December):1687–1691.

[35] Chen, J., Newhall, J., Xie, Z. R., Leckband, D., and Wu, Y. (2016). A Computational Model for Kinetic Studies of Cadherin Binding and Clustering. *Biophysical Journal*, 111(7):1507–1518.

[36] Chen, J., Weihs, D., and Vermolen, F. J. (2017). A model for cell migration in non-isotropic fibrin networks with an application to pancreatic tumor islets. *Biomechanics and Modeling in Mechanobiology*, pages 1–20.

[37] Chen, L., Vicente-Manzanares, M., Potvin-Trottier, L., Wiseman, P. W., and Horwitz, A. R. (2012). The integrin-ligand interaction regulates adhesion and migration through a molecular clutch. *PloS one*, 7(7):e40202.

[38] Chen, W. T. and Singer, S. J. (1982). Immunoelectron microscopic studies of the sites of cell-substratum and cell-cell contacts in cultured fibroblasts. *The Journal of cell biology*, 95(1):205–22.

[39] Cherry, J. L. and Adler, F. R. (2000). How to make a Biological Switch. *Journal of Theoretical Biology*, 203(2):117–133.

[40] Choi, C. K., Vicente-manzanares, M., Zareno, J., Leanna, A., Mogilner, A., Horwitz, A. R., and Engineering, B. (2008). Actin and α-actinin orchestrate the assembly and maturation of nascent adhesions in a myosin II motor-independent manner. *Nature cell biology*, 10(9):1039–1050.

[41] Christopher R. Jacobs, Hayden Huang, R. Y. K. (2012). *Introduction to Cell Mechanics and Mechanobiology*, volume 16.

[42] Chtcheglova, L. A., Wildling, L., Waschke, J., Drenckhahn, D., and Hinterdorfer, P. (2010). AFM functional imaging on vascular endothelial cells. *Journal of Molecular Recognition*, 23(6):589–596.

[43] Cirit, M., Krajcovic, M., Choi, C. K., Welf, E. S., Horwitz, A. F., and Haugh, J. M. (2010). Stochastic model of integrin-mediated signaling and adhesion dynamics at the leading edges of migrating cells. *PLoS computational biology*, 6(2):e1000688.

[44] Cochet-Escartin, O., Ranft, J., Silberzan, P., and Marcq, P. (2014). Border forces and friction control epithelial closure dynamics. *Biophysical Journal*, 106(1):65–73.

[45] Collins, J. J., Gardner, T. S., and Cantor, C. R. (2000). Construction of a genetic toggle switch in Escherichia coli. *Nature*, 403(6767):339–342.

[46] Condor, M. and Garcia-Aznar, J. M. (2017). A phenomenological cohesive model for the macroscopic simulation of cell-matrix adhesions. *Biomechanics and Modeling in Mechanobiology*, pages 1–18.

[47] Critchley, D. R. (2000). Focal adhesions - the cytoskeletal connection. *Current opinion in cell biology*, 12(1):133–9.

[48] De Pascalis, C. and Etienne-Manneville, S. (2017). Single and collective cell migration: the mechanics of adhesions. *Molecular Biology of the Cell*, 28(14):1833–1846.

[49] Dejana, E. and Orsenigo, F. (2013). Endothelial adherens junctions at a glance. *Journal of Cell Science*, 126(12):2545–2549.

[50] Dejana, E., Tournier-Lasserve, E., and Weinstein, B. M. (2009). The Control of Vascular Integrity by Endothelial Cell Junctions: Molecular Basis and Pathological Implications. *Developmental Cell*, 16(2):209–221.

[51] Del Amo, C., Borau, C., Movilla, N., Asín, J., and García-Aznar, J. M. (2017). Quantifying 3D chemotaxis in microfluidic-based chips with step gradients of collagen hydrogel concentrations. *Integr. Biol.*, 9(4):339–349.

[52] Deshpande, V., Mrksich, M., Mcmeeking, R., and Evans, A. (2008). A bio-mechanical model for coupling cell contractility with focal adhesion formation. *Journal of the Mechanics and Physics of Solids*, 56(4):1484–1510.

[53] Discher, D. E., Janmey, P., and Wang, Y.-L. (2005a). Tissue cells feel and respond to the stiffness of their substrate. *Science (New York, N.Y.)*, 310(5751):1139–43.

[54] Discher, D. E., Janmey, P., and Wang, Y.-l. (2005b). Tissue Cells Feel and Respond to the Stiffness of Their Substrate. *Science*, 310(5751):1139 LP – 1143.

[55] Dokukina, I. V. and Gracheva, M. E. (2010). A model of fibroblast motility on substrates with different rigidities. *Biophysical Journal*, 98(12):2794–2803.

[56] Dorland, Y. L. and Huveneers, S. (2017). Cell–cell junctional mechanotransduction in endothelial remodeling. *Cellular and Molecular Life Sciences*, 74(2):279–292.

[57] Dorn, J. F., Zhang, L., Phi, T.-T., Lacroix, B., Maddox, P. S., Liu, J., and Maddox, A. S. (2016). A theoretical model of cytokinesis implicates feedback between membrane curvature and cytoskeletal organization in asymmetric cytokinetic furrowing. *Molecular Biology of the Cell*, 27(8):1286–1299.

[58] Doyle, A. D., Petrie, R. J., Kutys, M. L., and Yamada, K. M. (2013). NIH Public Access. *Current opinion in cell biology*, 25(5):642–649.

[59] Doyle, P. S., Shaqfeh, E. S. G., and Gast, A. P. (1997). Dynamic simulation of freely draining flexible polymers in steady linear flows. *Journal of Fluid Mechanics*, 334:251–291.

[60] Drasdo, D. and Hoehme, S. (2012). Modeling the impact of granular embedding media, and pulling versus pushing cells on growing cell clones. *New Journal of Physics*, 14.

[61] Drees, F., Pokutta, S., Yamada, S., Nelson, W. J., and Weis, W. I. (2005). α-Catenin Is a Molecular Switch that Binds E-Cadherin-β-Catenin and Regulates Actin-Filament Assembly. *Cell*, 123(5):903–915.

[62] Elosegui-Artola, A., Bazellières, E., Allen, M. D., Andreu, I., Oria, R., Sunyer, R., Gomm, J. J., Marshall, J. F., Jones, J. L., Trepat, X., and Roca-Cusachs, P. (2014). Rigidity sensing and adaptation through regulation of integrin types. *Nature materials*, 13(6):631–7.

[63] Elosegui-Artola, A., Oria, R., Chen, Y., Kosmalska, A., Pérez-González, C., Castro, N., Zhu, C., Trepat, X., and Roca-Cusachs, P. (2016). Mechanical regulation of a molecular clutch defines force transmission and transduction in response to matrix rigidity. *Nature Cell Biology*, 18(5):540–548.

[64] Engler, A. J., Sen, S., Sweeney, H. L., and Discher, D. E. (2006). Matrix Elasticity Directs Stem Cell Lineage Specification. *Cell*, 126(4):677–689.

[65] Escribano, J., Sánchez, M. T., and García-Aznar, J. M. (2014). A discrete approach for modeling cell–matrix adhesions. *Computational Particle Mechanics*, 1(2):117–130.

[66] Escribano, J., Sánchez, M. T., and García-Aznar, J. M. (2015). Modeling the formation of cell-matrix adhesions on a single 3D matrix fiber. *Journal of Theoretical Biology*, 384:84–94.

[67] Escribano, J., Sunyer, R., Sánchez, M. T., Trepat, X., Roca-Cusachs, P., and García-Aznar, J. M. (2018). A hybrid computational model for collective cell durotaxis. *Biomechanics and Modeling in Mechanobiology*.

[68] Fackler, O. T. and Grosse, R. (2008). Cell motility through plasma membrane blebbing. *Journal of Cell Biology*, 181(6):879–884.

[69] Franz, C. M. (2005). Analyzing focal adhesion structure by atomic force microscopy. *Journal of Cell Science*, 118(22):5315–5323.

[70] Freddolino, P. L., Christopher B. Harrison, Y. L., and Schulten, K. (2010). Challenges in protein folding simulations: Timescale, representation, and analysis Peter. *Nat Phys.*, 6(10):751–758.

[71] Friedl, P. and Gilmour, D. (2009). Collective cell migration in morphogenesis, regeneration and cancer. *Nature reviews. Molecular cell biology*, 10(july):445–457.

[72] Friedl, P. and Wolf, K. (2010). Plasticity of cell migration: a multiscale tuning model. *The Journal of cell biology*, 188(1):11–9.

[73] Galle, J., Loeffler, M., and Drasdo, D. (2005). Modeling the Effect of Deregulated Proliferation and Apoptosis on the Growth Dynamics of Epithelial Cell Populations In Vitro. *Biophysical Journal*, 88(1):62–75.

[74] Gao, H., Qian, J., and Chen, B. (2011). Probing mechanical principles of focal contacts in cell-matrix adhesion with a coupled stochastic-elastic modelling framework. *Journal of the Royal Society, Interface / the Royal Society*, 8(62):1217–32.

[75] Gardel, M. L., Sabass, B., Ji, L., Danuser, G., Schwarz, U. S., and Waterman, C. M. (2008). Traction stress in focal adhesions correlates biphasically with actin retrograde fl ow speed. *Journal of Cell Biology*, 183(6):999–1005.

[76] Geiger, B., Bershadsky, A., Pankov, R., Yamada, K. M., and Correspondence, B. G. (2001). Transmembrane extracellular matrix-cytoskeleton crosstalk. *Nature Reviews |Molecular Cell Biology*, 2(November):793–805.

[77] Geiger, B., Spatz, J. P., and Bershadsky, A. D. (2009). Environmental sensing through focal adhesions. *Nature reviews. Molecular cell biology*, 10(1):21–33.

[78] Gerisch, A. and Painter, K. J. (2010). Mathematical modelling of cell adhesion and its applications to developmental biology and cancer invasion. In Chauvière, A., Preziosi, L., and Verdier, C., editors, *Cell Mechanics: From Single Scale-Based Models to Multiscale Modeling*, volume 2, chapter 12, pages 319–350. Chapman and Hall/CRC.

[79] Gonzalez-Valverde, I. and Garcia-Aznar, J. M. (2017). A hybrid computational model to explore the topological characteristics of epithelial tissues. *International Journal for Numerical Methods in Biomedical Engineering*, 33(11):1–16.

[80] Grimm, K. B., Oberleithner, H., and Fels, J. (2014). Fixed endothelial cells exhibit physiologically relevant nanomechanics of the cortical actin web. *Nanotechnology*, 25(21).

[81] Grinnell, F. (2008). Fibroblast mechanics in three-dimensional collagen matrices. *Journal of Bodywork and Movement Therapies*, 12(3):191–193.

[82] Grivennikov, S. I., Greten, F. R., and Karin, M. (2010). Immunity, inflammation, and cancer. *Cell*, 140(6):883–899.

[83] Haeger, A., Krause, M., Wolf, K., and Friedl, P. (2014). Cell jamming: Collective invasion of mesenchymal tumor cells imposed by tissue confinement. *Biochimica et biophysica acta*.

[84] Haeger, A., Wolf, K., Zegers, M. M., and Friedl, P. (2015). Collective cell migration: Guidance principles and hierarchies. *Trends in Cell Biology*, 25(9):556–566.

[85] Hartman, C. D., Isenberg, B. C., Chua, S. G., and Wong, J. Y. (2016). Vascular smooth muscle cell durotaxis depends on extracellular matrix composition. *Proceedings of the National Academy of Sciences of the United States of America*, 113(40):11190–11195.

[86] Harunaga, J. S. and Yamada, K. M. (2011). Cell-matrix adhesions in 3D. *Matrix biology : journal of the International Society for Matrix Biology*, 30(7-8):363–8.

[87] Hassinger, J. E., Oster, G., Drubin, D. G., and Rangamani, P. (2017). Design principles for robust vesiculation in clathrin-mediated endocytosis. *Proceedings of the National Academy of Sciences*, 114(7):E1118–E1127.

[88] Heemskerk, N., Schimmel, L., Oort, C., Van Rijssel, J., Yin, T., Ma, B., Van Unen, J., Pitter, B., Huveneers, S., Goedhart, J., et al. (2016). F-actin-rich contractile endothelial pores prevent vascular leakage during leukocyte diapedesis through local rhoa signalling. *Nature communications*, 7.

[89] Howard, J. (2002). Mechanics of motor proteins. In Flyvbjerg, F., Jülicher, F., Ormos, P., and David, F., editors, *Physics of bio-molecules and cells. Physique des biomol{é}cules et des cellules*, pages 69–94, Berlin, Heidelberg. Springer Berlin Heidelberg.

[90] Hughes, T. J. (1987). The Finite Element Method: Linear Static and Dynamic Finite Element Analysis.

[91] Huveneers, S., Oldenburg, J., Spanjaard, E., van der Krogt, G., Grigoriev, I., Akhmanova, A., Rehmann, H., and de Rooij, J. (2012). Vinculin associates with endothelial VE-cadherin junctions to control force-dependent remodeling. *Journal of Cell Biology*, 196(5):641–652.

[92] Jamali, Y., Azimi, M., and Mofrad, M. R. K. (2010). A sub-cellular viscoelastic model for cell population mechanics. *PLoS ONE*, 5(8).

[93] Jansen, K. A., Atherton, P., and Ballestrem, C. (2017). Mechanotransduction at the cell-matrix interface. *Seminars in Cell and Developmental Biology*, 71:75–83.

[94] Jia, D., Jolly, M. K., Boareto, M., Parsana, P., Mooney, S. M., Pienta, K. J., Levine, H., and Ben-Jacob, E. (2015). OVOL guides the epithelial-hybrid-mesenchymal transition. *Oncotarget*, 6(17):15436–48.

[95] Kabla, A. J. (2012). Collective cell migration: leadership, invasion and segregation. *Journal of The Royal Society Interface*, 9(77):3268–3278.

[96] Kanchanawong, P., Shtengel, G., Pasapera, A. M., Ramko, E. B., Davidson, M. W., Hess, H. F., and Waterman, C. M. (2010). Nanoscale architecture of integrin-based cell adhesions. *Nature*, 468(7323):580–4.

[97] Keren, K., Pincus, Z., Allen, G. M., Barnhart, E. L., Marriott, G., Mogilner, A., and Theriot, J. A. (2008). Mechanism of shape determination in motile cells. *Nature*, 453(7194):475–480.

[98] Kilian, K. A., Bugarija, B., Lahn, B. T., and Mrksich, M. (2010). Geometric cues for directing the differentiation of mesenchymal stem cells. *Proceedings of the National Academy of Sciences of the United States of America*, 107(11):4872–7.

[99] Kim, D.-H. and Wirtz, D. (2013). Focal adhesion size uniquely predicts cell migration. *FASEB journal : official publication of the Federation of American Societies for Experimental Biology*, 27(4):1351–61.

[100] Kim, M. C., Whisler, J., Silberberg, Y. R., Kamm, R. D., and Asada, H. H. (2015). Cell Invasion Dynamics into a Three Dimensional Extracellular Matrix Fibre Network. *PLoS Computational Biology*, 11(10):1–29.

[101] Kim, T., Hwang, W., and Kamm, R. D. (2007). Computational Analysis of a Cross-linked Actin-like Network. *Experimental Mechanics*, 49(1):91–104.

[102] Kim, T., Hwang, W., and Kamm, R. D. (2011). Dynamic role of cross-linking proteins in actin rheology. *Biophysical journal*, 101(7):1597–603.

[103] Kollman, P. a., Massova, I., Reyes, C., Kuhn, B., Huo, S., Chong, L., Lee, M., Lee, T., Duan, Y., Wang, W., Donini, O., Cieplak, P., Srinivasan, J., Case, D. a., and Cheatham, T. E. (2000). Calculating structures and free energies of complex molecules: combining molecular mechanics and continuum models. *Accounts of chemical research*, 33(12):889–97.

[104] Komarova, Y. and Malik, A. B. (2010). *Regulation of Endothelial Permeability via Paracellular and Transcellular Transport Pathways*, volume 72.

[105] Kong, D., Ji, B., and Dai, L. (2008). Stability of adhesion clusters and cell reorientation under lateral cyclic tension. *Biophysical journal*, 95(8):4034–44.

[106] Kong, F., García, A. J., Mould, a. P., Humphries, M. J., and Zhu, C. (2009). Demonstration of catch bonds between an integrin and its ligand. *The Journal of cell biology*, 185(7):1275–84.

[107] Kruse, K. and Komarova, Y. A. (2015). Tension across adherens junctions: when less is more. *Oncotarget*, 6(31):30433–4.

[108] Kubow, K. E., Conrad, S. K., and Horwitz, a. R. (2013). Matrix microarchitecture and myosin II determine adhesion in 3D matrices. *Current biology : CB*, 23(17):1607–19.

[109] Kulawiak, D. A., Camley, B. A., and Rappel, W.-J. (2016). Modeling Contact Inhibition of Locomotion of Colliding Cells Migrating on Micropatterned Substrates. *PLOS Computational Biology*, 12(12):1–25.

[110] Ladoux, B., Anon, E., Lambert, M., Rabodzey, A., Hersen, P., Buguin, A., Silberzan, P., and Mège, R.-M. (2010). Strength Dependence of Cadherin-Mediated Adhesions. *Biophysical Journal*, 98(4):534–542.

[111] Lang, N. R., Skodzek, K., Hurst, S., Mainka, A., Steinwachs, J., Schneider, J., Aifantis, K. E., and Fabry, B. (2015). Biphasic response of cell invasion to matrix stiffness in three-dimensional biopolymer networks. *Acta Biomaterialia*, 13:61–67.

[112] Lecuit, T. and Lenne, P.-F. (2007). Cell surface mechanics and the control of cell shape, tissue patterns and morphogenesis. *Nature reviews. Molecular cell biology*, 8(8):633–44.

[113] Lecuit, T. and Yap, A. S. (2015). E-cadherin junctions as active mechanical integrators in tissue dynamics. *Nature Cell Biology*, 17(5):533–539.

[114] Lee, K.-C. and Liu, A. J. (2009). Force-velocity relation for actin-polymerization-driven motility from Brownian dynamics simulations. *Biophysical journal*, 97(5):1295–304.

[115] Leong, F. Y. (2013). Physical explanation of coupled cell-cell rotational behavior and interfacial morphology: A particle dynamics model. *Biophysical Journal*, 105(10):2301–2311.

[116] Libby, P., Okamoto, Y., Rocha, V. Z., and Folco, E. (2010). Inflammation in atherosclerosis. *Circulation journal*, 74(2):213–220.

[117] Lin, S.-Z., Li, B., Xu, G.-K., and Feng, X.-Q. (2016). Collective dynamics of cancer cells confined in a confluent monolayer of normal cells. *Journal of Biomechanics*, 52:140–147.

[118] Liu, F., Mih, J. D., Shea, B. S., Kho, A. T., Sharif, A. S., Tager, A. M., and Tschumperlin, D. J. (2010). Feedback amplification of fibrosis through matrix stiffening and COX-2 suppression. *Journal of Cell Biology*, 190(4):693–706.

[119] Loeser, R. F. (2014). Integrins and chondrocyte-matrix interactions in articular cartilage. *Matrix biology : journal of the International Society for Matrix Biology*, 39:11–16.

[120] Lutz, B., Faber, M., Verma, A., Klumpp, S., and Schug, A. (2013). Differences between cotranscriptional and free riboswitch folding. *Nucleic acids research*, (i):1–10.

[121] Maaser, K., Wolf, K., Klein, C. E., Niggemann, B., Zänker, K. S., Bröcker, E. B., and Friedl, P. (1999). Functional hierarchy of simultaneously expressed adhesion receptors: integrin alpha2beta1 but not CD44 mediates MV3 melanoma cell migration and matrix reorganization within three-dimensional hyaluronan-containing collagen matrices. *Molecular biology of the cell*, 10(10):3067–79.

[122] Majumdar, R., Sixt, M., and Parent, C. A. (2014). New paradigms in the establishment and maintenance of gradients during directed cell migration. *Current Opinion in Cell Biology*, 30:33–40.

[123] Malet-Engra, G., Yu, W., Oldani, A., Rey-Barroso, J., Gov, N. S., Scita, G., and Dupré, L. (2015). Collective cell motility promotes chemotactic prowess and resistance to chemorepulsion. *Current Biology*, 25(2):242–250.

[124] Martin, P. (1997). Wound healing–aiming for perfect skin regeneration. *Science (New York, N.Y.)*, 276(5309):75–81.

[125] Martinelli, R., Zeiger, A. S., Whitfield, M., Sciuto, T. E., Dvorak, A., Van Vliet, K. J., Greenwood, J., and Carman, C. V. (2014). Probing the biomechanical contribution of the endothelium to lymphocyte migration: diapedesis by the path of least resistance. *Journal of Cell Science*, 127(17):3720–3734.

[126] Mayor, R. and Carmona-Fontaine, C. (2010). Keeping in touch with contact inhibition of locomotion. *Trends in Cell Biology*, 20(6):319–328.

[127] Méhes, E. and Vicsek, T. (2014). Collective motion of cells: from experiments to models. *Integr. Biol.*, 6(9):831–854.

[128] Merkher, Y. and Weihs, D. (2017). Proximity of Metastatic Cells Enhances Their Mechanobiological Invasiveness. *Annals of Biomedical Engineering*, 45(6):1399–1406.

[129] Milan, J.-l., Lavenus, S., Pilet, P., Louarn, G., Wendling, S., Heymann, D., Layrolle, P., and Chabrand, P. (2013). Computational model combined with in vitro experiments to analyse mechanotransduction during mesenchymal stem cell adhesion. *European Cells and Materials*, 25:97–113.

[130] Mizutani, K. and Takai, Y. (2016). Nectin spot: a novel type of nectin-mediated cell adhesion apparatus. *Biochemical Journal*, 473(18):2691–2715.

[131] Mogilner, a. and Rubinstein, B. (2005). The physics of filopodial protrusion. *Biophysical journal*, 89(2):782–95.

[132] Moreno-Arotzena, O., Borau, C., Movilla, N., Vicente-Manzanares, M., and García-Aznar, J. M. (2015). Fibroblast Migration in 3D is Controlled by Haptotaxis in a Non-muscle Myosin II-Dependent Manner. *Annals of Biomedical Engineering*, 43(12):3025–3039.

[133] Movilla, N., Borau, C., Valero, C., and García-Aznar, J. M. (2017). Degradation of extracellular matrix regulates osteoblast migration: A microfluidic-based study. *Bone*, 107:10–17.

[134] Mullin, J. M., Agostino, N., Rendon-Huerta, E., and Thornton, J. J. (2005). Keynote review: epithelial and endothelial barriers in human disease. *Drug discovery today*, 10(6):395–408.

[135] Münster, S., Jawerth, L. M., Leslie, B. a., Weitz, J. I., Fabry, B., and Weitz, D. a. (2013). Strain history dependence of the nonlinear stress response of fibrin and collagen networks. *Proceedings of the National Academy of Sciences of the United States of America*, 110(30):12197–202.

[136] Murray, P. J. and Wynn, T. A. (2011). Protective and pathogenic functions of macrophage subsets. *Nature reviews immunology*, 11(11):723–737.

[137] Nawabi, H., Briançon-Marjollet, A., Clark, C., Sanyas, I., Takamatsu, H., Okuno, T., Kumanogoh, A., Bozon, M., Takeshima, K., Yoshida, Y., Moret, F., Abouzid, K., and Castellani, V. (2010). A midline switch of receptor processing regulates commissural axon guidance in vertebrates. *Genes & development*, 24(4):396–410.

[138] Newell-Litwa, K. A., Horwitz, R., and Lamers, M. L. (2015). Non-muscle myosin II in disease: mechanisms and therapeutic opportunities. *Disease Models & Mechanisms*, 8(12):1495–1515.

[139] Nicolas, A., Geiger, B., and Safran, S. A. (2004). Cell mechanosensitivity controls the anisotropy of focal adhesions. *PNAS*, 101(34):12520–12525.

[140] Novikova, E. A., Raab, M., Discher, D. E., and Storm, C. (2017). Persistence-Driven Durotaxis: Generic, Directed Motility in Rigidity Gradients. *Physical Review Letters*, 118(7):1–5.

[141] Novikova, E. A. and Storm, C. (2013). Contractile fibers and catch-bond clusters: a biological force sensor? *Biophysical journal*, 105(6):1336–45.

[142] Olberding, J. E., Thouless, M. D., Arruda, E. M., and Garikipati, K. (2010). The non-equilibrium thermodynamics and kinetics of focal adhesion dynamics. *PloS one*, 5(8):e12043.

[143] Oldenburg, J. and De Rooij, J. (2014). Mechanical control of the endothelial barrier. *Cell and Tissue Research*, 355(3):545–555.

[144] Oria, R., Wiegand, T., Escribano, J., Elosegui-Artola, A., Uriarte, J. J., Moreno-Pulido, C., Platzman, I., Delcanale, P., Albertazzi, L., Navajas, D., Trepat, X., García-Aznar, J. M., Cavalcanti-Adam, E. A., and Roca-Cusachs, P. (2017). Force loading explains spatial sensing of ligands by cells. *Nature*.

[145] Paluch, E., Sykes, C., Prost, J., and Bornens, M. (2006). Dynamic modes of the cortical actomyosin gel during cell locomotion and division. *Trends in Cell Biology*, 16(1):5–10.

[146] Panorchan, P., George, J. P., and Wirtz, D. (2006). Probing Intercellular Interactions between Vascular Endothelial Cadherin Pairs at Single-molecule Resolution and in Living Cells. *Journal of Molecular Biology*, 358(3):665–674.

[147] Park, J. E. and Barbul, A. (2004). Understanding the role of immune regulation in wound healing. *The American Journal of Surgery*, 187(5, Supplement 1):S11 – S16.

[148] Parsons, J. T., Horwitz, A. R., and Schwartz, M. a. (2010). Cell adhesion: integrating cytoskeletal dynamics and cellular tension. *Nature Reviews Molecular Cell Biology*, 11(9):633–643.

[149] Pathak, A. (2016). Scattering of Cell Clusters in Confinement. *Biophysical Journal*, 111(7):1496–1506.

[150] Peng, L., Trucu, D., Lin, P., Thompson, A., and Chaplain, M. A. (2017). A Multiscale Mathematical Model of Tumour Invasive Growth. *Bulletin of Mathematical Biology*, 79(3):389–429.

[151] Petrie, R. J. and Yamada, K. M. (2012). At the leading edge of three-dimensional cell migration. *Journal of cell science*, 125(Pt 24):5917–26.

[152] Piana, S., Klepeis, J. L., and Shaw, D. E. (2014). Assessing the accuracy of physical models used in protein-folding simulations: quantitative evidence from long molecular dynamics simulations. *Current Opinion in Structural Biology*, 24:98–105.

[153] Plotnikov, S. V., Pasapera, A. M., Sabass, B., and Waterman, C. M. (2012). Force Fluctuations within Focal Adhesions Mediate ECM-Rigidity Sensing to Guide Directed Cell Migration. *Cell*, 151(7):1513–1527.

[154] Pollard, T. D. and Borisy, G. G. (2003). Cellular motility driven by assembly and disassembly of actin filaments. *Cell*, 112(4):453–65.

[155] Pollard, T. D. and Cooper, J. A. (2009). Actin, a Central Player in Cell Shape and Movement. *Science*, 326(5957):1208 LP – 1212.

[156] Ponti, A., Machacek, M., Gupton, S. L., Waterman-Storer, C. M., and Danuser, G. (2004). Two distinct actin networks drive the protrusion of migrating cells. *Science (New York, N.Y.)*, 305(5691):1782–6.

[157] Rabodzey, A., Alcaide, P., Luscinskas, F. W., and Ladoux, B. (2008). Mechanical Forces Induced by the Transendothelial Migration of Human Neutrophils. *Biophysical Journal*, 95(3):1428–1438.

[158] Reina-Romo, E., Gómez-Benito, M. J., García-Aznar, J. M., Domínguez, J., and Doblaré, M. (2010). Growth mixture model of distraction osteogenesis: Effect of pre-traction stresses. *Biomechanics and Modeling in Mechanobiology*, 9(1):103–115.

[159] Ren, X.-R., Ming, G.-L., Xie, Y., Hong, Y., Sun, D.-M., Zhao, Z.-Q., Feng, Z., Wang, Q., Shim, S., Chen, Z.-F., Song, H.-J., Mei, L., and Xiong, W.-C. (2004). Focal adhesion kinase in netrin-1 signaling. *Nature neuroscience*, 7(11):1204–12.

[160] Reymond, N., D'Água, B. B., and Ridley, A. J. (2013). Crossing the endothelial barrier during metastasis. *Nature Reviews Cancer*, 13(12):858–870.

[161] Ridley, A. J. (2011). Life at the leading edge. *Cell*, 145(7):1012–22.

[162] Ridley, A. J., Schwartz, M. a., Burridge, K., Firtel, R. a., Ginsberg, M. H., Borisy, G., Parsons, J. T., and Horwitz, A. R. (2003). Cell migration: integrating signals from front to back. *Science (New York, N.Y.)*, 302(5651):1704–9.

[163] Roca-Cusachs, P., Iskratsch, T., and Sheetz, M. P. (2012). Finding the weakest link: exploring integrin-mediated mechanical molecular pathways. *Journal of cell science*, 125(Pt 13):3025–38.

[164] Roca-Cusachs, P., Sunyer, R., and Trepat, X. (2013). Mechanical guidance of cell migration: Lessons from chemotaxis. *Current Opinion in Cell Biology*, 25(5):543–549.

[165] Rodriguez, E. K., Hoger, A., and McCulloch, A. D. (1994). Stress-dependent finite growth in soft elastic tissues. *Journal of Biomechanics*, 27(4):455–467.

[166] Rørth, P. (2011). Whence Directionality: Guidance Mechanisms in Solitary and Collective Cell Migration. *Developmental Cell*, 20(1):9–18.

[167] Ruoslahti, E. (1996). RGD and other recognition sequences for integrins. *Annual review of cell and developmental biology*, 12:697–715.

[168] Sabass, B. and Schwarz, U. S. (2010). Modeling cytoskeletal flow over adhesion sites: competition between stochastic bond dynamics and intracellular relaxation. *Journal of physics. Condensed matter : an Institute of Physics journal*, 22(19):194112.

[169] Sanz-Moreno, V., Gaggioli, C., Yeo, M., Albrengues, J., Wallberg, F., Viros, A., Hooper, S., Mitter, R., Féral, C. C., Cook, M., Larkin, J., Marais, R., Meneguzzi, G., Sahai, E., and Marshall, C. J. (2011). ROCK and JAK1 signaling cooperate to control actomyosin contractility in tumor cells and stroma. *Cancer cell*, 20(2):229–45.

[170] Sanz-Moreno, V. and Marshall, C. J. (2009). Rho-GTPase signaling drives melanoma cell plasticity. *Cell Cycle*, 8(10):1484–1487.

[171] Sarangapani, K. K., Qian, J., Chen, W., Zarnitsyna, V. I., Mehta, P., Yago, T., and Mcever, R. P. (2011). Regulation of Catch Bonds by Rate of Force Application *. *Journal of biological chemistry*, 286(37):32749–32761.

[172] Sauer, R. a. and Wriggers, P. (2009). Formulation and analysis of a three-dimensional finite element implementation for adhesive contact at the nanoscale. *Computer Methods in Applied Mechanics and Engineering*, 198(49-52):3871–3883.

[173] Schaefer, A. and Hordijk, P. L. (2015). Cell-stiffness-induced mechanosignaling–a key driver of leukocyte transendothelial migration. *J Cell Sci*, 128(13):2221–2230.

[174] Schaefer, A., te Riet, J., Ritz, K., Hoogenboezem, M., Anthony, E. C., Mul, F. P. J., de Vries, C. J., Daemen, M. J., Figdor, C. G., van Buul, J. D., and Hordijk, P. L. (2014). Actin-binding proteins differentially regulate endothelial cell stiffness, icam-1 function and neutrophil transmigration. *Journal of Cell Science*, 127(20):4470–4482.

[175] Schreiber, C. H., Stewart, M., and Duke, T. (2010). Simulation of cell motility that reproduces the force-velocity relationship. *Proceedings of the National Academy of Sciences of the United States of America*, 107(20):9141–6.

[176] Schwarz, U. S. and Gardel, M. L. (2012). United we stand: integrating the actin cytoskeleton and cell-matrix adhesions in cellular mechanotransduction. *Journal of cell science*, 125(Pt 13):3051–60.

[177] Schwarz, U. S. and Safran, S. a. (2013). Physics of adherent cells. *Reviews of Modern Physics*, 85(3):1327–1381.

[178] Selhuber-Unkel, C., Erdmann, T., López-García, M., Kessler, H., Schwarz, U. S., and Spatz, J. P. (2010). Cell adhesion strength is controlled by intermolecular spacing of adhesion receptors. *Biophysical journal*, 98(4):543–51.

[179] Sens, P. and Plastino, J. (2015). Membrane tension and cytoskeleton organization in cell motility. *Journal of Physics Condensed Matter*, 27(27).

[180] Sepúlveda, N., Petitjean, L., Cochet, O., Grasland-Mongrain, E., Silberzan, P., and Hakim, V. (2013). Collective Cell Motion in an Epithelial Sheet Can Be Quantitatively Described by a Stochastic Interacting Particle Model. *PLoS Computational Biology*, 9(3).

[181] Shemesh, T., Geiger, B., Bershadsky, A. D., and Kozlov, M. M. (2005). Focal adhesions as mechanosensors: a physical mechanism. *Proceedings of the National Academy of Sciences of the United States of America*, 102(35):12383–8.

[182] Singh, S. P., Schwartz, M. P., Lee, J. Y., Fairbanks, B. D., and Anseth, K. S. (2014). A peptide functionalized poly(ethylene glycol) (PEG) hydrogel for investigating the influence of biochemical and biophysical matrix properties on tumor cell migration. *Biomaterials Science*, 2(7):1024.

[183] Smith, L. A., Aranda-Espinoza, H., Haun, J. B., Dembo, M., and Hammer, D. A. (2007). Neutrophil Traction Stresses are Concentrated in the Uropod during Migration. *Biophysical Journal*, 92(7):L58–L60.

[184] Soler, M. a. and Faísca, P. F. N. (2013). Effects of knots on protein folding properties. *PloS one*, 8(9):e74755.

[185] Stefanoni, F., Ventre, M., Mollica, F., and Netti, P. A. (2011). A numerical model for durotaxis. *Journal of Theoretical Biology*, 280(1):150–158.

[186] Steketee, M. B. and Tosney, K. W. (2002). Three functionally distinct adhesions in filopodia: shaft adhesions control lamellar extension. *The Journal of neuroscience*, 22(18):8071–83.

[187] Strilic, B. and Offermanns, S. (2017). Intravascular Survival and Extravasation of Tumor Cells. *Cancer Cell*, 32(3):282–293.

[188] Suarez, C. and Kovar, D. R. (2016). Internetwork competition for monomers governs actin cytoskeleton organization. *Nature Reviews Molecular Cell Biology*, 17(12):799–810.

[189] Sunyer, R., Conte, V., Escribano, J., Elosegui-Artola, A., Labernadie, A., Valon, L., Navajas, D., Garcia-Aznar, J. M., Munoz, J. J., Roca-Cusachs, P., and Trepat, X. (2016). Collective cell durotaxis emerges from long-range intercellular force transmission. *Science*, 353(6304):1157–1161.

[190] Tambe, D. T., Corey Hardin, C., Angelini, T. E., Rajendran, K., Park, C. Y., Serra-Picamal, X., Zhou, E. H., Zaman, M. H., Butler, J. P., Weitz, D. A., Fredberg, J. J., and Trepat, X. (2011). Collective cell guidance by cooperative intercellular forces. *Nature Materials*, 10(6):469–475.

[191] te Boekhorst, V., Preziosi, L., and Friedl, P. (2016). Plasticity of Cell Migration In Vivo and In Silico. *Annual Review of Cell and Developmental Biology*, 32(1):491–526.

[192] Theveneau, E., Marchant, L., Kuriyama, S., Gull, M., Moepps, B., Parsons, M., and Mayor, R. (2010). Collective Chemotaxis Requires Contact-Dependent Cell Polarity. *Developmental Cell*, 19(1):39–53.

[193] Thievessen, I., Thompson, P. M., Berlemont, S., Plevock, K. M., Plotnikov, S. V., Zemljic-Harpf, A., Ross, R. S., Davidson, M. W., Danuser, G., Campbell, S. L., and Waterman, C. M. (2013). Vinculin-actin interaction couples actin retrograde flow to focal adhesions, but is dispensable for focal adhesion growth. *The Journal of cell biology*, 202(1):163–77.

[194] Trichet, L., Le Digabel, J., Hawkins, R. J., Vedula, S. R. K., Gupta, M., Ribrault, C., Hersen, P., Voituriez, R., and Ladoux, B. (2012). Evidence of a large-scale mechanosensing mechanism for cellular adaptation to substrate stiffness. *Proceedings of the National Academy of Sciences*, 109(18):6933–6938.

[195] Ulrich, T. A., De Juan Pardo, E. M., and Kumar, S. (2009). The mechanical rigidity of the extracellular matrix regulates the structure, motility, and proliferation of glioma cells. *Cancer Research*, 69(10):4167–4174.

[196] Urban, E., Jacob, S., Nemethova, M., Resch, G. P., and Small, J. V. (2010). Electron tomography reveals unbranched networks of actin filaments in lamellipodia. *Nature Cell Biology*, 12(5):429–435.

[197] Uyaver, S. and Hansmann, U. H. E. (2014). Multicanonical Monte Carlo simulations of a de novo designed protein with end-to-end β-sheet. *The Journal of chemical physics*, 140(6):065101.

[198] Valent, E. T., van Nieuw Amerongen, G. P., van Hinsbergh, V. W. M., and Hordijk, P. L. (2016). Traction force dynamics predict gap formation in activated endothelium. *Experimental Cell Research*, 347(1):161–170.

[199] Van Liedekerke, P., Palm, M. M., Jagiella, N., and Drasdo, D. (2015). Simulating tissue mechanics with agent-based models: concepts, perspectives and some novel results. *Computational Particle Mechanics*, 2(4):401–444.

[200] Vermolen, F., Arkesteijn, E., and Gefen, A. (2016). Modelling the immune system response to epithelial wound infections. *Journal of Theoretical Biology*, 393:158–169.

[201] Vermolen, F. J., van der Meijden, R. P., Van Es, M., Gefen, A., and Weihs, D. (2015). Towards a Mathematical Formalism for Semi-stochastic Cell-Level Computational Modeling of Tumor Initiation. *Annals of Biomedical Engineering*, 43(7):1680–1694.

[202] Vestweber, D. (2015). How leukocytes cross the vascular endothelium. *Nature Reviews Immunology*, 15(11):692–704.

[203] Viet, M. H. (2012). *Numerical study of protein-ligand binding: implications for alzheimer's disease and influenza virus*. PhD thesis.

[204] Vogel, V. and Sheetz, M. (2006). Local force and geometry sensing regulate cell functions. *Nature reviews. Molecular cell biology*, 7(4):265–75.

[205] Waisman, H. and Fish, J. (2008). A heterogeneous space - time full approximation storage multilevel method for molecular dynamics simulations. *Int. J. Numer. Meth. Engng*, 73(May 2007):407–426.

[206] Weichsel, J. and Schwarz, U. S. (2010). Two competing orientation patterns explain experimentally observed anomalies in growing actin networks. *Proceedings of the National Academy of Sciences of the United States of America*, 107(14):6304–9.

[207] Wolf, K., Mazo, I., Leung, H., Engelke, K., von Andrian, U. H., Deryugina, E. I., Strongin, A. Y., Bröcker, E.-B., and Friedl, P. (2003). Compensation mechanism in tumor cell migration: mesenchymal-amoeboid transition after blocking of pericellular proteolysis. *The Journal of cell biology*, 160(2):267–77.

[208] Wolfenson, H., Meacci, G., Liu, S., Stachowiak, M. R., Iskratsch, T., Ghassemi, S., Roca-Cusachs, P., O'Shaughnessy, B., Hone, J., and Sheetz, M. P. (2016). Tropomyosin controls sarcomere-like contractions for rigidity sensing and suppressing growth on soft matrices. *Nature Cell Biology*, 18(1):33–42.

[209] Wozniak, M. a. and Chen, C. S. (2009). Mechanotransduction in development: a growing role for contractility. *Nature reviews. Molecular cell biology*, 10(1):34–43.

[210] Yamada, K., Pankov, R., and Cukierman, E. (2003). Dimensions and dynamics in integrin function. *Brazilian Journal of Medical and Biological Research*, 36(8):959–966.

[211] Yang, J. and Weinberg, R. A. (2008). Epithelial-Mesenchymal Transition: At the Crossroads of Development and Tumor Metastasis. *Developmental Cell*, 14(6):818–829.

[212] Yao, M., Goult, B. T., Chen, H., Cong, P., Sheetz, M. P., and Yan, J. (2014). Mechanical activation of vinculin binding to talin locks talin in an unfolded conformation. *Scientific reports*, 4:4610.

[213] Yoshida, K. and Soldati, T. (2006). Dissection of amoeboid movement into two mechanically distinct modes. *Journal of Cell Science*, 119(18):3833–3844.

[214] Yu, G., Feng, J., Man, H., and Levine, H. (2017). Phenomenological modeling of durotaxis. *Physical Review E*, 96(1):1–6.

[215] Zaidel-Bar, R., Itzkovitz, S., Ma'ayan, A., Iyengar, R., and Geiger, B. (2007). Functional atlas of the integrin adhesome. *Nature cell biology*, 9(8):858–67.

[216] Zamir, E. and Geiger, B. (2001). Molecular complexity and dynamics of cell-matrix adhesions. *Journal of cell science*, 114(Pt 20):3583–90.

[217] Zhang, H., Berg, J. S., Li, Z., Wang, Y., Lång, P., Sousa, A. D., Bhaskar, A., Cheney, R. E., and Strömblad, S. (2004). Myosin-X provides a motor-based link between integrins and the cytoskeleton. *Nature cell biology*, 6(6):523–31.

[218] Zimmermann, J., Brunner, C., Enculescu, M., Goegler, M., Ehrlicher, A., Käs, J., and Falcke, M. (2012). Actin filament elasticity and retrograde flow shape the force-velocity relation of motile cells. *Biophysical journal*, 102(2):287–95.